

**A Comparison of Photophysical Properties of A  
Chiral Perylene Monoimide with 3,4,9,10-  
Perylenetetracarboxylic Acid**

**Haval Mohammed Ali**

Submitted to the  
Institute of Graduate Studies and Research  
in partial fulfillment of the requirements for the Degree of

Master of Science  
in  
Chemistry

Eastern Mediterranean University  
January 2014  
Gazimağusa, North Cyprus

Approval of the Institute of Graduate Studies and Research

---

Prof. Dr. Elvan Yılmaz  
Director

I certify that this thesis satisfies the requirements as a thesis for the degree of Master of Science in Chemistry.

---

Prof. Dr. Mustafa Halilsoy  
Chair, Department of Chemistry

We certify that we have read this thesis and that in our opinion it is fully adequate in scope and quality as a thesis for the degree of Master of Science in Chemistry.

---

Prof. Dr. Huriye İcil  
Supervisor

---

Examining Committee

1. Prof. Dr. Huriye İcil
2. Asst. Prof. Dr. Hatice Nilay Hasipođlu
3. Asst. Prof. Dr. Mustafa Erkut Özser

## ABSTRACT

The perylene chromophore with versatile substituents offers strong absorption in the visible region with high molar extinction coefficients. Moreover, they are capable of emitting light with high fluorescence quantum yields near unity. The four carbonyl groups present in the core structure facilitate ease of accepting electrons and therefore perylene dyes play an important role for dye sensitized solar cells.

In this project, perylene -3,4,9,10 tetracarboxylic acid (PTCA) and perylene-3,4-dicarboxylic-9,10-(R)-(+)–1–phenylethyl)-carboximide (R-CPMI) were synthesized and their photophysical properties were compared. The synthesized compounds were characterized by FT-IR spectroscopy and photophysical properties were studied by absorption and emission spectroscopy.

All the synthesized dyes have very high molar absorptivities. The highest value is obtained for R-CPMI  $114000 \text{ M}^{-1} \text{ cm}^{-1}$ . PTCA and PDA absorption spectra indicate aggregation formation where dye-dye molecular interaction in PTCA is higher than PDA. Introducing a chiral substituent at one end of the PTCA breaks dye-dye molecular interaction in polar aprotic solvents. R-CPMI absorption spectrum in polar protic solvent displays a 9 nm blue shift due to hydrogen bonding.

**Keywords:** Perylene diimide, perylene monoimide, perylene carboxylic acid monoimide, perylene tetracarboxylic acid

## ÖZ

Perilen boyaları çok yönlü sübstitüentlerle görünür bölgede, yüksek molar absorplama sabitleri ile güçlü absorblama sunmaktadırlar. Ayrıca, bire yakın floresan kuantum verimleri ile ışık yayma yeteneğine sahiptirler. Perilenin çekirdek yapısında bulunan dört karbonil grubu elektron alabilme özelliğini kolaylaştırmakta ve bu nedenle, perilen boyaları güneş pillerinde önemli rol oynamaktadırlar.

Bu projede, perilen-3,4,9,10 tetrakarboksilik asit (PTCA) ve perilen-3,4-dikarboksilik-9, 10- (R)-(+)–1–feniletıl)–karboksimid (R-CPMI) sentezlenmiş ve bunların fotofiziksel özellikleri karşılaştırılmıştır. Sentezlenen bileşikler FT-IR spektroskopisi ile karakterize edilmiş ve fotofiziksel özellikleri absorpsiyon ve emisyon spektroskopisi ile incelenmiştir.

Sentezlenen tüm boyalar çok yüksek molar absorplama özelliğine sahiptir. En yüksek değer  $114000 \text{ M}^{-1} \text{ cm}^{-1}$  olarak R-CPMI için elde edilmiştir. PTCA ve PDA absorpsiyon spektrumları her iki bileşikte de agregasyon oluşumunu göstermekte ve boya-boya moleküler etkileşiminin PTCA'de PDA'e göre daha yüksek olduğu tespit edilmiştir. PTCA'in bir ucunda bir kiral sübstitüe bağlanması ile polar aprotik çözücü maddeler içerisinde boya-boya moleküler etkileşiminin kırıldığı tespit edilmiştir. R-CPMI'in polar protik çözücüdeki absorpsiyon spektrumu, hidrojen bağı nedeni ile, 9 nm daha kısa dalga boylu bölgeye kayma olduğunu göstermektedir.

**Anahtar kelimeler:** Perilen diimid, perilen monoimid, perilen karboksilik asit monoimide, perilen tetrakarboksilik asit

*To my beloved Prophet **Muhammad**  
peace and blessings be upon him and  
his family and his companions  
who filled the world of his light and  
mercy*

*Whose praise God (And We have not  
sent you, [O Muhammad], except as a  
mercy to the worlds)*

# ACKNOWLEDGEMENT

Bismillahi Al-Rahmani Al-Rahim

Praise be to Allah, Lord of the Worlds, and peace and blessings be upon our Prophet Muhammad and his family and his companions.

After that I would like firstly to offer my thanks to my esteemed supervisor Professor Dr. Huriye Icil, that we learned from her ethics and knowledge, and for giving me the opportunity to work with her group in this interesting field. I would like to mention also that she always treat every one of her group as one of her family, in many occasions she round up her students on a dinner party at her house or in a restaurant for the sake of deepen the friendship between each other. I won't forget her patience, wisdom, and the magnificent style in delivering lecture. Often she talked about her experience in life to give us the outcome of her experience. For all of these and more I hope the best for her and her family.

I would like also to thank everyone encourage me and help me to finish my synthesis in laboratory, specially Dr. Duygu Uzun and Dr. Jagadeesh Babu Bodapati, and also I would like thank Prof. Dr. Huriye İcil Organic Group members for their assistance and friendship.

To my beloved mother Alia Ftah Ahmed; To my Honorable father Mohammad Ali Mohammad; To my excellency uncle..... Dr. Zaki Ali Mohammad who encouraged me and support me; To my brother Dilshad and my sesters Shelan, Asmaa, Iman and Hajer; To my grandfather's and grandmother's, uncles and aunties;

To my relatives; To all my friends; To all my brothers in Islam; To my tribe and nation.

Finally I ask my god ALLAH to accept my work as right deeds.

# TABLE OF CONTENTS

ABSTRACT.....	iii
ÖZ .....	iv
ACKNOWLEDGEMENT .....	vi
LIST OF TABLES .....	x
LIST OF ILLUSTRATIONS.....	xiv
LIST OF SYMBOLS/ABBREVIATIONS .....	xv
1 INTRODUCTION.....	1
2 THEORETICAL .....	9
2.1 Properties of Perylene Monoimide and Diimide Dyes .....	9
2.1.1 Optical Characteristics of Perylene Monoimide and Diimide Dyes .....	9
2.1.2 Electron Acceptor Properties of Perylene Monoimide and Diimide Dyes for Photovoltaic Applications.....	12
2.1.3 Binding Properties of Perylene Monoimide Dyes for Photovoltaic Applications .....	13
2.2 The Future and Commercialization of Dye Sensitized Solar Cells.....	14
3 EXPERIMENTAL .....	17
3.1 Materials .....	17
3.2 Instruments.....	17
3.3 Methods of Synthesis.....	18
3.4 Synthesis of N, N' -bis (( <i>R</i> ) – (+) – 1– phenylethyl) 3, 4, 9, 10- perylenbis (dicarboximide) (PDI) .....	21
3.5 Synthesis of N- (( <i>R</i> ) – (+) – 1 – phenylethyl) – 3 , 4 , 9 , 10 - perylene-tetracarboxylic -3,4-anhydride-9,10-imide (R-PMI) .....	21

3.8 General Reaction Mechanism of Perylene Dyes .....	24
4 DATA AND CALCULATIONS .....	26
4.1 Calculations of Fluorescence Quantum Yield ( $\Phi_f$ ) .....	26
4.2 Calculations of Maximum Extinction Co-efficients ( $\epsilon_{\max}$ ) .....	28
4.3 Calculations of Half-width of the Selected Absorption ( $\Delta\nu_{1/2}$ ).....	30
4.4 Calculations of Theoretical Radiative Lifetimes ( $\tau_0$ ).....	33
4.5 Calculation of Theoretical Fluorescence Lifetime ( $\tau_f$ ) .....	35
4.6 Calculations of Fluorescence Rate Constants ( $k_f$ ).....	36
4.7 Calculations of Oscillator Strengths ( $f$ ) .....	37
4.8 Calculations of Singlet Energies ( $E_s$ ) .....	39
4.9 Calculations of Optical Band Gap Energies ( $E_g$ ) .....	40
5 RESULTS AND DISCUSSION .....	84
5.1 Synthesis of the Perylene Dyes .....	84
5.2 Solubility of the Perylene Dyes.....	85
5.3 Analysis of FTIR Spectra.....	86
5.4 Interpretation of UV-vis Spectra .....	87
5.5 Interpretation of Emission Spectra .....	89
6 CONCLUSION.....	92
REFERENCES .....	95

## LIST OF TABLES

Table 4.1 Fluorescence Quantum Yields of PTCA and R-CPMI.....	28
Table 4.2. Molar absorptivities of PTCA, PDA and R-CPMI.....	30
Table 4.3 Half-widths of the selected absorptions of compounds PTCA, PDA and R-CPMI.....	32
Table 4.4 Theoretical radiative lifetimes of compounds PTCA, PDA and R- CMPI.....	34
Table 4.5 Theoretical Fluorescence Lifetimes ( $\tau_f$ ) of PTCA and R-CPMI in different solvents.....	35
Table 4.6 Theoretical fluorescence rate constant of compounds PTCA, PDA and R-CPMI.....	37
Table 4.7 Oscillator strengths of the PTCA, PDA and R-CPMI.....	38
Table 4.8 The singlet energies of PTCA, PDA and R-CPMI.....	40
Table 4.9 Band gap energies of PTCA, PDA and R-CPMI.....	42
Table 5.1 Solubility of PTCA, PDA and R-CPMI.....	85

## LIST OF FIGURES

Figure 1. 1. Perylene core.....	1
Figure 1. 2 PDA .....	3
Figure 1. 3 PMI .....	3
Figure 1. 4 PDI.....	3
Figure 1. 5 Model of a Silicon solar cell .....	5
Figure 1. 6 A simple DSSCs.....	6
Figure 1. 7 PTCA.....	8
Figure 1. 8 R-CPMI.....	8
Figure 2. 1 Absorption spectrum of PDI .....	10
Figure 2. 2 Fluorescence Emission spectrum of PDI.....	10
Figure 2. 3 The structures bay and peri substitutions positions at PMI [16].....	11
Figure 2. 4 Binding of nanocrystalline TiO <sub>2</sub> with Carboxylic acid group. ....	14
Figure 4. 1 Absorption spectrum of PTCA in DMSO at concentration of $1 \times 10^{-5}$ M. .....	29
Figure 4. 2 Absorption spectrum of PTCA in DMSO and half-width representation .....	31
Figure 4. 3 Absorption spectrum of PTCA in DMSO and the cut-off wavelength ..	41
Figure 4. 4 FTIR spectrum of chiral PDI .....	43
Figure 4.5 FTIR spectrum of R-PMI.....	44
Figure 4.6 FTIR spectrum of R-CPMI .....	45
Figure 4.7 FTIR spectrum of PTCA .....	46
Figure 4.8 FTIR spectrum of PDA.....	47
Figure 4.9 Absorption spectrum of PTCA in DMSO.....	48
Figure 4.10 Absorption spectrum of PTCA in DMSO microfiltered.....	49

Figure 4.11 Absorption spectrum of PTCA in DMSO and DMSO microfiltered ....	50
Figure 4.12 Absorption spectrum of PTCA in DMF .....	51
Figure 4.13 Absorption spectrum of PTCA in DMF microfiltered .....	52
Figure 4.14 Absorption spectrum of PTCA in DMF and DMF microfiltered .....	53
Figure 4.15 Absorption spectrum of PTCA in DMF and DMSO .....	54
Figure 4.16 Absorption spectrum of R-CPMI in DMSO .....	55
Figure 4.17 Absorption spectrum of R-CPMI in DMF .....	56
Figure 4.18 Absorption spectrum of R-CPMI in Chloroform .....	57
Figure 4.19 Absorption spectrum of R-CPMI in MeOH .....	58
Figure 4.20 Absorption spectrum of R-CPMI in DMF, DMSO, CHL and MeOH ..	59
Figure 4.21 Absorption spectrum of PDA in DMSO .....	60
Figure 4.22 Absorption spectrum of PDA in DMSO microfiltered .....	61
Figure 4.23 Absorption spectrum of PDA in DMSO and DMSO microfiltered .....	62
Figure 4.24 Absorption spectrum of PDA in DMF .....	63
Figure 4.25 Absorption spectrum of PDA in DMF microfiltered .....	64
Figure 4. 26 Absorption spectrum of PDA in DMF and DMF microfiltered .....	65
Figure 4. 27 Absorption spectrum of PDA in DMF and DMSO .....	66
Figure 4.28 Emission spectrum of PTCA in DMSO at $\lambda_{exc} = 485$ nm .....	67
Figure 4. 29 Emission spectrum of PTCA in DMF at $\lambda_{exc} = 485$ nm .....	68
Figure 4.30 Emission spectrum of PTCA in DMF and DMSO at $\lambda_{exc} = 485$ nm .....	69
Figure 4.31 Emission spectrum of R-CPMI in DMSO at $\lambda_{exc} = 485$ nm .....	70
Figure 4.32 Emission spectrum of R-CPMI in DMF at $\lambda_{exc} = 485$ nm .....	71
Figure 4.33 Emission spectrum of R-CPMI in Chloroform at $\lambda_{exc} = 485$ nm .....	72
Figure 4.34 Emission spectrum of R-CPMI in MeOH at $\lambda_{exc} = 485$ nm .....	73

Figure 4.35 Emission spectrum of R-CPMI in DMF, DMSO, CHL and MeOH at $\lambda_{exc} = 485$ nm .....	74
Figure 4.36 Emission spectrum of PDA in DMSO M.F. at $\lambda_{exc} = 485$ nm .....	75
Figure 4.37 Emission spectrum of PDA in DMF M.F. at $\lambda_{exc} = 485$ nm .....	76
Figure 4.38 Emission spectrum of PDA in DMF and DMSO at $\lambda_{exc} = 485$ nm .....	77
Figure 4.39 Comparison of Absorbance and Emission of PTCA in DMSO .....	78
Figure 4.40 Comparison of Absorbance and Emission of PTCA in DMF .....	79
Figure 4.41 Comparison of Absorbance and Emission of R-CPMI in DMSO .....	80
Figure 4.42 Comparison of Absorbance and Emission of R-CPMI in DMF .....	81
Figure 4.43 Comparison of Absorbance and Emission of R-CPMI in CHL .....	82
Figure 4.44 Comparison of Absorbance and Emission of R-CPMI in MeOH .....	83

## LIST OF ILLUSTRATIONS

Scheme 3.1 Synthesis of perylene tetracarboxylic acid (PTCA). .....	18
Scheme 3.2 Synthetic route of chiral perylene dicarboxylic acid carboximide (R-CPMI). .....	18
Scheme 3.3 Synthesis of N,N'-bis((R)-(+)-1-phenylethyl)3,4,9,10-perylenbis(dicarboximide) (PDI) [30]. .....	19
Scheme 3.4 Synthesis of N-((R)-(+)-1-phenylethyl)-3,4,9,10-perylenetetracarboxylic-3,4-anhydride-9,10-imide (R-PMI). .....	20
Scheme 3.5 Synthesis of chiral perylene-3,4-dicarboxylic-9,10-(R)-(+)-1-phenylethyl-carboximide (R-CPMI). .....	20

## LIST OF SYMBOLS/ABBREVIATIONS

$\text{\AA}$	Armstrong
<b>cm</b>	Centimeter
$^{\circ}\text{C}$	Degrees Celcius
$\Delta \bar{\nu}_{1/2}$	Half-width of the selected absorption
$\epsilon_{\text{max}}$	Maximum extinction coefficient
$E_s$	Singlet energy
$f$	Oscillator strength
$\lambda_{\text{exc}}$	Excitation wavelength
$\lambda_{\text{max}}$	Absorption wavelength maximum
$\tau_0$	Theoretical radiative lifetime
$\tau_f$	Fluorescence lifetime
$\Phi_f$	Fluorescence quantum yield
<b>nm</b>	Nanometer
<b>CHCl<sub>3</sub></b>	Chloroform
<b>CHL</b>	Chloroform

<b>DMF</b>	N,N'-dimethylformamide
<b>DMSO</b>	N,N'-dimethyl sulfoxide
<b>FT-IR</b>	Fourier Transform Infrared Spectroscopy
<b>HCl</b>	Hydrochloric acid
<b>KBr</b>	Potassium bromide
$k_d$	Rate constant of Radiationless deactivation
$k_f$	Theoretical fluorescence rate constant
<b>KOH</b>	Potassium hydroxide
<b>M</b>	molar concentration
<b>MeOH</b>	Methanol
<b>UV-vis</b>	Ultraviolet visible absorption spectroscopy

# Chapter 1

## INTRODUCTION

The chemical structure of perylene consists of five benzene rings, arising from the interconnection of two naphthalene units, which attached together by covalent bonds, as shown in the Figure 1.1.

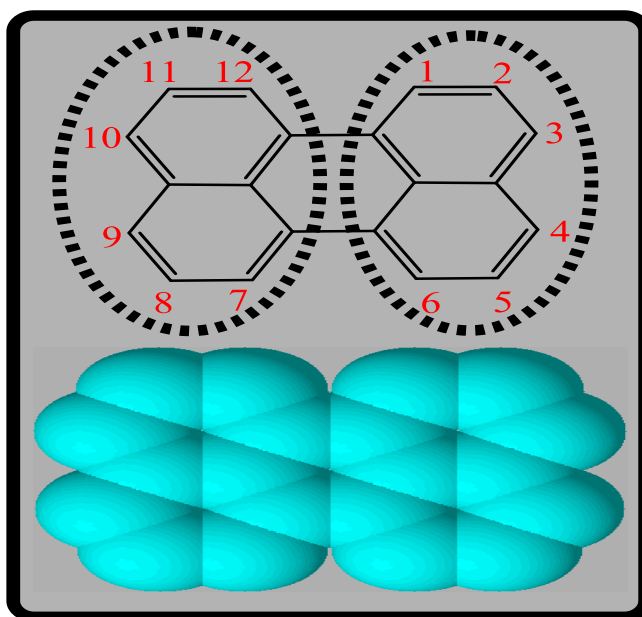


Figure 1. 1. Perylene core

One century ago, perylene dyes were discovered by Kardos in 1913. Perylene monoimide (PMI) and perylene diimide (PDI) as shown in Figure 1.3 and 1.4, respectively, are synthesized from perylene dianhydride (PDA) (Figure 1.2), where oxygen atoms are replaced by nitrogen atom, on the other hand, carbonyl groups are linked to benzene rings in peri positions which represented by carbon numbers (3,4,9,10) as shown in the Figure 1.1 and nitrogen atom is associated with two of

carbonyl groups to forms imides. The carbonyl groups provide the electron withdrawing property for the perylene dyes [1]. Thus perylene derivatives will subordination fast electron transfer and used as essential electron acceptors [2]. The conjugated  $\pi$ -system for both PMI and PDI molecules provide a perfect electron delocalization and this electron accepting feature in collaboration with high stabilities of these compounds make them the best in the area of electronics.

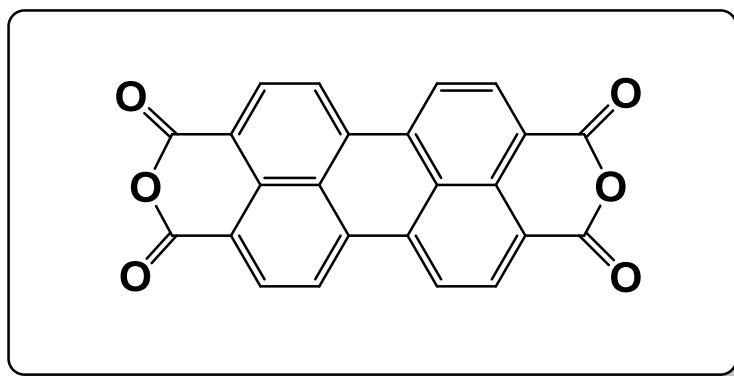


Figure 1. 2 PDA

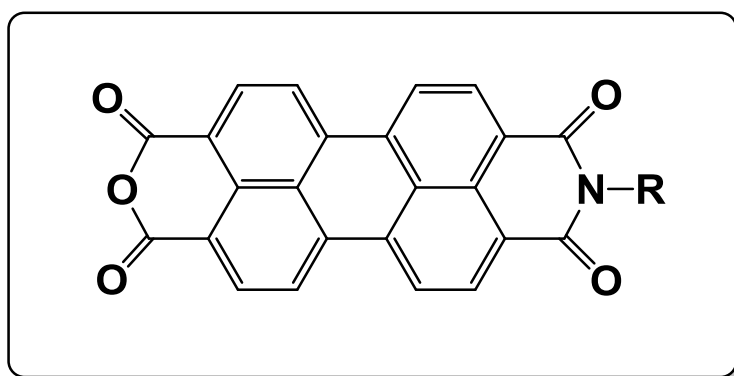


Figure 1. 3 PMI

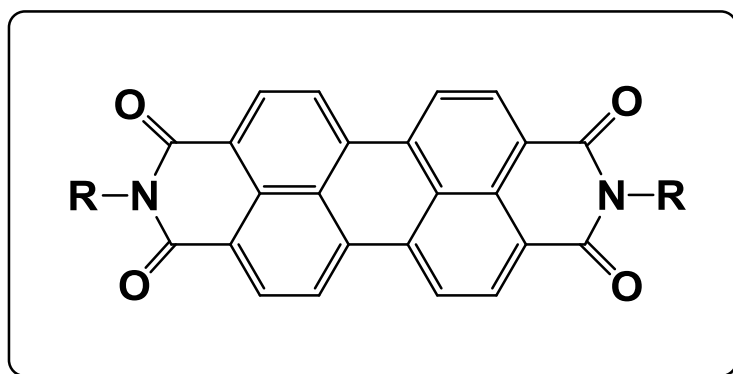


Figure 1. 4 PDI

One of the issue of perylene diimides is their low solubilities in common organic solvents which is arising from the presence of conjugated  $\pi$ -system that gives the rigidity feature of the compounds. Introducing long alkyl or aryl group substituents on the bay and ortho positions of perylene dye which represented by carbon numbers (1,6,7,12) and (2,5,8,11), respectively, as shown in Figure 1.1, and in addition, to nitrogen atom sites for PMI and PDI, will increase the solubility of perylene derivatives in many organic solvents [3]. On the other hand, their low solubility will be a benefit for some of their applications [4]. Beside the solubility's of perylene diimides, their optical properties like absorption wavelengths, HOMO/LUMO energies and also the spatial characteristics of the molecular orbitals are affected directly on the nature of the substituents, as well as the site that are attached to the perylene molecule [5].

Therefore, according to the application preferences it is possible to introduce different substituents to the perylene molecule and design functional perylene diimides for the required application. Although most of the perylene diimides has low solubility with common organic solvents, however, all the perylene derivatives are soluble in concentrated sulphuric acid through the positive hydrogen ion (protonation), which make a bathochromic shift of the absorption of 80 nm.

The unique properties of perylene dyes and its derivatives enabled them to be one of the best organic materials that undergo many technology application, for example organic light emitting diodes (OLED), liquid crystal displays (LCD), organic field effect transistors (OFET), dye lasers, dye sensitized solar cells (DSSCs), photodynamic therapy and photosensitizers in chemical oxidations [3].

Solar cells are apparatuses which transform sunlight into electrical power. There is many application in our daily life which possess this technology like in solar panel on roofs, water pump and small calculator. The majority of the trade mark solar cells are manufactured from silicon semiconductor. Figure 1.5 shows an example of silicon solar cell [6].

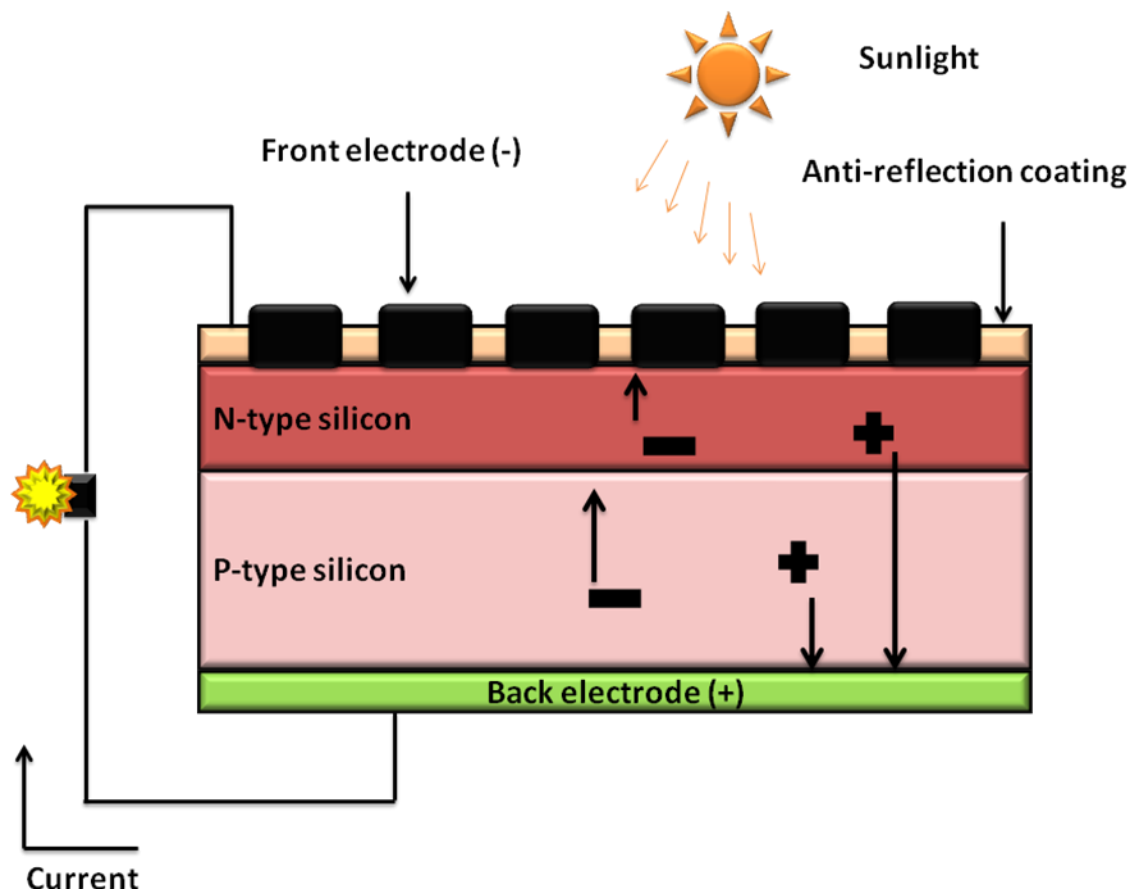


Figure 1. 5 Model of a Silicon solar

Beside the silicon solar cells, as a new generation, Dye-Sensitized Solar Cell (DSSCs) was first prepared by Grätzel and O'Regan in 1991, that is called 'Grätzel cell' and they are organic-based solar cells. The DSSCs are mostly inexpensive by comparing to silicon solar cells and is important to develop this type of solar cells [7]. Figure 1.6 shows an example of DSSCs [8].

Perylene diimides, due to their outstanding properties, are used as organic dye in the DSSCs. According to the working principle of DSSCs, the perylene dyes are used as electron accepting materials together with an electron donating substances and then the dyes is binding to nanocrystalline titanium dioxide ( $\text{TiO}_2$ ) [7, 9].

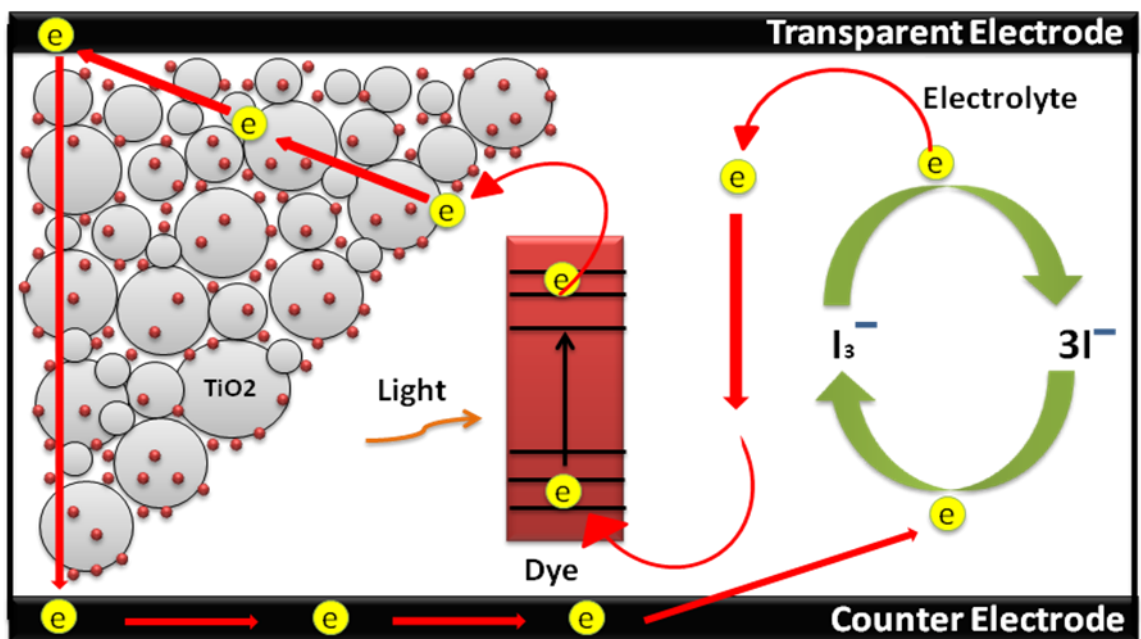


Figure 1. 6 A simple DSSCs

In general, the efficiencies of DSSCs cells even by using perylene dyes and its derivatives are lower than the silicon solar cells efficiencies. However, according to the ease of fabrication, band gap range, toxicity of materials and excellent absorption coefficients DSSCs are more valuable than silicon solar cells especially

for future research. Therefore, lots of efforts are spending to develop new perylene derivatives to increase the efficiencies [10].

In this research, two perylene derivatives perylene tetracarboxylic acid (PTCA) and chiral perlyene dicarboxylic acid carboximide (R-CPMI) were synthesized for solar cell applications (Figure 1.7–1.8). Perylene dianhydride (PDA) was also used for comparison. The synthesized compounds were characterized in detail by FTIR, UV-vis and fluorescence spectroscopy measurements. These compounds are potential dyes for DSSCs and therefore their binding properties to nanocrystalline TiO<sub>2</sub> will be investigated in future.

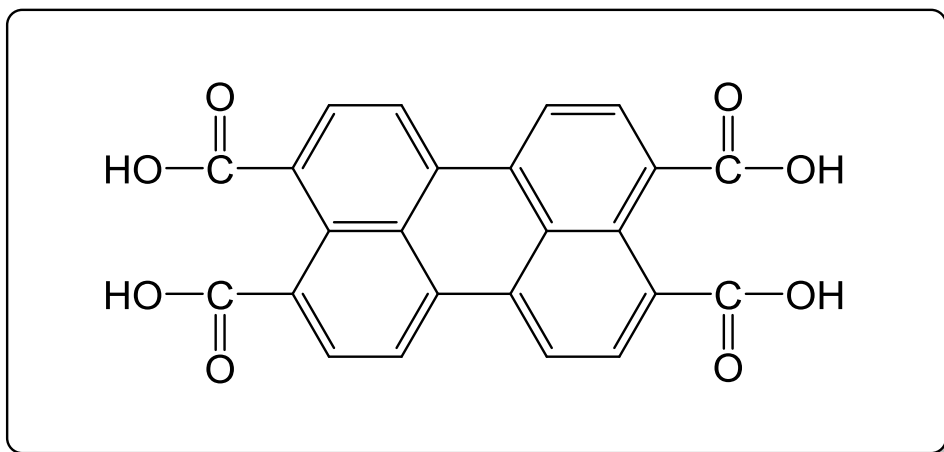


Figure 1. 7 PTCA

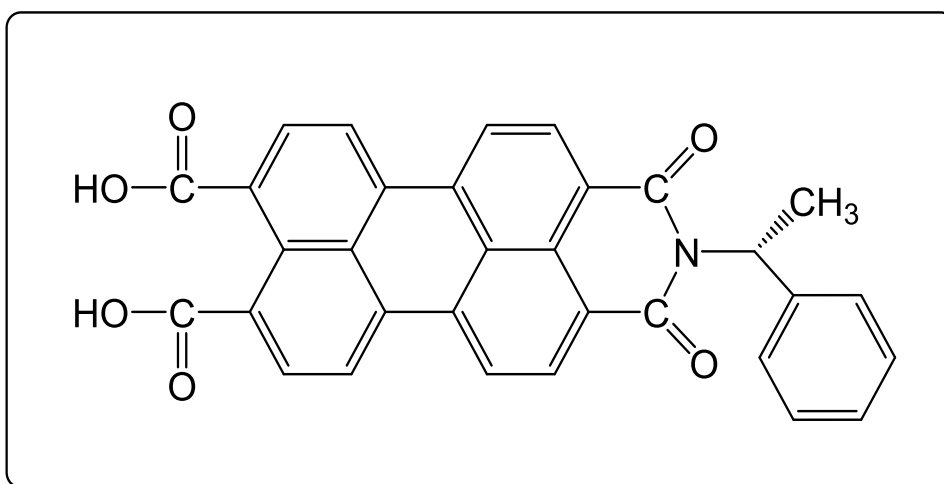


Figure 1. 8 R-CPMI

## Chapter 2

### THEORETICAL

#### 2.1 Properties of Perylene Monoimide and Diimide Dyes

Perylene family were considered as one of the most important pigments and dyes. In general, perylene derivatives exhibit a lot of interested characteristics such as electrochemical properties, photo and thermal stable, inexpensive, nontoxic dye and they have high fluorescence quantum yield and molar absorptivity. Perylene monoimides and diimides are some of perylene derivatives that belong to perylene family, therefore, they have a lot of properties that enable them to be used as important dyes with different efficiencies. On the other hand, the disadvantage of the perylene derivatives is their poor solubility in the common organic solvents [11-12].

##### 2.1.1 Optical Characteristics of Perylene Monoimide and Diimide Dyes

Perylenemonoimide (PMI) derivatives in thin films and in different solutions exhibit good optical properties such as high extinction coefficient and high fluorescence quantum yield [13, 14].

As shown in Figure 2.1 and 2.2, the perylenemonoimide (PMI) and diimide (PDI) dyes have similar absorption and emission spectra. The absorption range is in between 400-600 nm and emission range is in between 500-700 nm [15].

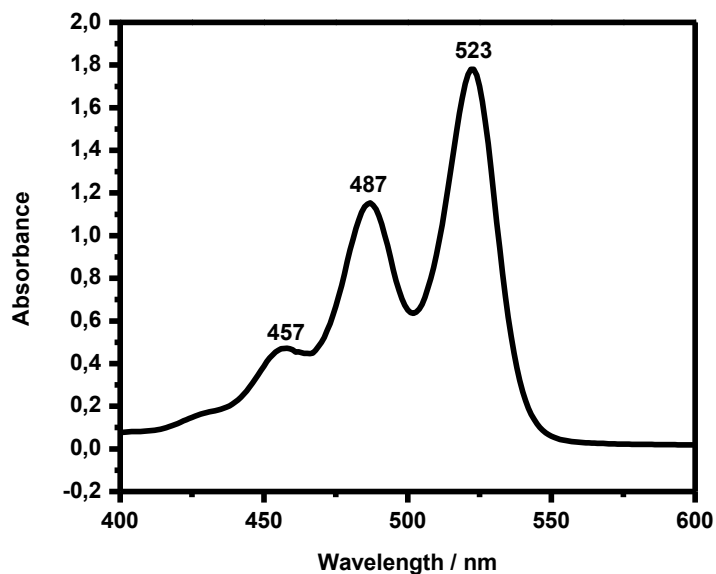


Figure 2. 1 Absorption spectrum of PDI

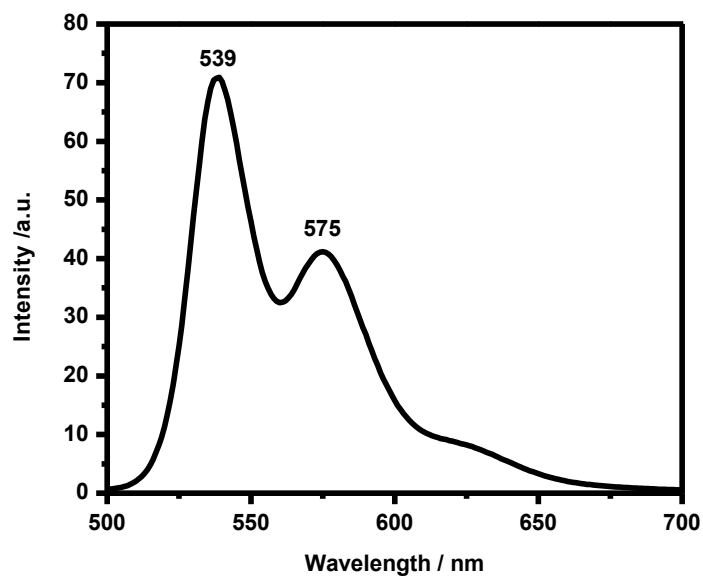


Figure 2. 2 Fluorescence Emission spectrum of PDI

The optical features of PMI derivatives can be affected by the position of the substituents. The effect of peri and bay functional groups were studied where, in general, the PMI with bay group substituents have higher  $\lambda_{\max}$  and molar absorptivity ( $\epsilon_{\max}$ ) than that have peri group substituents. The Figure 2.3 illustrate the structures of PMI with bay and peri substitutions positions [12, 16].

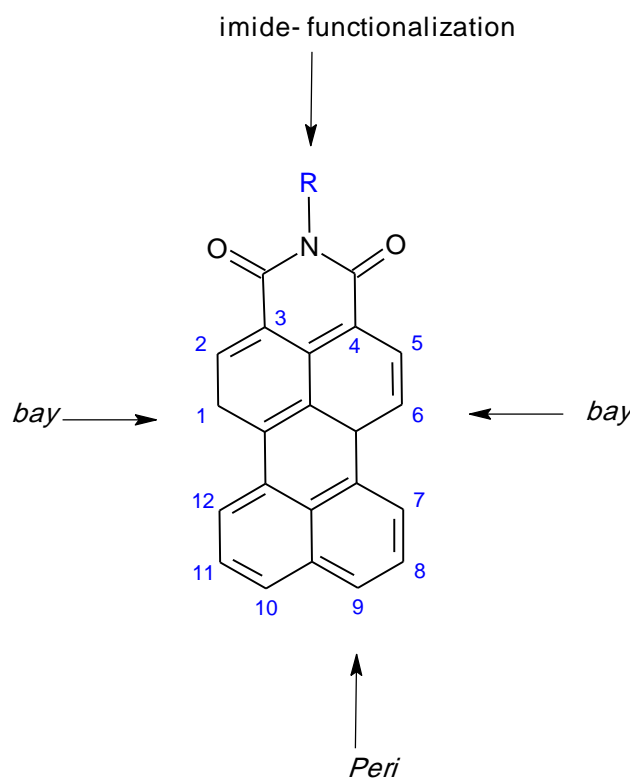


Figure 2. 3 The structures bay and peri substitutions positions at PMI [16].

Perylene diimides (PDI) derivatives also exhibit excellent optical features and thermal stability. PDI derivatives are attractive dyes because of their features of high molar absorptivity, high fluorescence quantum yield and photostability. They exhibit long singlet energy transfer life time. PDIs has absorbance in the visible range wavelength (400 – 600) nm and molar extinction coefficient about ( $\epsilon = 10^5 \text{ M}^{-1} \text{ cm}^{-1}$ ) [12, 17].

PMIs and PDIs also exhibit broad band absorption features in the NIR region. The advantages of absorption the wavelength in the NIR region will lead to enhancing the exothermic electron injection from the excited singlet state to the conduction band of  $\text{TiO}_2$  electrode [16].

### 2.1.2 Electron Acceptor Properties of Perylene Monoimide and Diimide Dyes for Photovoltaic Applications

In addition to the mentioned optical properties of perylene monoimide and diimide dyes, the electrochemical properties are another important property of the perylene derivatives. In general, perylene derivatives are well-known as n-type material with good electron acceptor feature. These properties in addition to the high thermal stability of PMIs and PDIs give them advantages for using in photovoltaic applications [16].

The imide group of PMIs can be used as electron acceptor. The presence of electron donating substituent group on different positions of the PMIs lead to build “push-pull” characters of PMIs. However, push-pull characters intramolecular charge transfer occurred because the  $\pi$ -conjugation via  $\pi$ -conducting bridge (D- $\pi$ -A) between the electron donor (D) and acceptor (A) [11].

The substituent positions of the PMIs can affect the intramolecular charge transfer. By comparing the intramolecular charge transfer of PMIs that have a functional group in the bay position with PMIs that have the same functional group in the peri-position, the intramolecular charge transfer of the bay position is higher [18]. Also, the attached donor substituent at PMIs can also affect the electron injection from the dye to the band gap of TiO<sub>2</sub> semiconductor [18].

One of the attractive properties of PDIs in solar cells applications is their high electron transport features than high energy conversion efficiency. The intramolecular charge transfer of PDIs is due to the mobility of electron through  $\pi$ - $\pi$  stacking. The presence of substituents in the bay position of PDI can easily tuning the HOMO and LUMO level of the PDIs. Therefore, the power conversion

efficiency increases due to the increasing of the light harvesting and the injections of electrons to the conducting band of TiO<sub>2</sub> [19].

Other parameter that affect on the mobility of the PDIs is the type of the PDIs attached electron donor functional group substituents [19-20]. Photoinduced electron transfer (PET) from various electron donating substituents at the bay region of PDIs shows that the electron mobility of sulfur containing substituents is relatively low according to its unsuitable packing in the films [19].

### **2.1.3 Binding Properties of Perylene Monoimide Dyes for Photovoltaic Applications**

The electron injection rate between the perylene dye and semiconductor nanoparticles surface can be affected by the binding strength between them. The binding strength depends on the number, position and type of anchoring groups. However, in general, the binding strength increases with increasing the number of anchoring groups [21].

Carboxylic acid usually selected as anchoring group according to its strength adsorption on the nanoparticles surface. The binding strength of perylene monoimide using carboxylic acid as anchoring group with various position at perylene core was studied. The results shows that the electron injection rate can be controlled by the carboxylic acid anchoring group positions [22]. Figure 2.4 shows binding of nanocrystalline TiO<sub>2</sub> with carboxylic acid group.

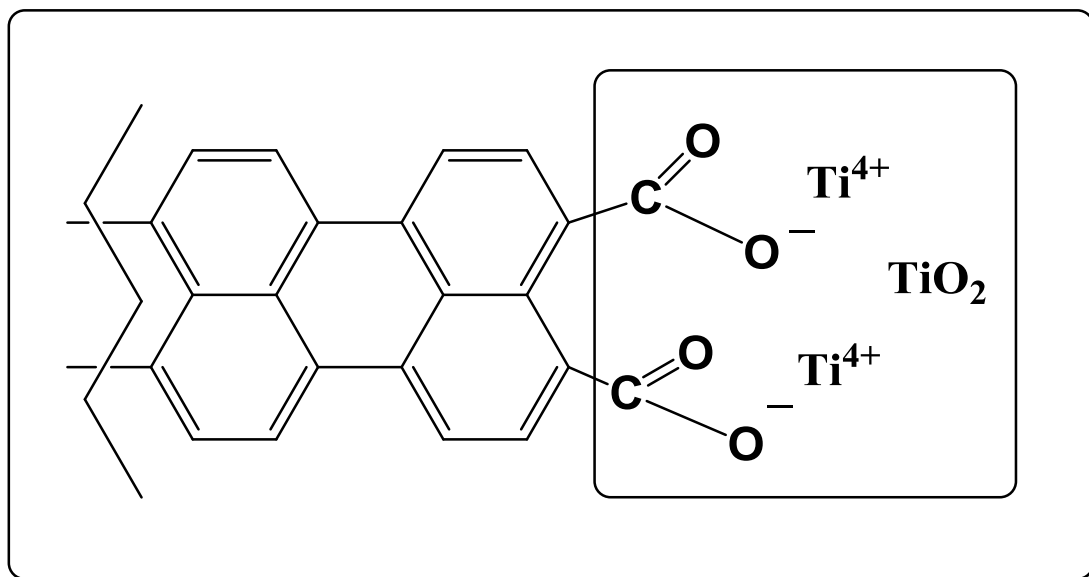


Figure 2. 4 Binding of nanocrystalline TiO<sub>2</sub> with Carboxylic acid group.

## 2.2 The Future and Commercialization of Dye Sensitized Solar Cells

Getting on the electric power from the sun is a cheap source, it is considered as a solution for a lot of problems including global warming and the concomitant problems. It is also a solution for the issue of limited fossil fuels such as oil [23].

The conversion of solar energy into the electrical form of energy is called photovoltaics. The next level of this conversion would be to convert the solar energy directly into some sort of chemical energy and this kind of artificial photosynthesis type of chemical conversion which is also very important and interesting for future. Today most of the solar energy panels for photovoltaics are based on silicon which is either single crystalline very high quality or multi crystalline or even amorphous type.

The new model of solar cells which goes in the direction of using organic materials, are in principle cheaper in production than that of the silicon crystalline form. On

the other hand, silicon is not safe environmentally and that's why it is very important to develop this type of solar cells. With the new model of solar cells, which is based on organic and hybrid types, larger area surfaces are coated easily and this reduce the prices and this is one of the state of art in today's research. Lots of efforts spend for the preparation of this new type organic semiconductor. Today, the best solar cells with organic hybrid systems are based on ideal titanium dioxide particles. The conversion efficiency of the organic hybrid solar cells is nowadays above 11% [24], this is of course less than silicon crystalline efficiency where it is about 47.5% [25]. Although, organic solar cell has lower efficiencies than silicone solar cells, the progress in organic solar cells has remarkable improvement in the last ten years and growing day by day. Therefore, this speed and good progress in organic solar cells will improve the efficiencies to 40% soon [26, 27].

There is a great challenge to design, develop and synthesize new organic materials. These organic materials would have environmental stability so that they can be used outside the buildings under very harsh circumstances like rain, heat, oxygen and dust. Another challenge for the organic hybrid solar cells is their long term stability.

In commercial studies, the greater issue is the chemical constancy. Organic materials that are used in solar cells applications have additional features compared to inorganic materials. First, the low cost of organic materials and also their easy fabrication than inorganic materials. Second, they are applicable on larger surfaces. Gaining flexibility to battery by using different organic materials allows it to increase its scope of application area. Furthermore, the synthesis of these organic materials with more superior attributes from various reagents and reactants is another most important part of the improvement of organic solar cells. Solar cells

with conjugated polymers are utilizing as organic material because it has a greater molar absorption coefficient compared to inorganic based cells [26].

## Chapter 3

### EXPERIMENTAL

#### 3.1 Materials

Perylene -3,4,9,10-tetracarboxylic dianhydride, potassium hydroxide, hydrochloric acid, isoquinoline, zinc acetate, (*R*)-(+)-1-phenylethylamine were obtained from Sigma-Aldrich. All the chemicals were used without further purifications. Some of the common organic solvents were distilled according to literature [28]. For the ultraviolet and emission spectroscopy measurements all the solvents used were in spectroscopic grade and were also obtained from Sigma-Aldrich.

#### 3.2 Instruments

##### Infrared Spectra

JASCO FT-IR spectrophotometer was used to record FTIR spectra by using KBr pellets.

##### Ultraviolet (UV-vis) Absorption Spectra

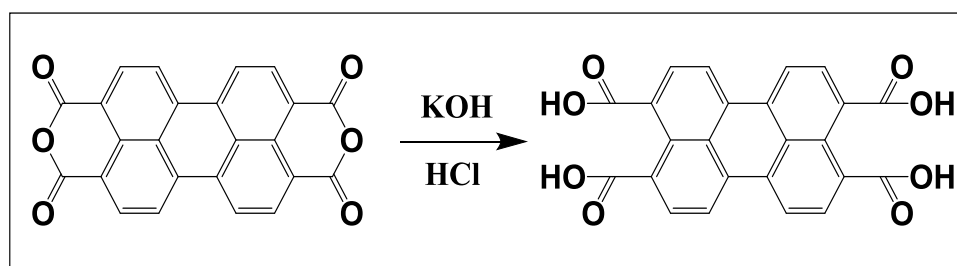
Varian Cary-100 spectrophotometer was used to record UV-vis absorption spectra in solutions.

##### Emission Spectra

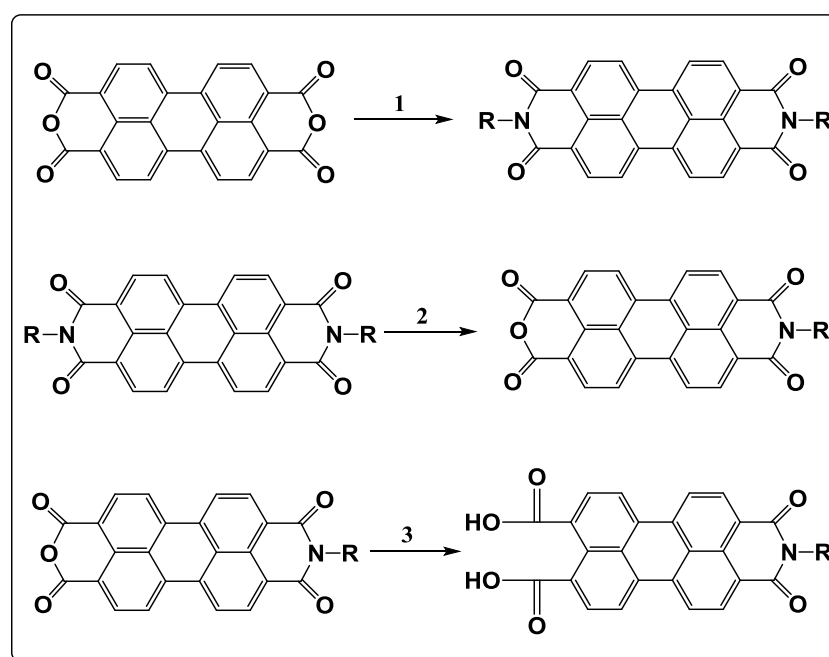
Emission spectra were measured by using a Varian Cary Eclipse Fluorescence spectrophotometer.

### 3.3 Methods of Synthesis

The aim of this study is to synthesize new perylene dyes for solar cells applications. The synthesized perylene derivatives were designed especially to have a potential for  $\text{TiO}_2$  binding. In this thesis, first of all perylene -3,4,9,10 tetracarboxylic acid (PTCA) was synthesized from commercially available perylene -3,4,9,10-tetracarboxylic dianhydride (PDA), as it is shown in Scheme 3.1. Secondly, chiral perylene dicarboxylic acid carboximide (R-CPMI) was synthesized in three step as shown in Scheme 3.2.

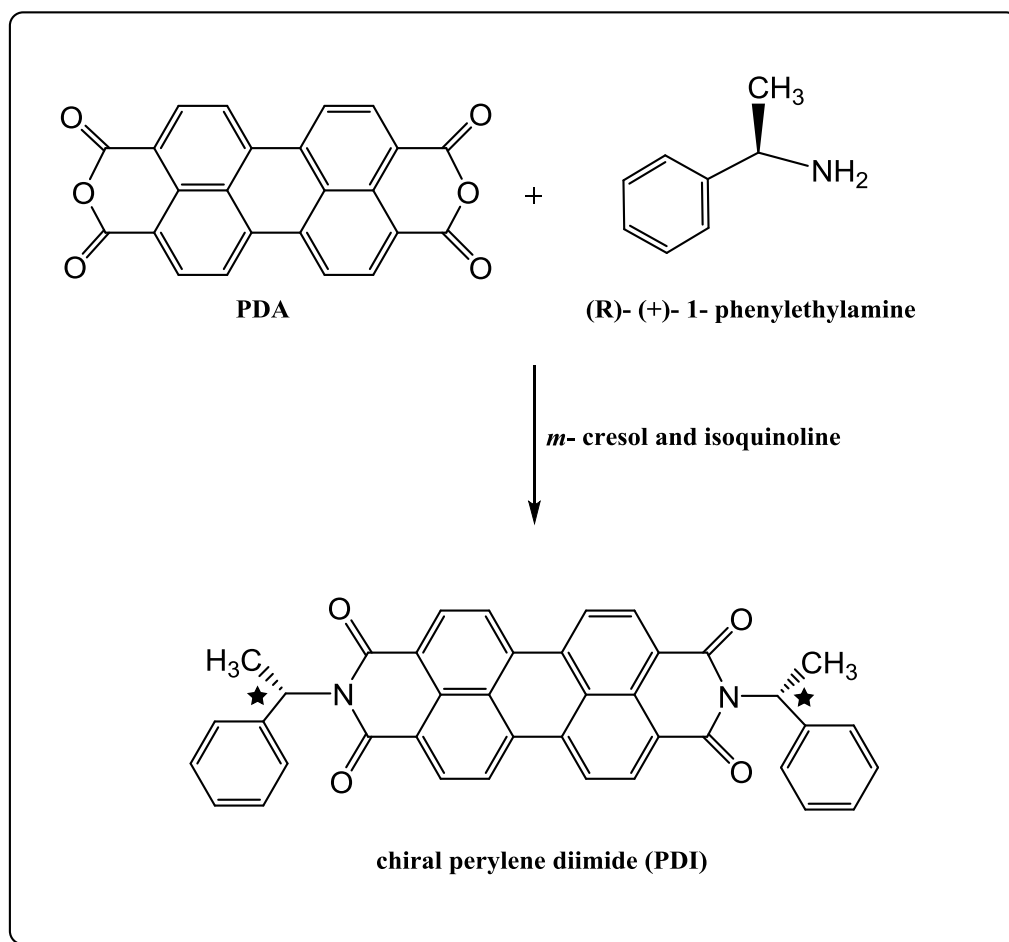


Scheme 3.1 Synthesis of perylene tetracarboxylic acid (PTCA).



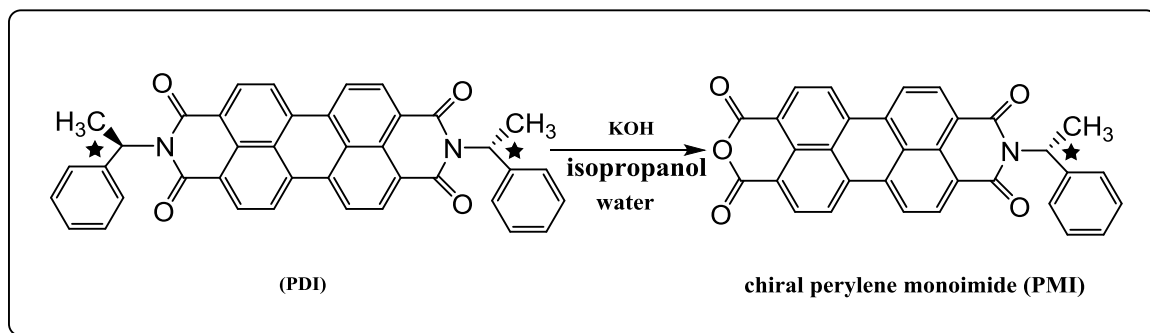
Scheme 3. 2 Synthetic route of chiral perylene dicarboxylic acid carboximide (R-CPMI).

As it is shown in Scheme 3.1, from the perylene dianhydride, perylene tetracarboxylic acid was synthesized in the presence of KOH [29]. As it is shown in Scheme 3.2, chiral perylene dicarboxylic acid carboximide (R-CPMI) was synthesized in three steps. In the first step, as shown in Scheme 3.3 a chiral PDI was synthesized in the presence of *m*-cresol and isoquinoline.



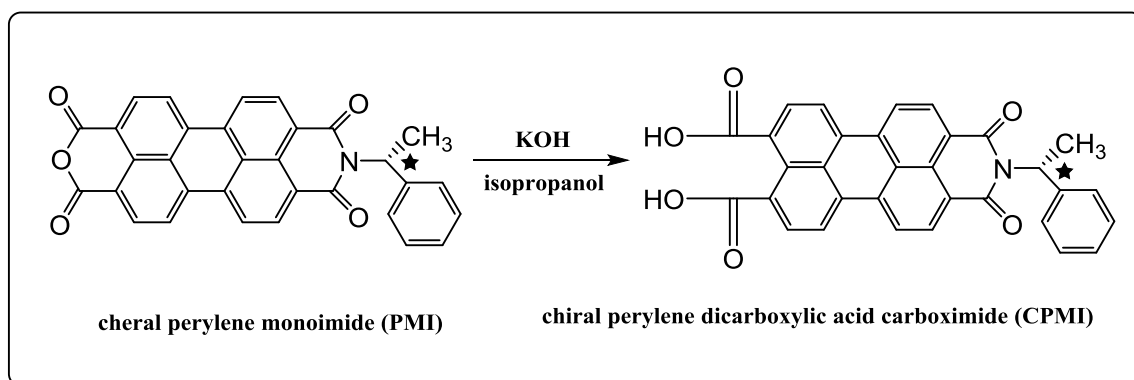
Scheme 3. 3 Synthesis of N,N'-bis((*R*)-(+)–1–phenylethyl)3,4,9,10-perylenenbis(dicarboximide) (PDI) [30].

In the second step, as it is shown in Scheme 3.4, in the presence of KOH, isopropanol and water, perylene monoimide (R-PMI) was synthesized from the synthesized PDI.



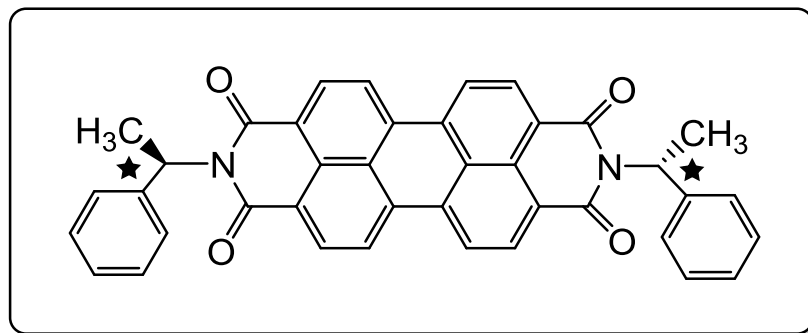
Scheme 3. 4 Synthesis of N-((*R*)-(+)–1–phenylethyl)-3,4,9,10-perylenetetracarboxylic-3,4-anhydride-9,10-imide (*R*-PMI).

As it is shown in Scheme 3.5, in the third step, in the presence of KOH and isopropanol chiral perylene dicarboxylic acid carboximide (*R*-CPMI) was synthesized from synthesized chiral perylene monoimide (*R*-PMI).



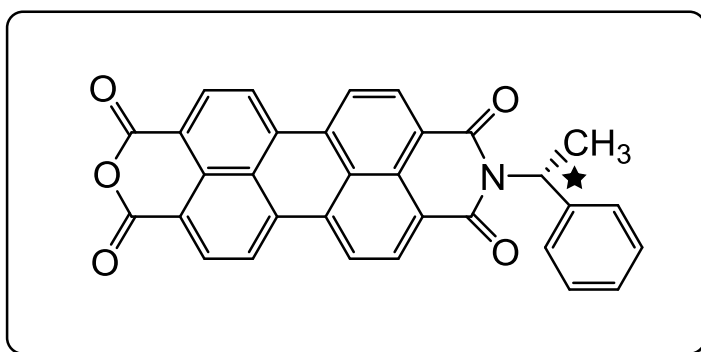
Scheme 3. 5 Synthesis of chiral perylene-3,4-dicarboxylic-9,10-(*R*)-(+)–1–phenylethyl)-carboximide (*R*-CPMI).

### 3.4 Synthesis of N, N' -bis ((R) – (+) – 1– phenylethyl) 3, 4, 9, 10- perylenenbis (dicarboximide) (PDI)



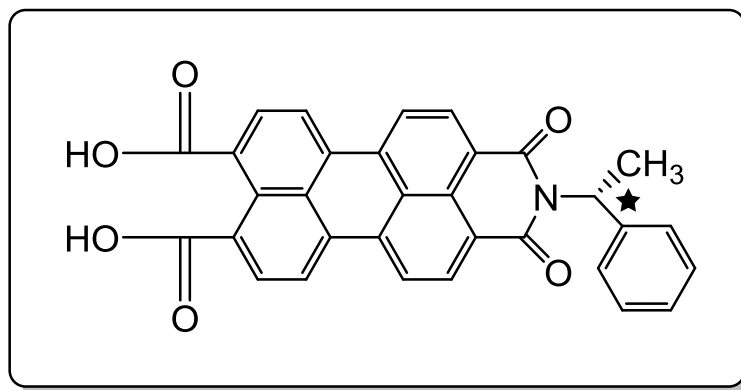
The chiral PDI was successfully synthesized and characterized according to the procedure reported in Ahmad H. MS thesis [10].

### 3.5 Synthesis of N- ((R) – (+) – 1 – phenylethyl) – 3 , 4 , 9 , 10 - perylenetetracarboxylic -3,4-anhydride-9,10-imide (R-PMI)



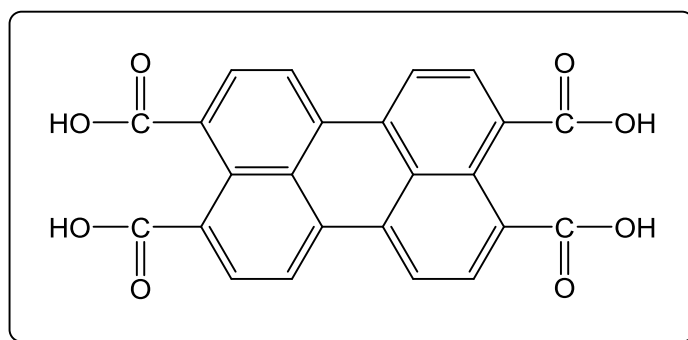
The chiral R-PMI was successfully synthesized and characterized according to the procedure reported in Ahmad H. MS thesis [10].

### 3.6 Synthesis of chiral perylene-3,4-dicarboxylic-9,10-(R)-(+)–1-phenylethyl)-carboximide (R-CPMI)



The chiral R-CPMI was successfully synthesized and characterized according to the procedure reported in Ahmad H. MS thesis [10].

### 3.7 Synthesis of perylene -3,4,9,10 tetracarboxylic acid (PTCA)



Perylene dianhydride (PDA) (1g, 2.5 mmol) was refluxed with 50 mL of a 5% aqueous solution of KOH by stirring for 12 h at 65 °C. After refluxed, the cold solution was acidified drop wise with 0.1 M of hydrochloric acid at room temperature until the pH was 4–5. At this pH, a red precipitate was formed and was filtered off to get the red powdered PTCA. The product was purified by soxhlet extraction with water and dried in vacuum oven for 24 hour at 100 °C.

**Yield:** 90 %.

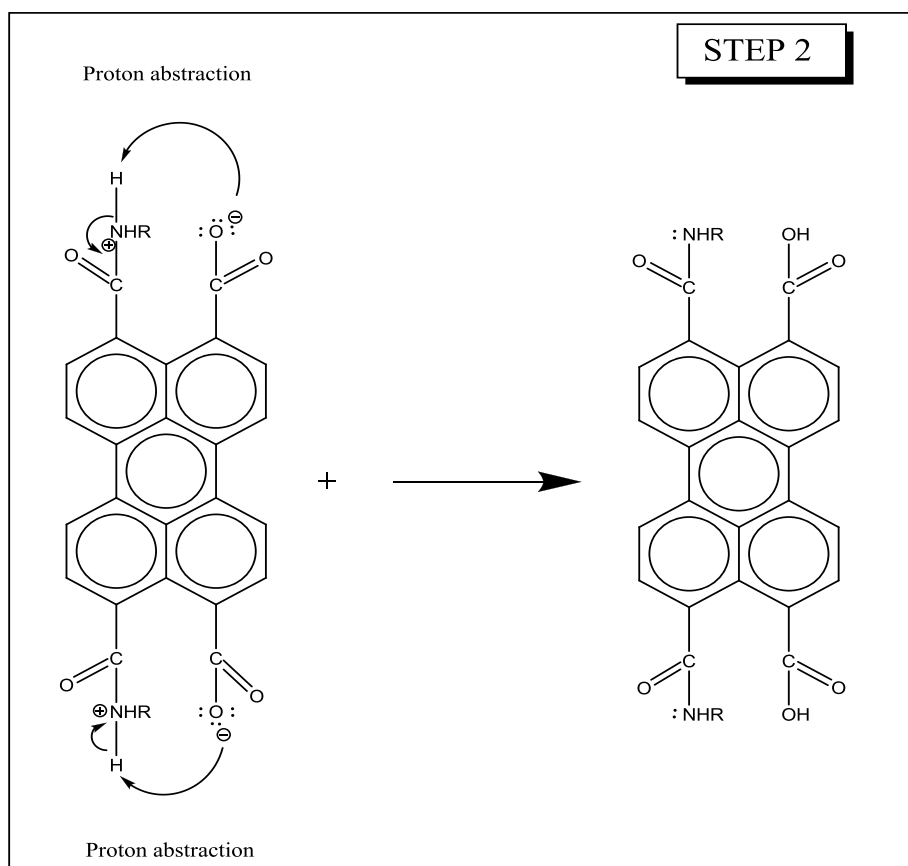
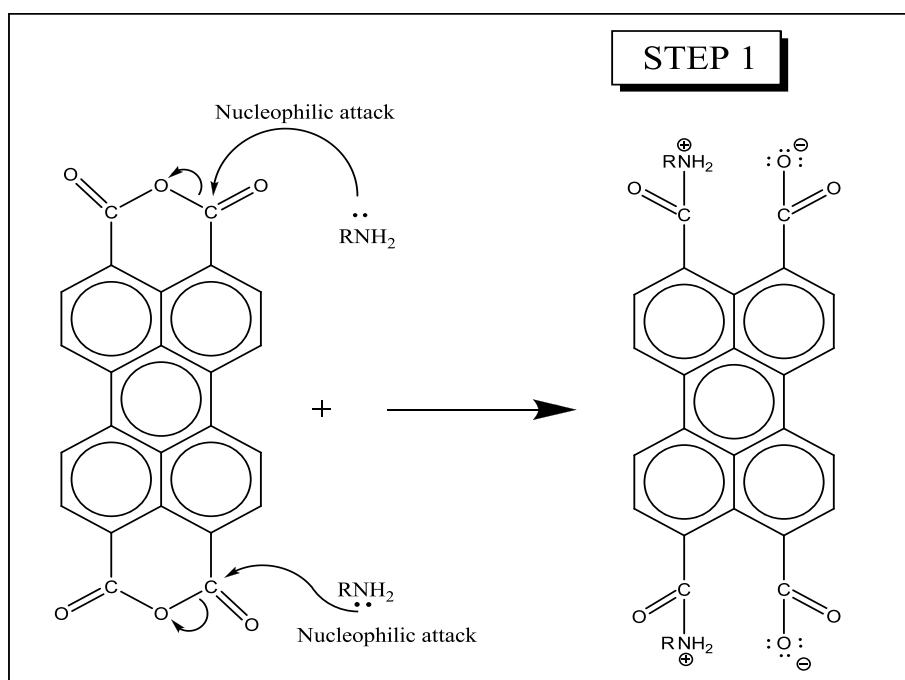
**Color:** Red

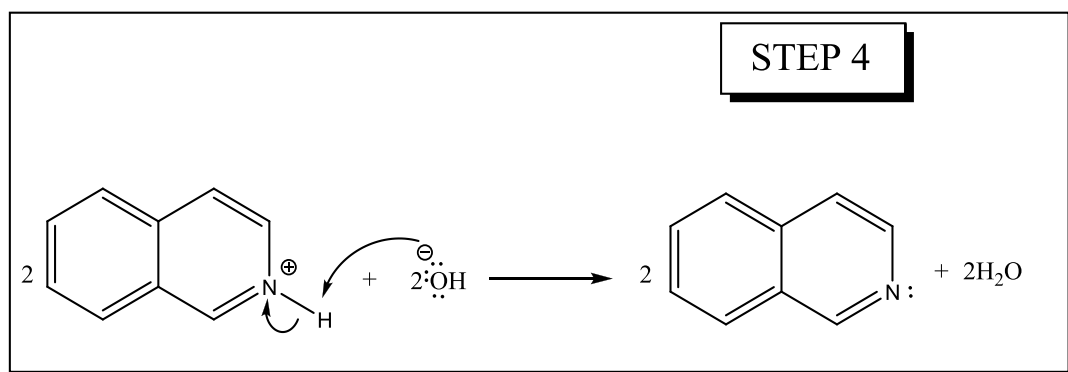
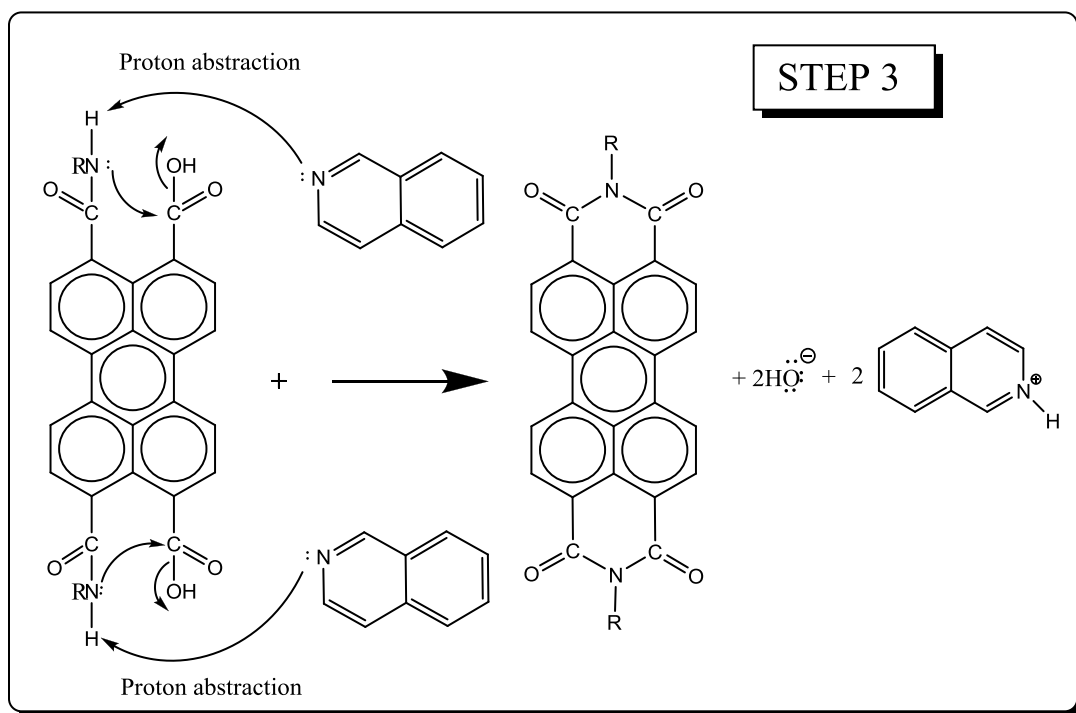
**FT-IR: (KBr,  $\text{cm}^{-1}$ ):**  $\nu = 3440, 3114, 2924, 1777, 1596, 1403, 1297, 1013, 734$ .

**UV-vis (DMSO) ( $\lambda_{\text{max}}$  / nm; ( $\epsilon_{\text{max}}$  /  $\text{L}\cdot\text{mol}^{-1}\cdot\text{cm}^{-1}$ ):** 483, 516, 557(51000)

**Fluorescence (DMSO) ( $\lambda_{\text{max}}$  / nm):** 535, 575, 625

### 3.8 General Reaction Mechanism of Perylene Dyes





## Chapter 4

### DATA AND CALCULATIONS

#### 4.1 Calculations of Fluorescence Quantum Yield ( $\Phi_f$ )

The fluorescence quantum yield is the ratio of absorbed photons to emitted photons through fluorescence and formulated as:

$$\Phi = \frac{\text{number of moles of product formed}}{\text{number of photons of radiation absorbed}}$$

Fluorescence quantum yield is an important parameter to indicate the properties of a molecule if it emits all the absorbed light or if it deactivates the absorbed light by heat. Williams et al. method is one of the well known comparative methods that is used in order to calculate  $\Phi_f$  of a compound by using well standard samples that are characterized and its  $\Phi_f$  is known [31]. It is considered that, at the same excitation wavelength, both the test and standard compounds solutions have absorbed equal number of photons. The ratio of integrated fluorescence intensities of the two solutions of compounds gives the quantum yield value. The unknown compound  $\Phi_f$  value is calculated by using the given equation below and a standard compound that its  $\Phi_f$  is known.

$$\Phi_f = \frac{A_{std}}{A_u} \times \frac{S_u}{S_{std}} \times \left[ \frac{n_u}{n_{std}} \right]^2 \times \Phi_{std}$$

- $\Phi_f$ : Fluorescence quantum yield of unknown
- $A_{std}$ : Absorbance of the reference at the excitation wavelength
- $A_u$ : Absorbance of the unknown at the excitation wavelength
- $S_{std}$ : The integrated emission area across the band of reference
- $S_u$ : The integrated emission area across the band of unknown
- $n_{std}$ : Refractive index of reference solvent
- $n_u$ : Refractive index of unknown solvent
- $\Phi_{std}$ : Fluorescence quantum yield of reference. [31, 32]

The fluorescence quantum yields of the synthesized perylene dyes were calculated by using the N,N'-bis(dodecyl)-3,4,9,10-perylenebis(discarboximide) as reference compound and its  $\Phi_f = 1$  in chloroform [32]. All the perylene dyes including the reference that used in the  $\Phi_f$  calculations were excited at the wavelength,  $\lambda_{exc} = 485$  nm.

#### **$\Phi_f$ calculation of PTCA in DMSO**

The reference is N,N'-bis(dodecyl)-3,4,9,10-perylenebis(discarboximide) [32].

$$\Phi_{std} = 1 \text{ in chloroform}$$

$$A_{std} = 0.1055$$

$$A_u = 0.0998$$

$$S_u = 2085.85$$

$$S_{std} = 4129.22$$

$$\Phi_f = \frac{0.1055}{0.0998} \times \frac{2085.85}{4129.22} \times \left[ \frac{1.479}{1.446} \right]^2 \times 1$$

$$\Phi_f = 0.56$$

Table 4.1 shows the fluorescence quantum yield of the synthesized PTCA and R-CPMI.

**Table 4.1 Fluorescence Quantum Yields of PTCA and R-CPMI**

<b>Compound</b>	<b>Solvent</b>	$\Phi_f$
<b>PTCA</b>	DMSO	0.56
<b>R-CPMI</b>	DMSO	0.74
<b>R-CPMI</b>	MeOH	0.24
<b>R-CPMI</b>	CHL	0.32

## **4.2 Calculations of Maximum Extinction Co-efficients ( $\epsilon_{\max}$ )**

Beer-Lambert law was applied to calculate the Extinction co-efficients ( $\epsilon_{\max}$ ) for PTCA, PDA and R-CPMI.

The formula of Beer-lambert law is described as shown bellow.

$$\epsilon_{\max} = \frac{A}{c l}$$

Where

$\epsilon_{\max}$ : Maximum extinction co-efficient in  $L.mol^{-1}.cm^{-1}$  at  $\lambda_{\max}$

**A:** Absorbance

**c:** Concentration in  $mol.L^{-1}$

**l:** path length in cm

The calculation of PTCA

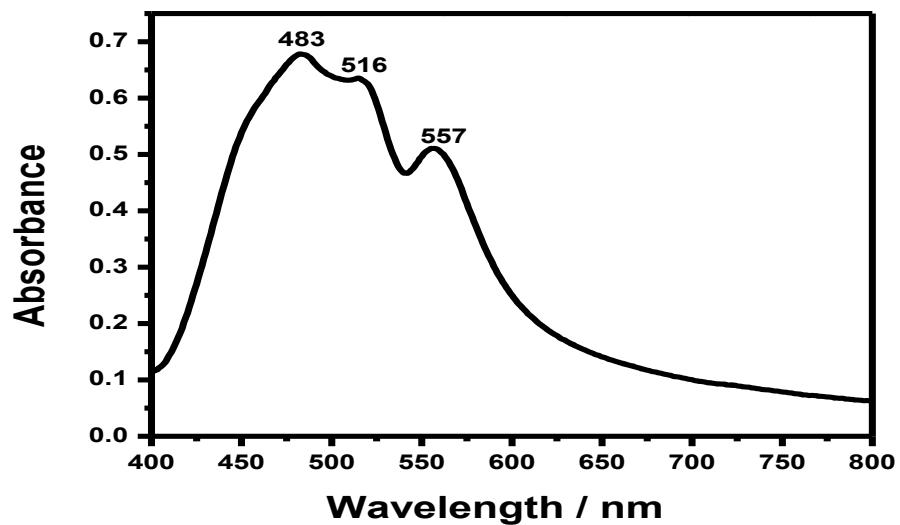


Figure 4. 1 Absorption spectrum of PTCA in DMSO at concentration of  $1 \times 10^{-5}$  M.

According to Figure 4.1, the absorbance is 0.51 at concentration of  $1 \times 10^{-5}$  M at  $\lambda_{\max}$  = 557 nm.

$$\epsilon_{\max} = \frac{0.51}{1 \times 10^{-5} \text{ M} \times 1 \text{ cm}} = 51000 \text{ L. mol}^{-1} \cdot \text{cm}^{-1}$$

$$\epsilon_{\max} \text{ for PTCA} = 51000 \text{ L. mol}^{-1} \cdot \text{cm}^{-1}$$

Table 4.2 shows the calculated molar absorptivities of all the compounds

Table 4.2. Molar absorptivities of PTCA, PDA and R-CPMI

Compound	Solvent	Conc. (M)	A	$\lambda_{\max}$ (nm)	$\epsilon_{\max}$ ( $M^{-1} cm^{-1}$ )
PTCA	DMSO	$1 \times 10^{-5}$	0.51	557	51000
PTCA	DMSO	$1 \times 10^{-5}$	0.64	516	64000
PTCA	DMF	$1 \times 10^{-5}$	0.66	559	66000
PTCA	DMF	$1 \times 10^{-5}$	0.80	514	80000
PDA	DMSO	$1 \times 10^{-5}$	0.61	587	61000
PDA	DMSO	$1 \times 10^{-5}$	0.57	522	57000
PDA	DMF	$1 \times 10^{-5}$	0.19	588	19000
PDA	DMF	$1 \times 10^{-5}$	0.21	517	21000
R-CPMI	DMSO	$1 \times 10^{-5}$	1	525	100000
R-CPMI	DMF	$1 \times 10^{-5}$	1.14	522	114000

### 4.3 Calculations of Half-width of the Selected Absorption ( $\Delta\bar{\nu}_{1/2}$ )

The full width at half width maximum is called half-width maximum of selected wavelength.

The formula that used for the calculation  $\Delta\bar{\nu}_{1/2}$  is given bellow.

$$\Delta\bar{\nu}_{1/2} = \bar{\nu}_1 - \bar{\nu}_2$$

Where

$\bar{\nu}_1$  and  $\bar{\nu}_2$  : the frequencies from the absorption spectrum in  $cm^{-1}$

$\Delta\bar{\nu}_{1/2}$  : the half-width of the selected maximum absorption in  $cm^{-1}$

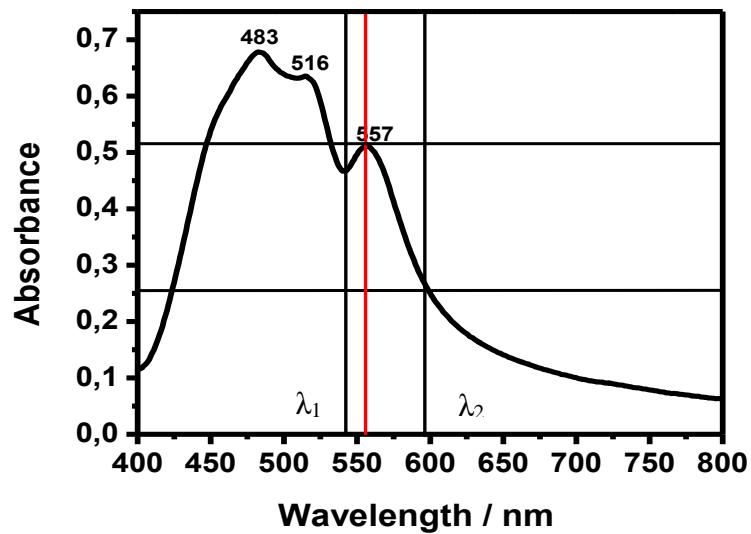


Figure 4. 2 Absorption spectrum of PTCA in DMSO and half-width representation

According to Figure 4.2;

$$\lambda_{\max} = 557 \text{ nm}$$

$$\text{half-width absorption} = 0.255$$

$$\lambda_1 = 541.44 \text{ nm}$$

$$\lambda_2 = 596.35 \text{ nm}$$

$$\lambda_1 = 541.44 \text{ nm} \times \frac{10^{-9} \text{ m}}{1 \text{ nm}} \times \frac{1 \text{ cm}}{10^{-2} \text{ m}} = 5.4144 \times 10^{-5} \text{ cm}$$

$$\bar{\nu}_1 = \frac{1}{5.4144 \times 10^{-5} \text{ cm}} = 18469.27 \text{ cm}^{-1}$$

$$\lambda_2 = 596.35 \text{ nm} \times \frac{10^{-9} \text{ m}}{1 \text{ nm}} \times \frac{1 \text{ cm}}{10^{-9} \text{ m}} = 5.9635 \times 10^{-5} \text{ cm}$$

$$\bar{\nu}_2 = \frac{1}{5.9635 \times 10^{-5} \text{ cm}} = 16768.68 \text{ cm}^{-1}$$

$$\Delta\bar{\nu}_{1/2} = \bar{\nu}_1 - \bar{\nu}_2 = 18469.27 \text{ cm}^{-1} - 16768.68 \text{ cm}^{-1} = 1700.59 \text{ cm}^{-1}$$

In order to calculate the theoretical radiative lifetimes of the synthesized compounds, it is necessary to determine the half-widths of the compounds. As it is shown above, the half-widths were calculated for PDA and R-CPMI. All the results were listed in Table 4.2 as show bellow.

Table 4.3 Half-widths of the selected absorptions of compounds PTCA, PDA and R-CPMI

<b>Compound</b>	<b>Solvent</b>	$\lambda_{\max}$ (nm)	$\lambda_1$ (nm)	$\lambda_2$ (nm)	$\bar{\nu}_{1/2}$ (cm <sup>-1</sup> )
<b>PTCA</b>	DMSO	557	541.44	596.35	1700.59
<b>PTCA</b>	DMSO	516	508.04	554.95	1663.84
<b>PTCA</b>	DMF	559	541.44	605.06	1941.98
<b>PTCA</b>	DMF	514	501.82	556.55	1720.48
<b>PDA</b>	DMSO	587	545.35	754.33	5080.05
<b>PDA</b>	DMSO	522	494.53	625.67	4238.36
<b>PDA</b>	DMF	588	545.53	763.92	5240.42
<b>PDA</b>	DMF	517	496.13	566.14	2492.53
<b>R-CPMI</b>	DMSO	525	504.93	535.93	1145.57
<b>R-CPMI</b>	DMF	522	501.73	532.29	1130.74

#### 4.4 Calculations of Theoretical Radiative Lifetimes ( $\tau_0$ )

The theoretical radiative lifetime is calculated by using the equation shown below. It is postulated that in the absence of nonradiative transition the theoretical lifetime of an excited molecule can be calculated as [33].

$$\tau_0 = \frac{3.5 \times 10^8}{\bar{\nu}_{\max}^2 \times \epsilon_{\max} \times \Delta\bar{\nu}_{1/2}}$$

Where

$\tau_0$ : Theoretical radiative lifetime in ns

$\bar{\nu}_{\max}$ : Mean frequency of the maximum absorption band in  $\text{cm}^{-1}$

$\epsilon_{\max}$ : The maximum extinction co-efficient in  $\text{L. mol}^{-1} \text{cm}^{-1}$  at the maximum absorption wavelength,  $\lambda_{\max}$

$\Delta\bar{\nu}_{1/2}$ : Half-width of the selected absorption in units of  $\text{cm}^{-1}$

##### Theoretical Radiative Lifetime of PTCA:

From Figure 4.2 and 4.3,

$$\lambda_{\max} = 557 \text{ nm}$$

$$\lambda_{\max} = 557 \text{ nm} \times \frac{10^{-9} \text{ m}}{1 \text{ nm}} \times \frac{1 \text{ cm}}{10^{-2} \text{ m}} = 5.57 \times 10^{-5} \text{ cm}$$

$$\bar{\nu}_{\max} = \frac{1}{5.57 \times 10^{-5} \text{ cm}} = 17953.32 \text{ cm}^{-1}$$

$$\bar{\nu}_{\max}^2 = (17953.32 \text{ cm}^{-1})^2 = 3.22 \times 10^8 \text{ cm}^{-2}$$

The theoretical radiative lifetime;

$$\tau_0 = \frac{3.5 \times 10^8}{\bar{\nu}_{\max}^2 \times \epsilon_{\max} \times \Delta\bar{\nu}_{1/2}} = \frac{3.5 \times 10^8}{3.22 \times 10^8 \times 51000 \times 1700.59}$$

$$\tau_0 = 1.25 \times 10^{-8} \text{ s}$$

$$\tau_0 = 1.25 \text{ ns}$$

The theoretical radiative lifetimes of all the synthesized compounds PTCA, PDA and R-CMPI were calculated by using the same way and all the results were listed in Table 4.4.

Table 4.4 Theoretical radiative lifetimes of compounds PTCA, PDA and R-CMPI

Compound	Solvent	$\lambda_{\max}$ (nm)	$\epsilon_{\max}$ ( $\text{M}^{-1} \text{cm}^{-1}$ )	$(\nu_{\max}^2)$ $\text{cm}^{-2}$	$\Delta\nu_{1/2}$ ( $\text{cm}^{-1}$ )	$\tau_0$ (s)
PTCA	DMSO	557	51000	$3.22 \times 10^8$	1700.59	$1.25 \times 10^{-8}$
PTCA	DMSO	516	64000	$3.75 \times 10^8$	1663.84	$8.77 \times 10^{-9}$
PTCA	DMF	559	66000	$3.20 \times 10^8$	1941.98	$8.54 \times 10^{-9}$
PTCA	DMF	514	97000	$3.78 \times 10^8$	1959.63	$6.73 \times 10^{-9}$
PDA	DMSO	587	61000	$2.89 \times 10^8$	5080.05	$3.90 \times 10^{-9}$
PDA	DMSO	522	57000	$3.67 \times 10^8$	4238.36	$3.10 \times 10^{-9}$
PDA	DMF	588	19000	$2.89 \times 10^8$	5240.42	$1.21 \times 10^{-8}$
PDA	DMF	517	21000	$3.74 \times 10^8$	2492.53	$1.79 \times 10^{-8}$
R-CMPI	DMSO	525	100000	$3.63 \times 10^8$	1145.57	$8.41 \times 10^{-9}$
R-CMPI	DMF	522	114000	$3.67 \times 10^8$	1271.88	$7.40 \times 10^{-9}$

#### 4.5 Calculation of Theoretical Fluorescence Lifetime ( $\tau_f$ )

The average time that a molecule stays in the excited state before fluorescence is called fluorescence lifetime. Below equation is used to calculate the theoretical fluorescence lifetimes in nanosecond [33].

$$\tau_f = \tau_0 \cdot \Phi_f$$

$\tau_0$ : Theoretical radiative lifetime in nano seconds

$\Phi_f$ : Fluorescence quantum yield

##### Theoretical fluorescence lifetime calculation of PTCA in DMSO:

$$\tau_f = \tau_0 \cdot \Phi_f$$

$$\tau_f = 8.77 \text{ ns} \times 0.56 = 4.91 \text{ ns}$$

Table 4.5 shows the theoretical fluorescence lifetime ( $\tau_f$ ) that was calculated for the synthesized compounds in different solvents.

Table 4.5 Theoretical Fluorescence Lifetimes ( $\tau_f$ ) of PTCA and R-CPMI in different solvents.

Compound	Solvent	$\Phi_f$	$\tau_0$ (ns)	$\tau_f$ (ns)
PTCA	DMSO	0.56	8.77	4.91
R-CPMI	DMSO	0.74	8.41	6.22

## 4.6 Calculations of Fluorescence Rate Constants ( $k_f$ )

The theoretical fluorescence rate constant for PTCA, PDA and R-CPMI are calculated from the given equation:

$$k_f = \frac{1}{\tau_0}$$

Where

$k_f$ : fluorescence rate constant in  $s^{-1}$

$\tau_0$ : theoretical radiative lifetime in s

**Fluorescence Rate Constant for PTCA in DMSO at  $\lambda_{\max} = 557\text{nm}$ :**

$$k_f = \frac{1}{1.25 \times 10^{-9}} = 8.0 \times 10^7 \text{ s}^{-1}$$

The theoretical fluorescence rate constant of all the synthesized compounds PTCA, PDA and R-CMPI were calculated by using the same equation and all the results were listed in Table 4.6.

Table 4.6 Theoretical fluorescence rate constant of compounds PTCA, PDA and R-CPMI

Compound	Solvent	$\lambda_{\max}$ (nm)	$\tau_0$ (s)	$k_f$ (s <sup>-1</sup> )
PTCA	DMSO	557	$1.25 \times 10^{-8}$	$8.0 \times 10^7$
PTCA	DMSO	516	$8.77 \times 10^{-9}$	$11.4 \times 10^7$
PTCA	DMF	559	$8.54 \times 10^{-9}$	$11.7 \times 10^7$
PTCA	DMF	514	$6.73 \times 10^{-9}$	$14.8 \times 10^7$
PDA	DMSO	587	$3.90 \times 10^{-9}$	$25.6 \times 10^7$
PDA	DMSO	522	$3.10 \times 10^{-9}$	$32.3 \times 10^7$
PDA	DMF	588	$1.21 \times 10^{-8}$	$8.26 \times 10^7$
PDA	DMF	517	$1.79 \times 10^{-8}$	$5.59 \times 10^7$
R-CPMI	DMSO	525	$8.41 \times 10^{-9}$	$11.9 \times 10^7$
R-CPMI	DMF	522	$7.40 \times 10^{-9}$	$13.5 \times 10^7$

#### 4.7 Calculations of Oscillator Strengths ( $f$ )

The strength of an electronic transition is expressed as oscillator strength which is a dimensionless quantity. The oscillator strength is calculated from the given formula

$$f = 4.32 \times 10^{-9} \Delta\bar{\nu}_{1/2} \epsilon_{\max}$$

Where

$f$ : Oscillator strength

$\Delta\bar{\nu}_{1/2}$ : Half-width of the selected absorption in units of cm<sup>-1</sup>

$\epsilon_{\max}$ : Maximum extinction co-efficient in L.mol<sup>-1</sup> . cm<sup>-1</sup> at  $\lambda_{\max}$

**Oscillator strength of PTCA in DMSO at  $\lambda_{\max} = 557$  nm**

$$f = 4.32 \times 10^{-9} \Delta\bar{\nu}_{1/2} \epsilon_{\max}$$

$$f = 4.32 \times 10^{-9} \times 1700.59 \times 51000$$

$$f = 0.37$$

The calculated oscillator strengths of the synthesized perylene derivatives PTCA, PDA and R-CPMI listed in Table 4.7.

Table 4.7 Oscillator strengths of the PTCA, PDA and R-CPMI

<b>Compound</b>	<b>Solvent</b>	$\lambda_{\max}$ (nm)	$\bar{\nu}_{1/2}$ ( $\text{cm}^{-1}$ )	$\epsilon_{\max}$ ( $\text{M}^{-1} \text{cm}^{-1}$ )	$f$
<b>PTCA</b>	DMSO	557	1700.59	51000	0.37
<b>PTCA</b>	DMSO	516	1663.84	64000	0.46
<b>PTCA</b>	DMF	559	1941.98	66000	0.55
<b>PTCA</b>	DMF	514	1959.63	80000	0.59
<b>PDA</b>	DMSO	587	5080.05	61000	1.34
<b>PDA</b>	DMSO	522	4238.36	57000	1.04
<b>PDA</b>	DMF	588	5240.42	19000	0.43
<b>PDA</b>	DMF	517	2492.53	21000	0.23
<b>R-CPMI</b>	DMSO	525	1145.57	100000	0.49
<b>R-CPMI</b>	DMF	522	1271.88	114000	0.56

## 4.8 Calculations of Singlet Energies ( $E_s$ )

The amount of energy necessary for an electronic transition from ground state to excited state is called singlet energy. Singlet energy is calculated from the given formula

$$E_s = \frac{2.86 \times 10^5}{\lambda_{\max}}$$

Where

$E_s$  : Singlet energy in kcal mol<sup>-1</sup>

$\lambda_{\max}$  : The maximum absorption wavelength in Å

**Singlet energy for PTCA in DMSO at  $\lambda_{\max} = 557$  nm:**

$$E_s = \frac{2.86 \times 10^5}{\lambda_{\max}} = \frac{2.86 \times 10^5}{5570} = 51.3 \text{ kcal mol}^{-1}$$

The singlet energies of the synthesized perylene derivatives PTCA, PDA and R-CPMI listed in Table 4.8.

Table 4. 8 The singlet energies of PTCA, PDA and R-CPMI

Compound	Solvent	$\lambda_{\text{max}}$ (Å)	$E_s$ (kcal mol <sup>-1</sup> )
PTCA	DMSO	5570	51.3
PTCA	DMSO	5160	55.4
PTCA	DMF	5590	51.2
PTCA	DMF	5140	55.6
PDA	DMSO	5870	48.7
PDA	DMSO	5220	54.8
PDA	DMF	5880	48.6
PDA	DMF	5170	55.3
R-CPMI	DMSO	5250	54.5
R-CPMI	DMF	5220	54.8

#### 4.9 Calculations of Optical Band Gap Energies ( $E_g$ )

HOMO and LUMO energy levels are very important parameters especially for solar cell applications. Band gap energy provides important information about HOMO and LUMO energy levels. It can be calculated by using below equation.

$$E_g = \frac{1240 \text{ eV nm}}{\lambda}$$

Where

$E_g$  : Band gap energy in eV

$\lambda$  : Cut-off wavelength of the absorption band gap in nm

### Band gap energy for PTCA in DMSO:

As shown in Figure 4.3, the cut-off wavelength of the absorption band is obtained by extrapolating the maximum absorption band to zero absorbance.

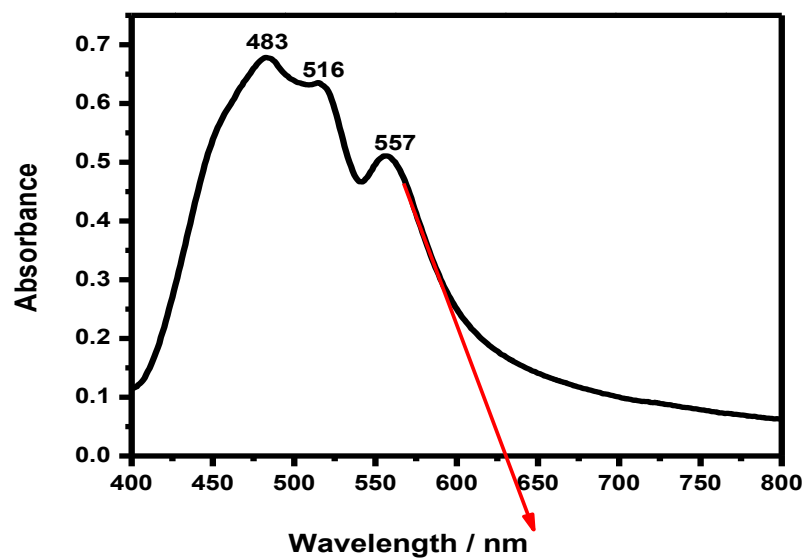


Figure 4. 3 Absorption spectrum of PTCA in DMSO and the cut-off wavelength

$$E_g = \frac{1240 \text{ eV}}{\lambda} = \frac{1240 \text{ eV}}{630.30} = 1.97 \text{ eV}$$

The bang gap energies of all the compounds PTCA, PDA and R-CPMI were calculated by using the same equation and listed in Table 4.7.

Table 4.9 Band gap energies of PTCA, PDA and R-CPMI

<b>Compound</b>	<b>Solvent</b>	<b><math>\lambda_{\max}</math> (nm)</b>	<b>Cut-off <math>\lambda</math> (nm)</b>	<b><math>E_g</math> (eV)</b>
<b>PTCA</b>	DMSO	557	630.30	1.97
<b>PTCA</b>	DMSO	516	592.27	2.09
<b>PTCA</b>	DMF	559	643.27	1.93
<b>PTCA</b>	DMF	514	589.78	2.10
<b>PDA</b>	DMSO	587	835.36	1.52
<b>PDA</b>	DMSO	522	672.59	1.68
<b>PDA</b>	DMF	588	823.81	1.50
<b>PDA</b>	DMF	517	857.30	2.14
<b>R-CPMI</b>	DMSO	525	548.56	2.26
<b>R-CPMI</b>	DMF	522	542.34	2.29

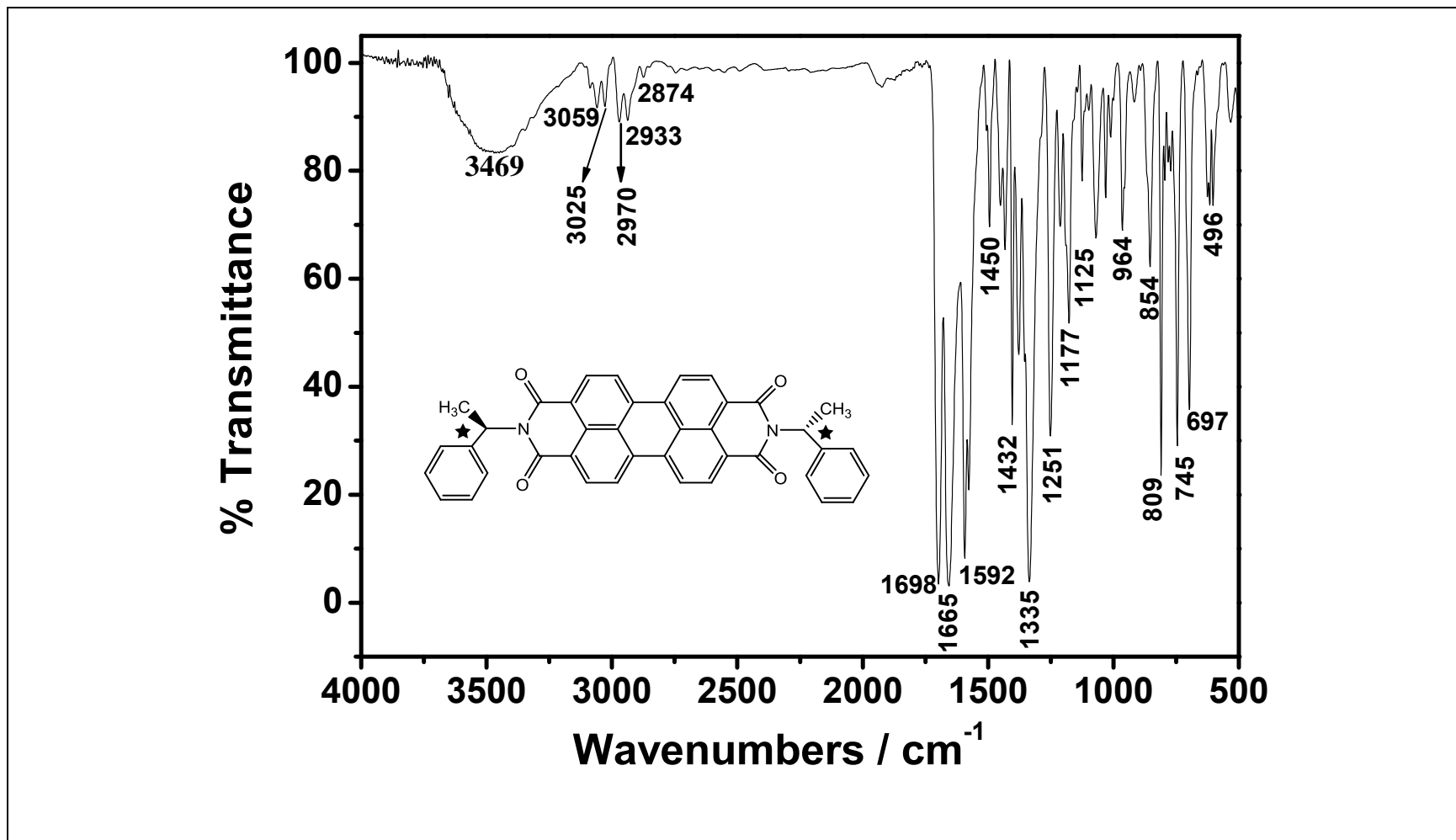


Figure 4. 4 FTIR spectrum of chiral PDI

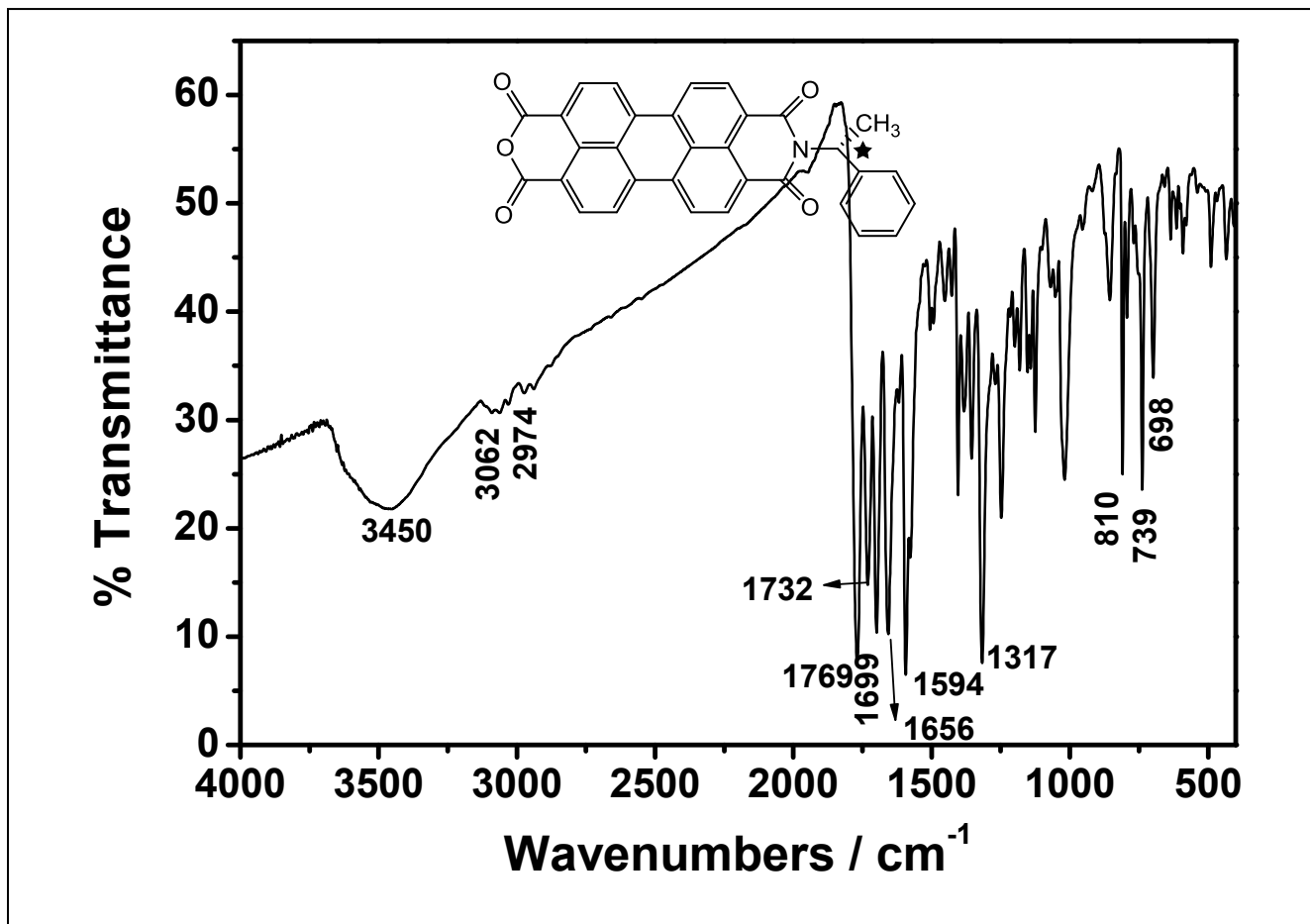


Figure 4.5 FTIR spectrum of R-PMI

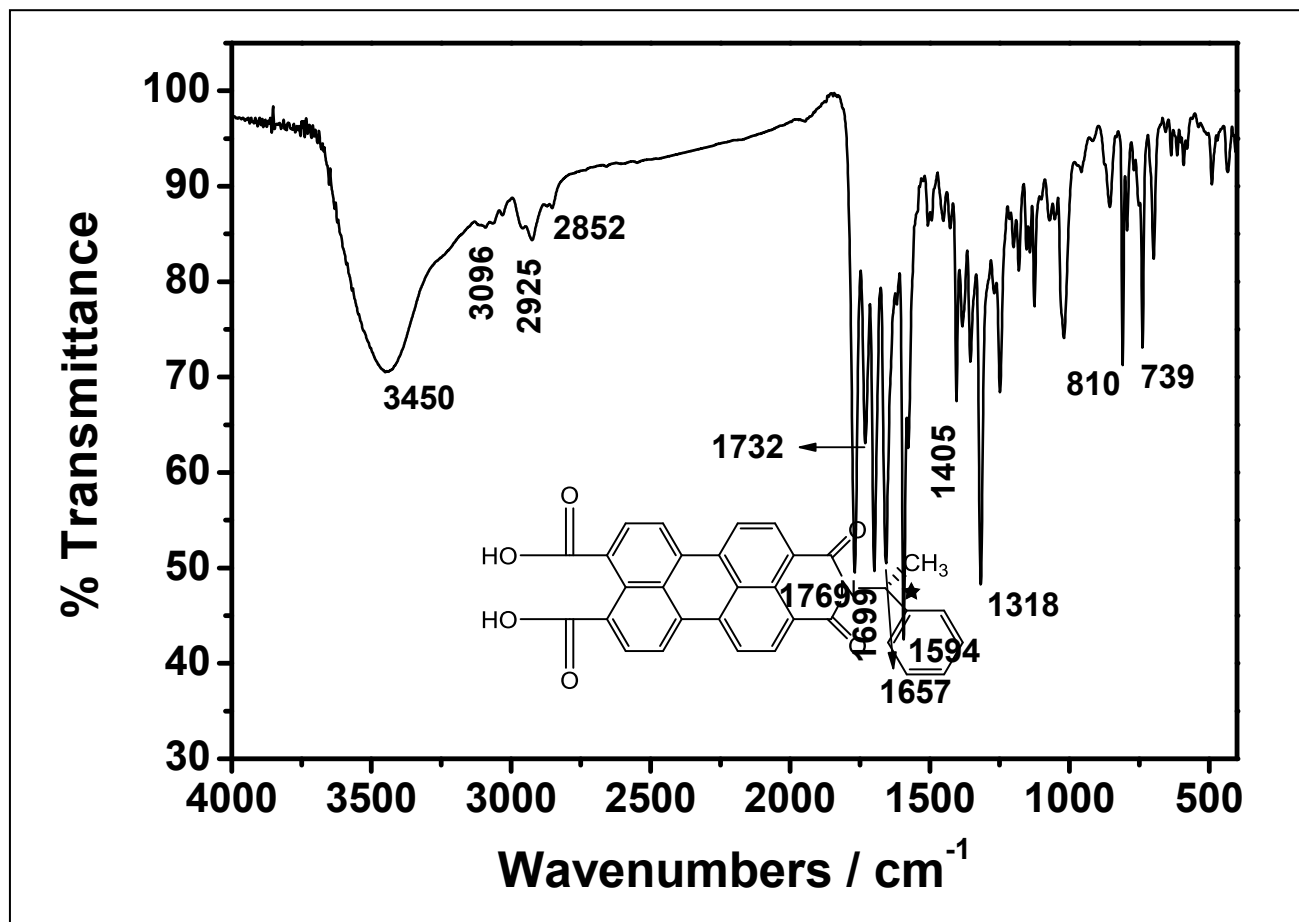


Figure 4.6 FTIR spectrum of R-CPMI

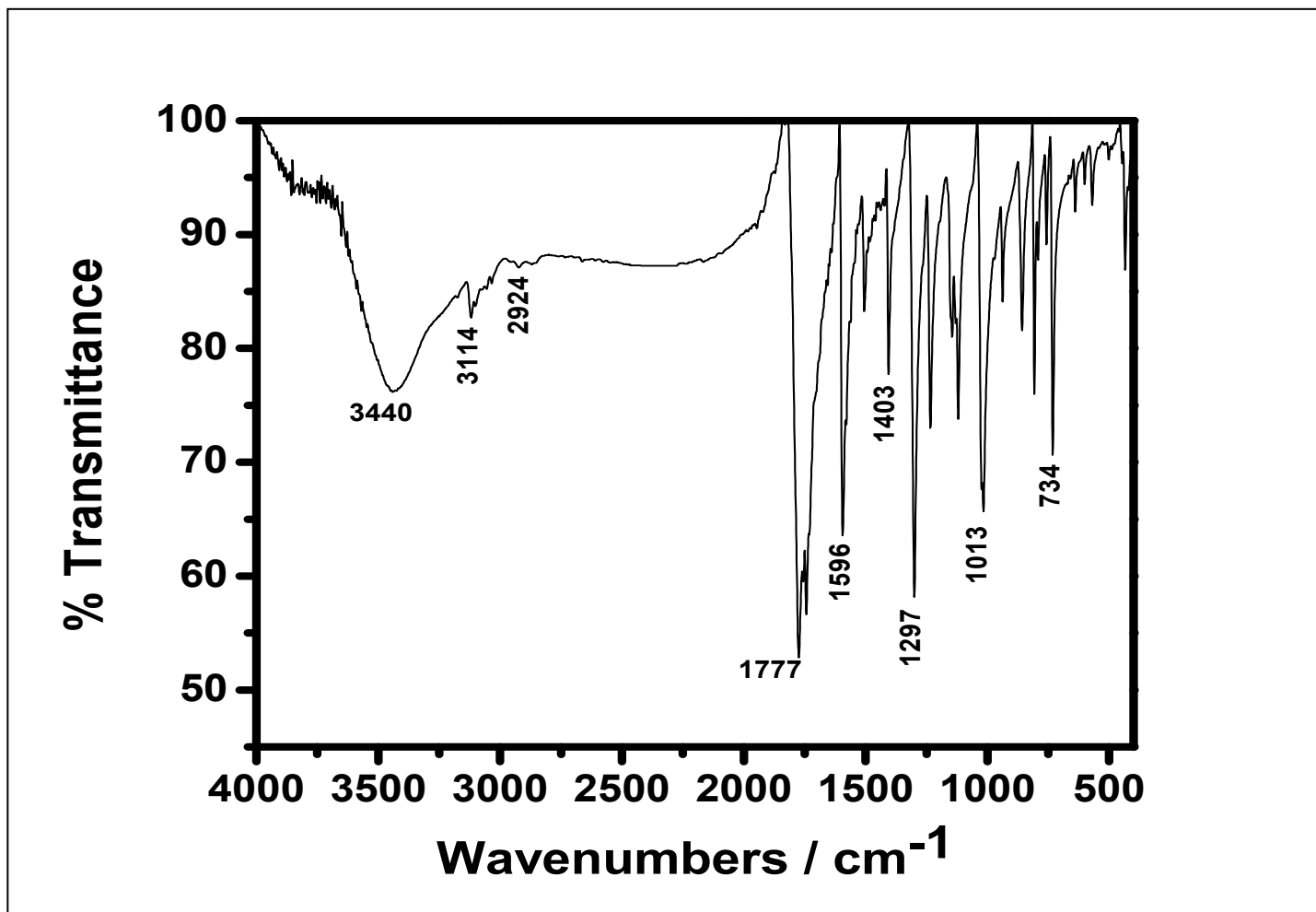


Figure 4.7 FTIR spectrum of PTCA

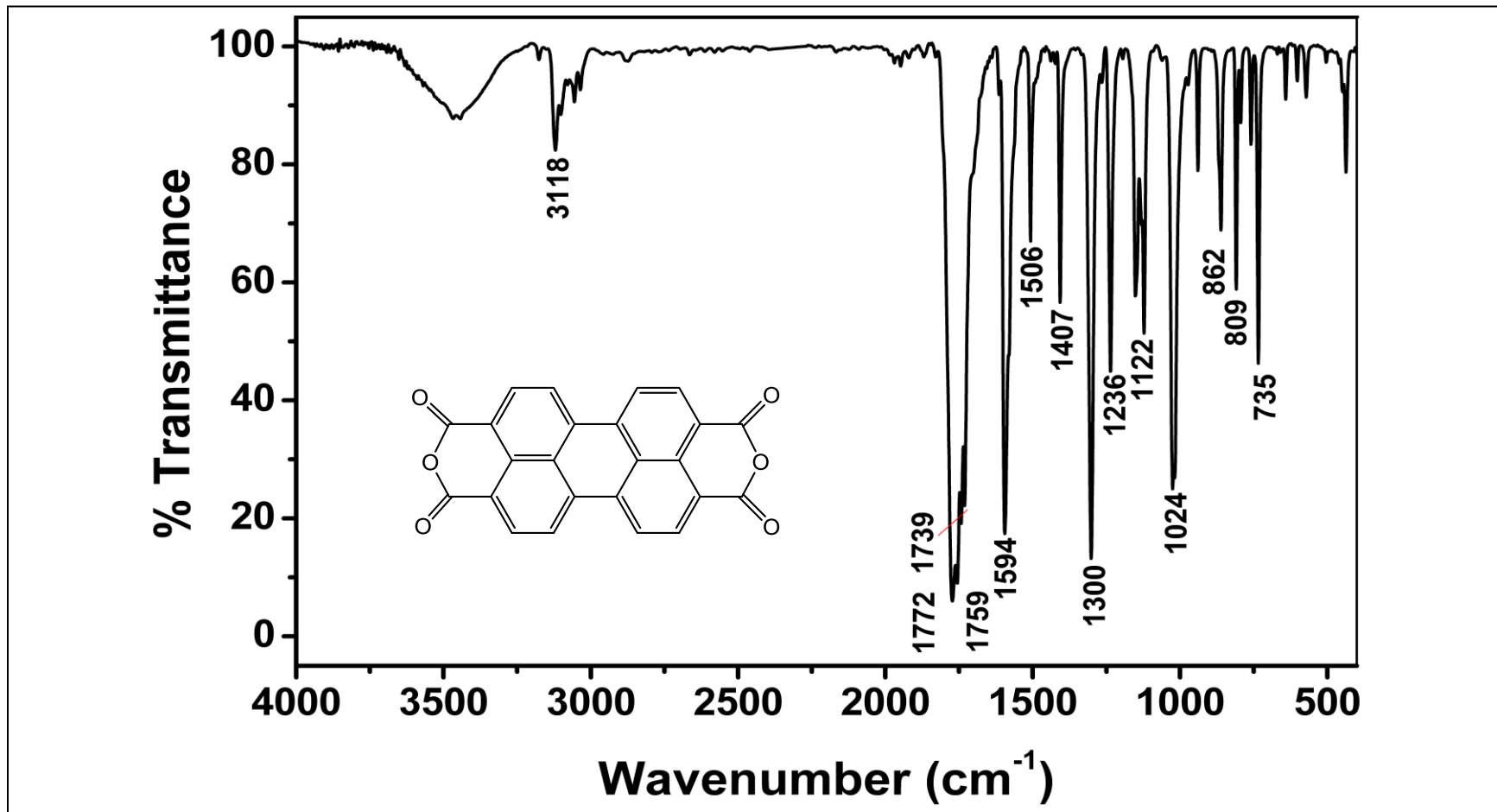


Figure 4.8 FTIR spectrum of PDA

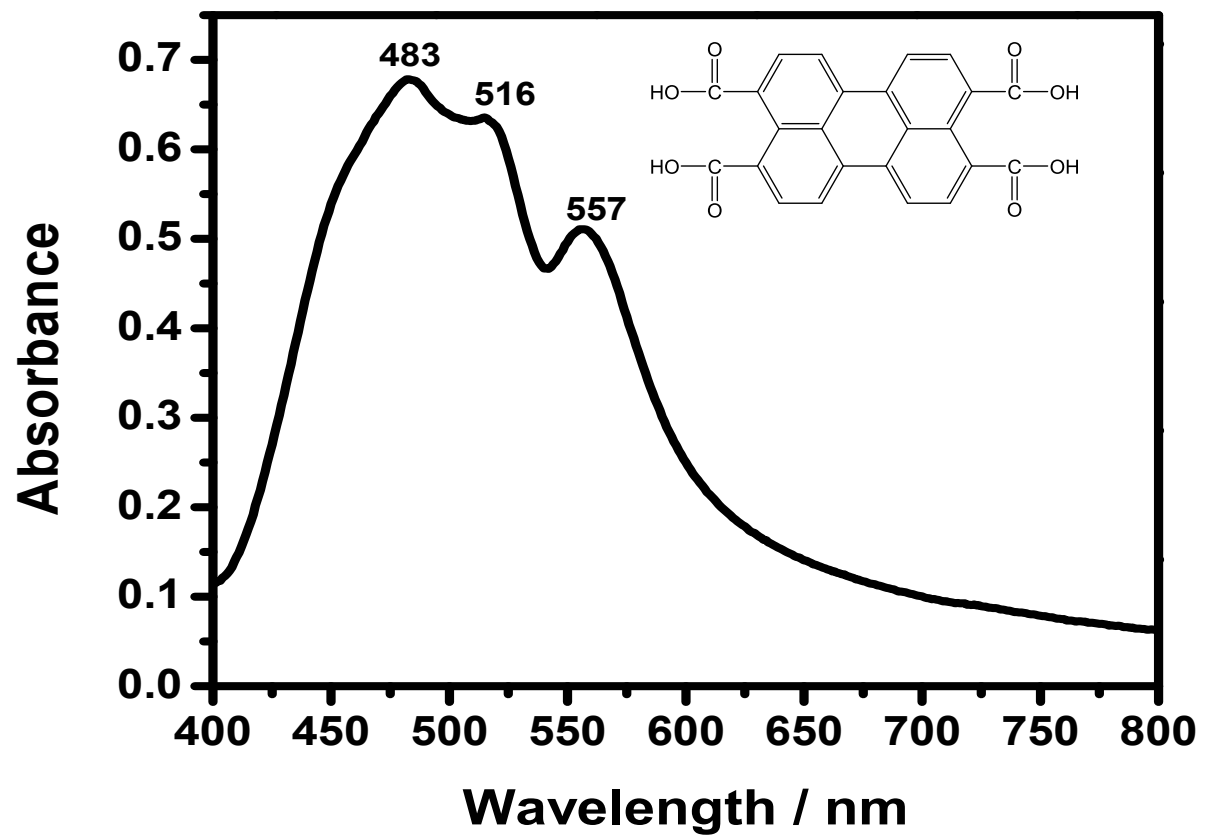


Figure 4.9 Absorption spectrum of PTCA in DMSO

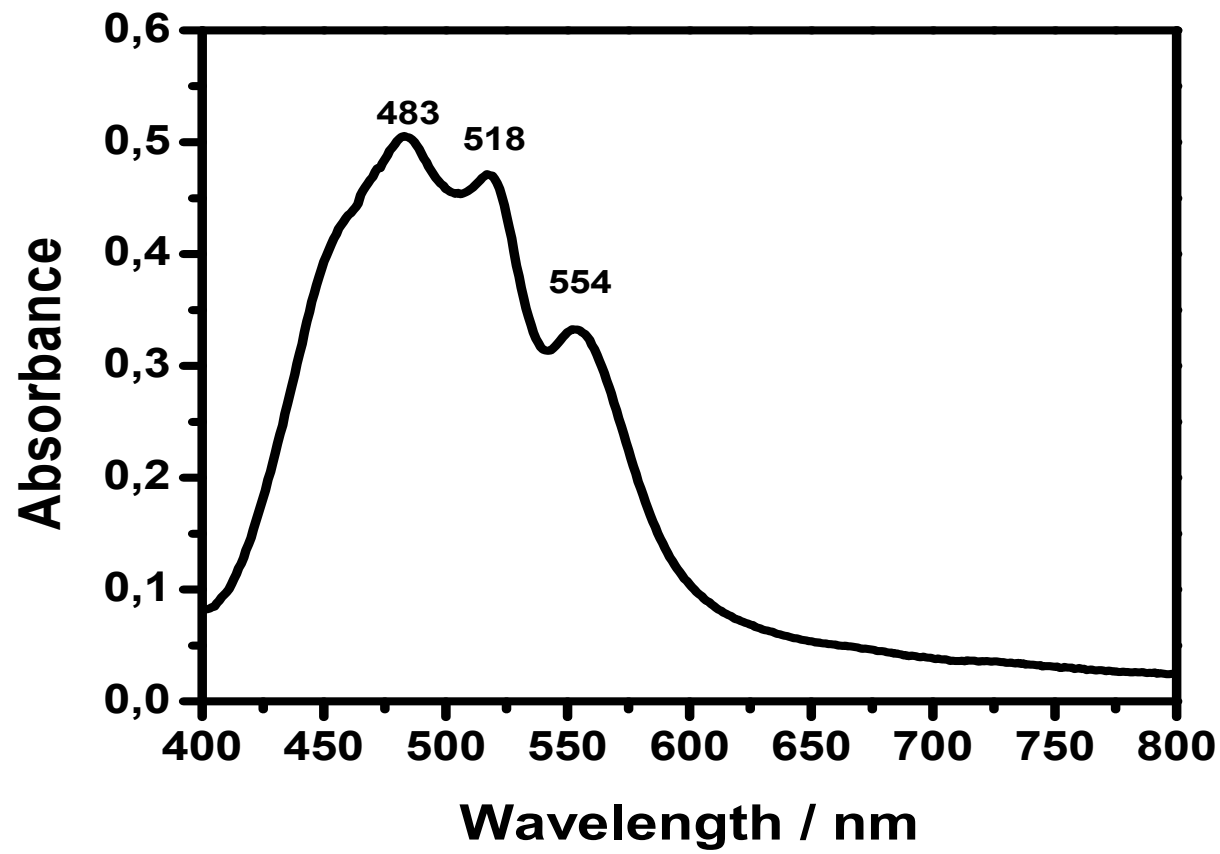


Figure 4.10 Absorption spectrum of PTCA in DMSO microfiltered

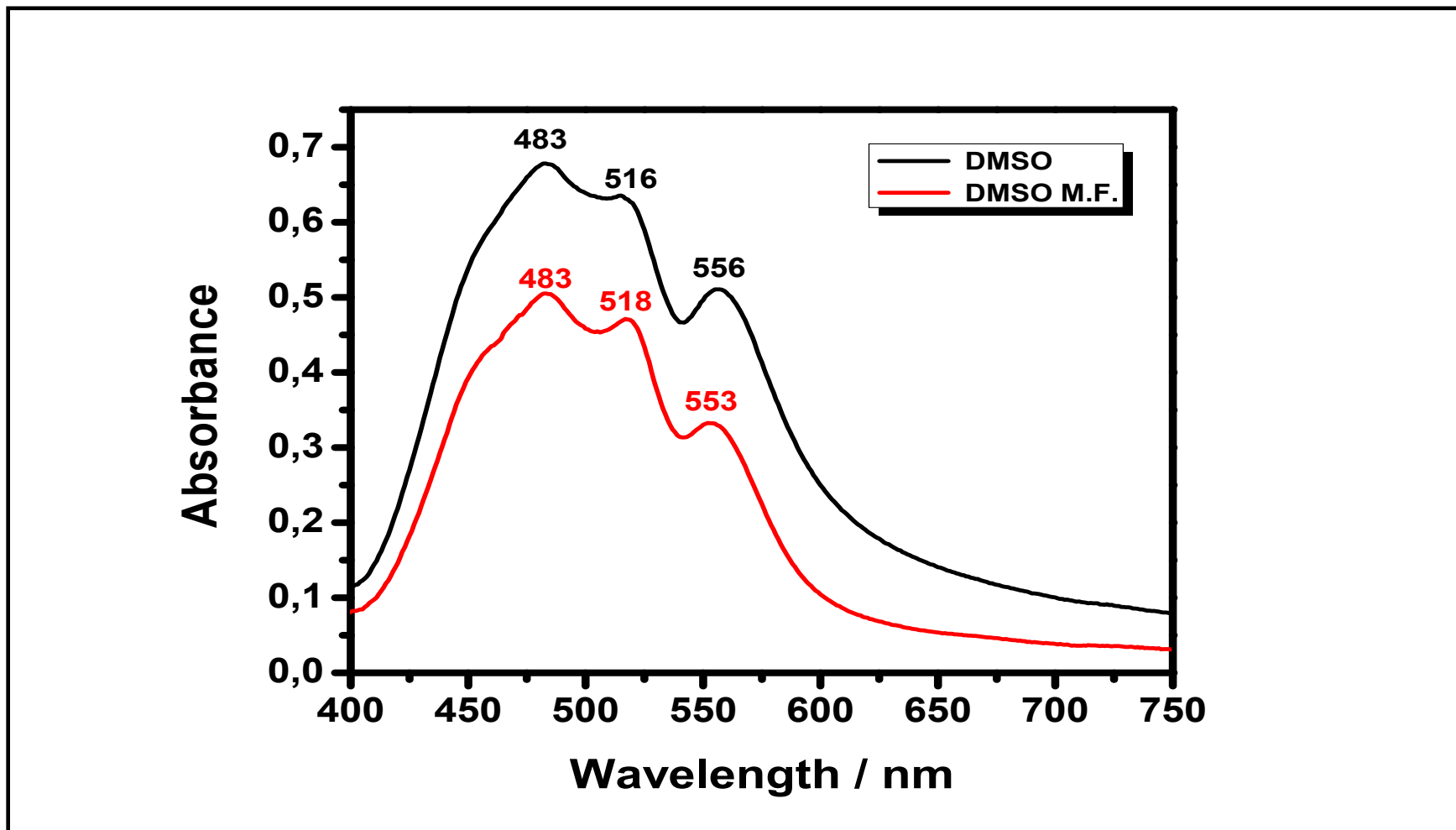


Figure 4.11 Absorption spectrum of PTCA in DMSO and DMSO microfiltered

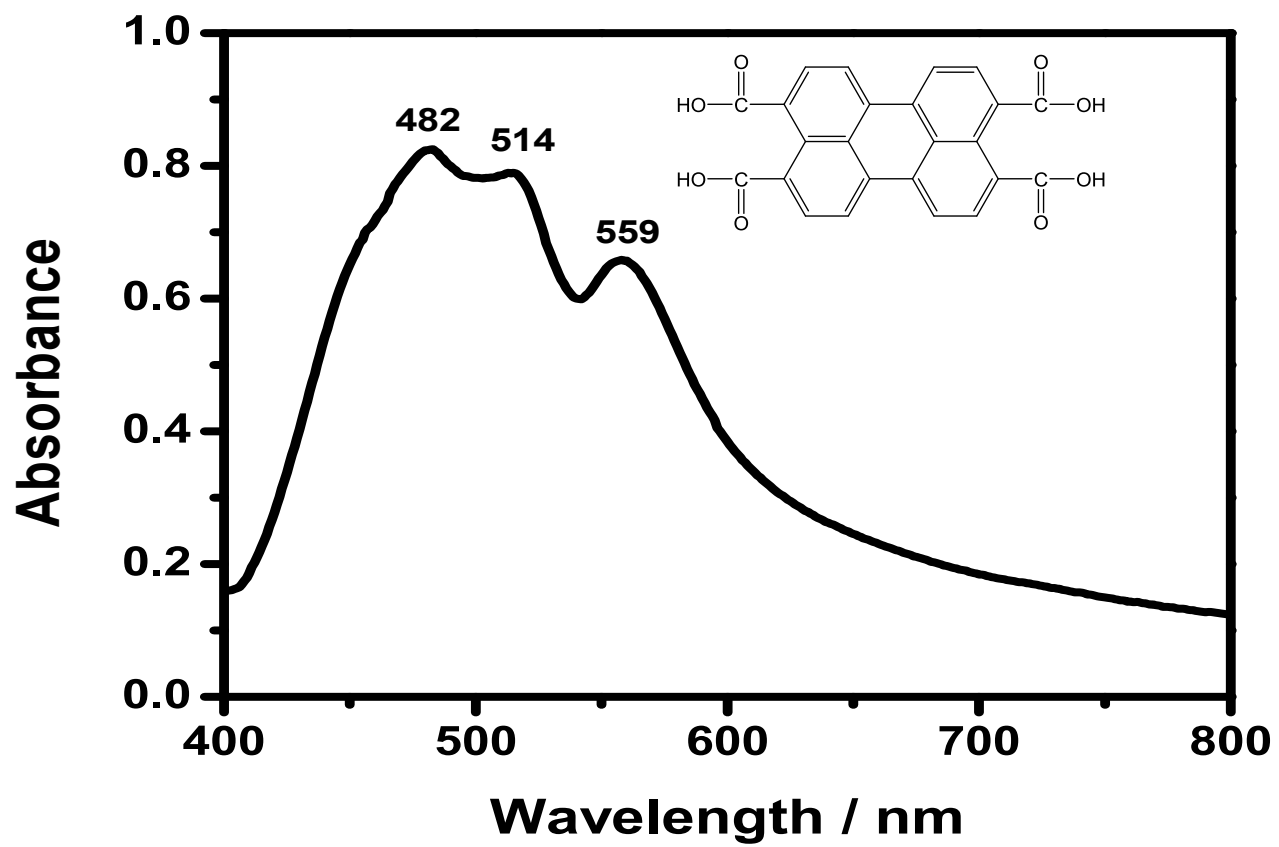


Figure 4.12 Absorption spectrum of PTCA in DMF

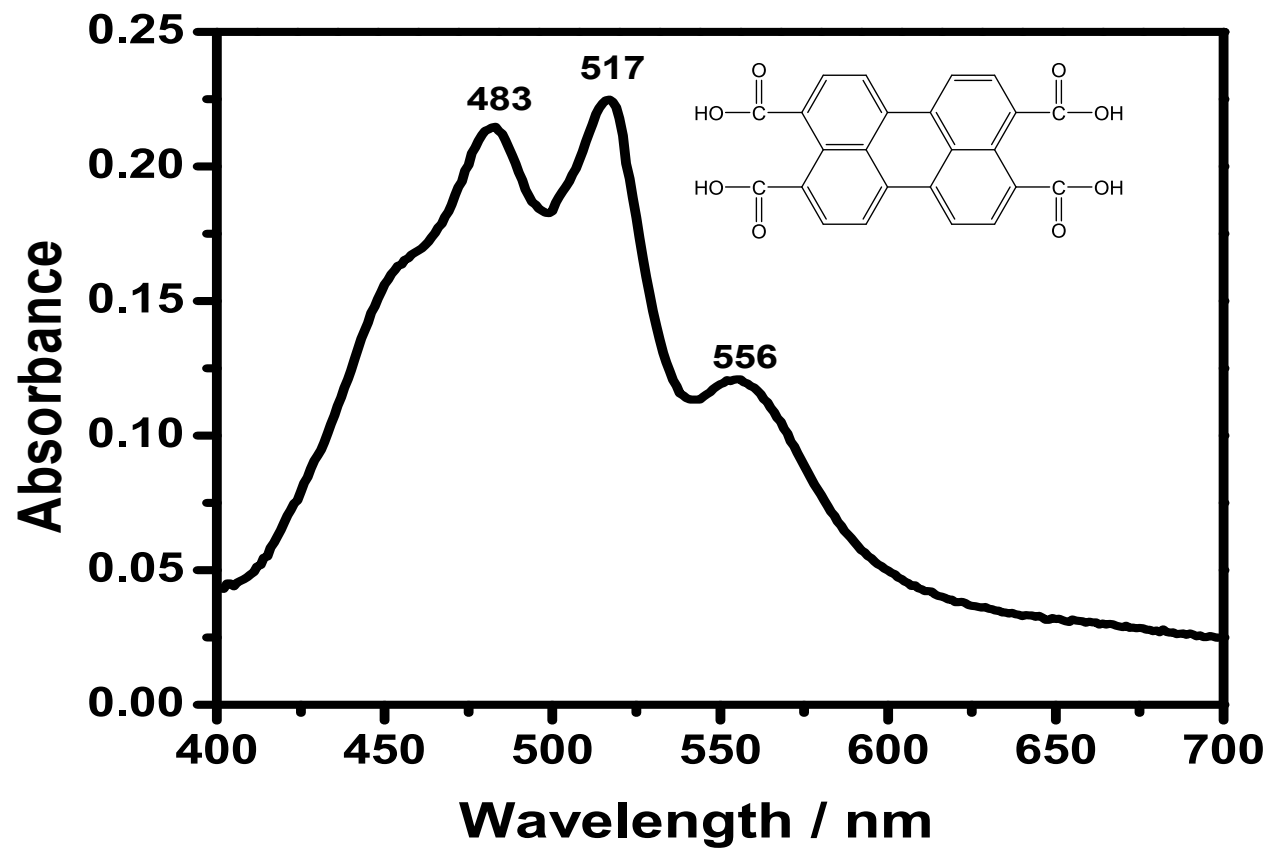


Figure 4.13 Absorption spectrum of PTCA in DMF microfiltered

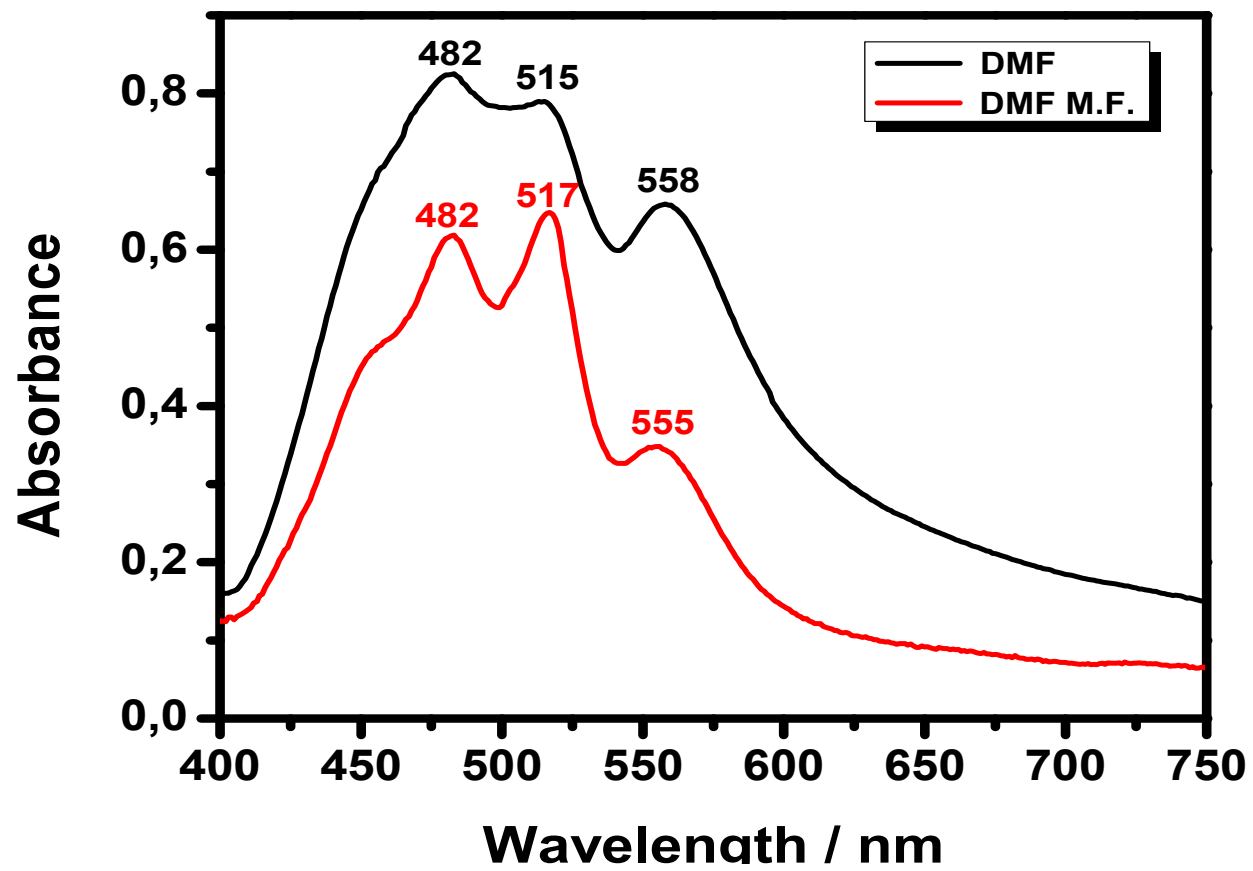


Figure 4.14 Absorption spectrum of PTCA in DMF and DMF microfiltered

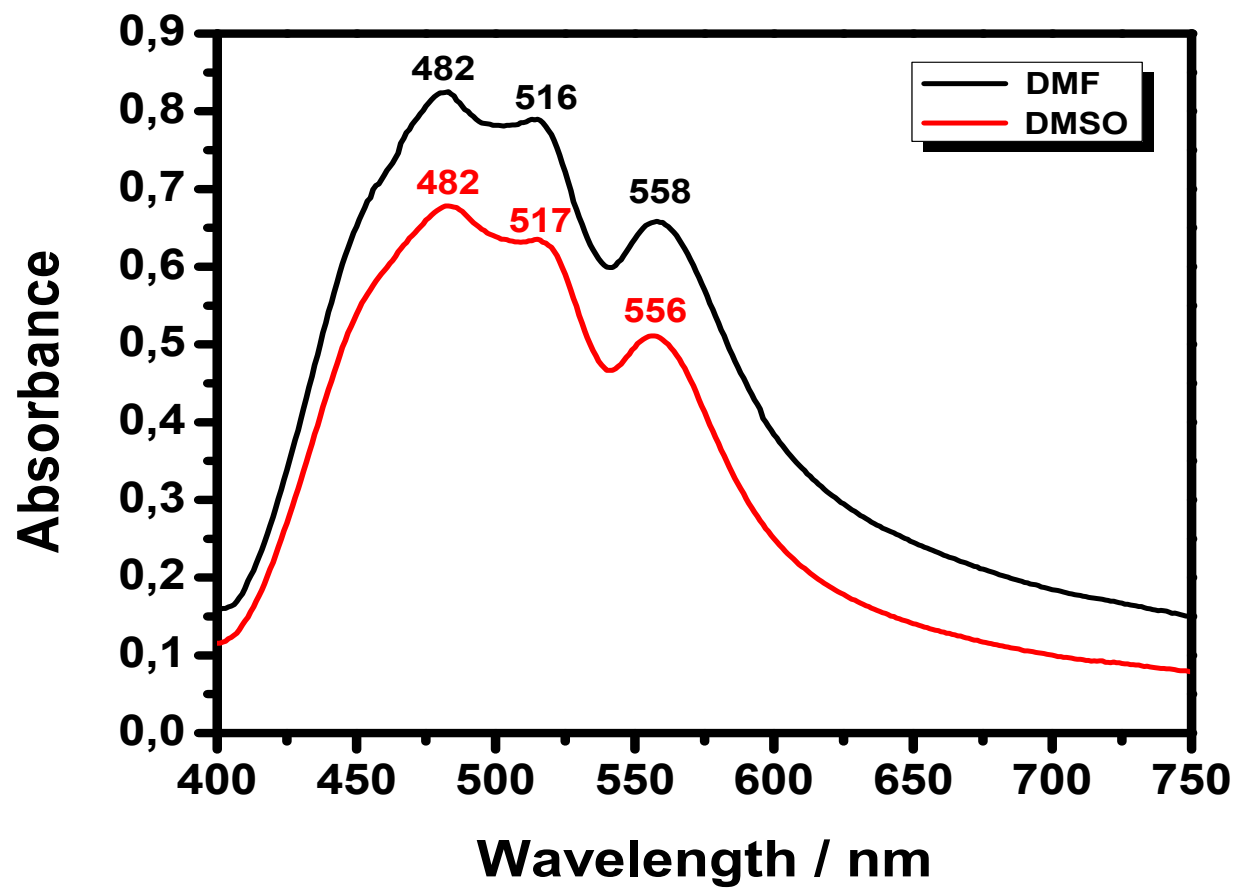


Figure 4.15 Absorption spectrum of PTCA in DMF and DMSO

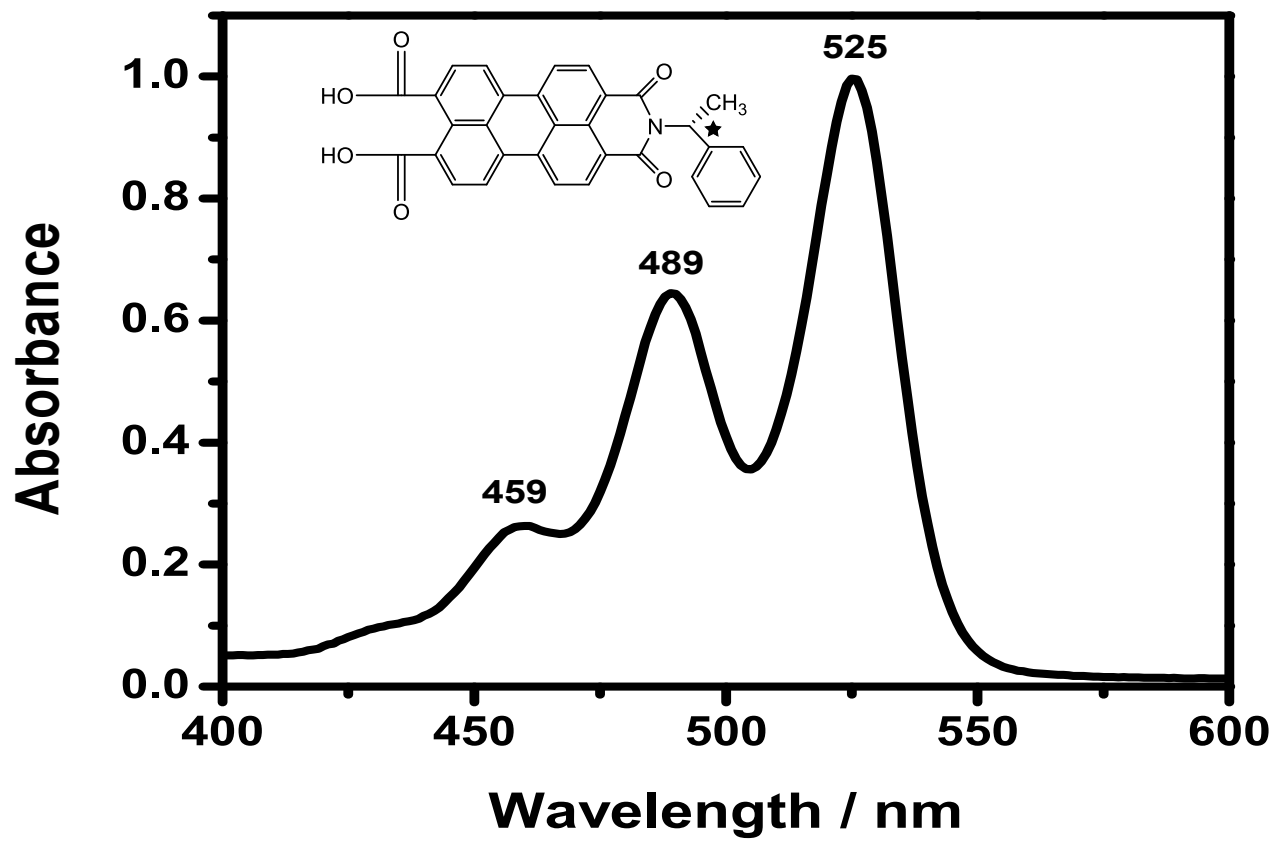


Figure 4.16 Absorption spectrum of R-CPMI in DMSO

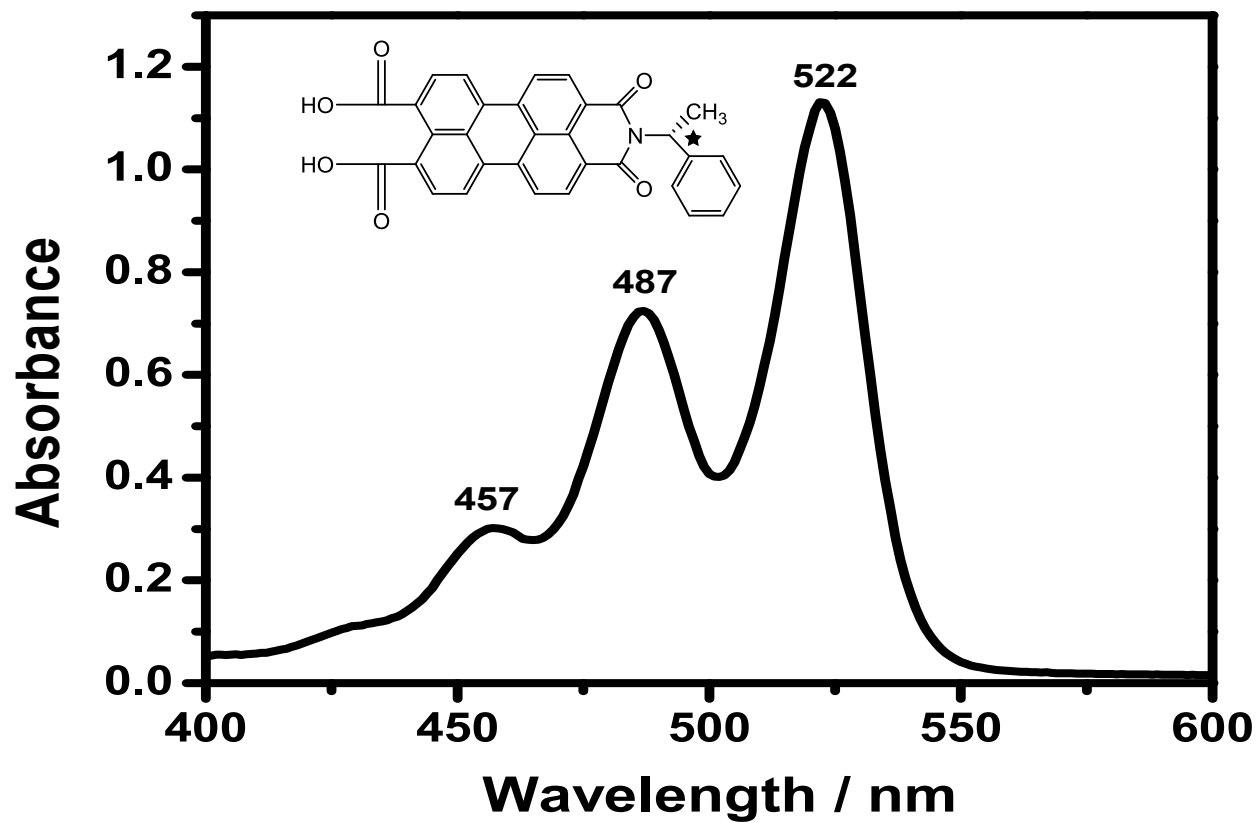


Figure 4.17 Absorption spectrum of R-CPMI in DMF

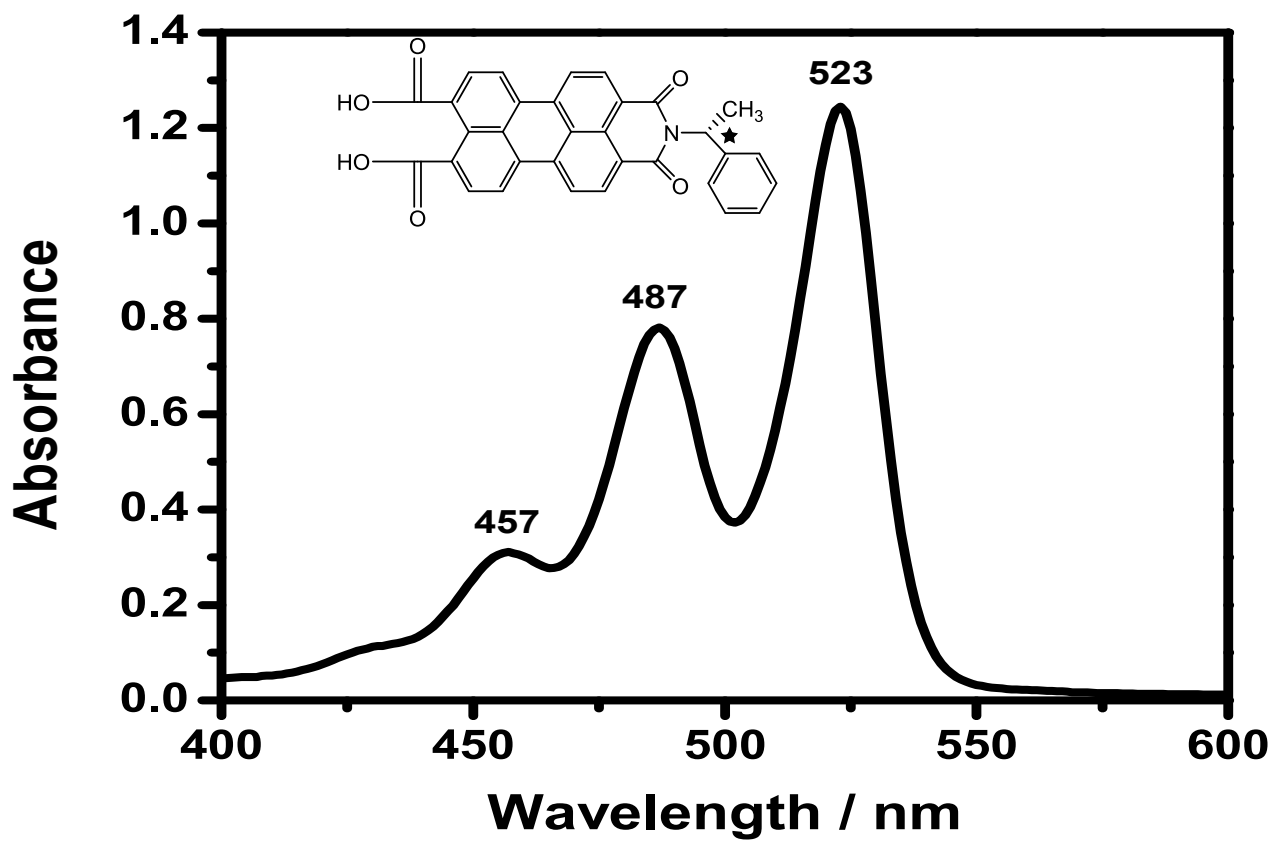


Figure 4.18 Absorption spectrum of R-CPMI in Chloroform

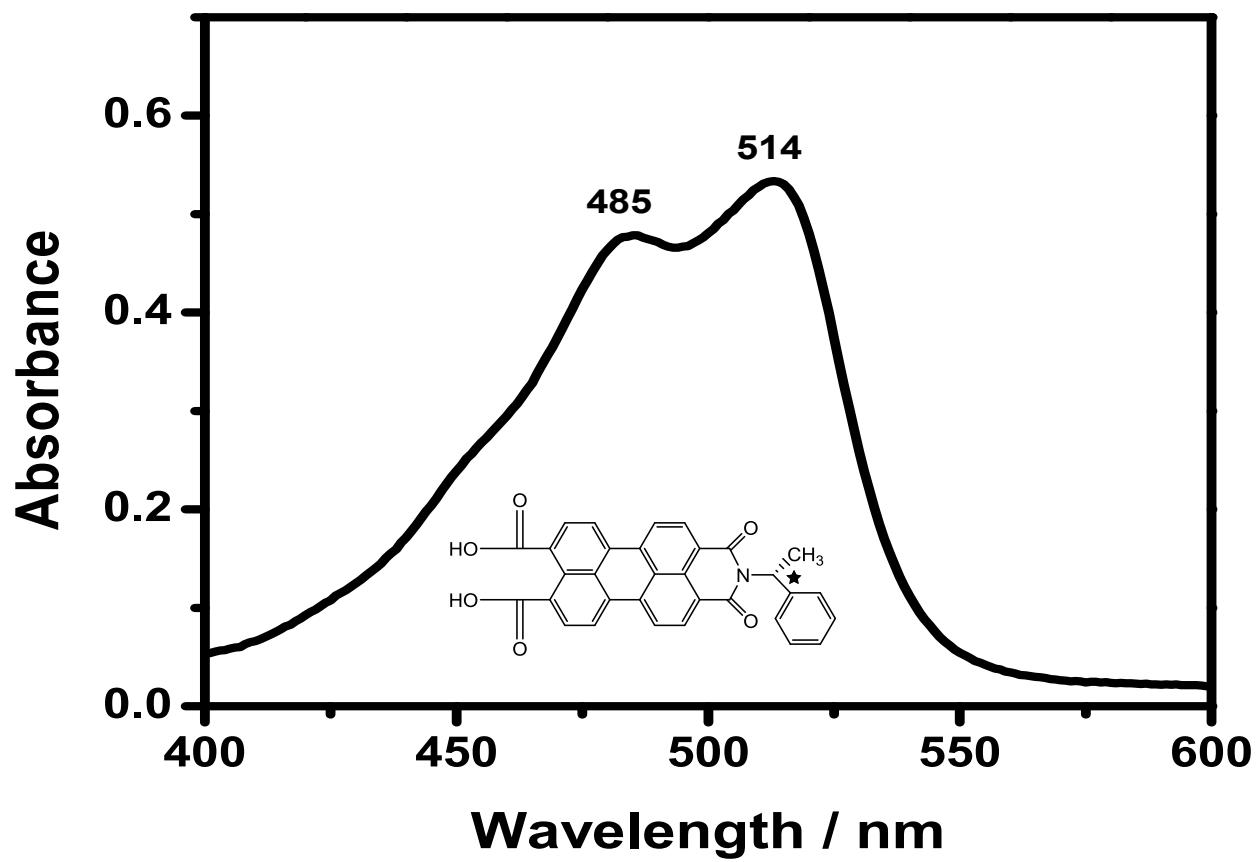


Figure 4.19 Absorption spectrum of R-CPMI in MeOH

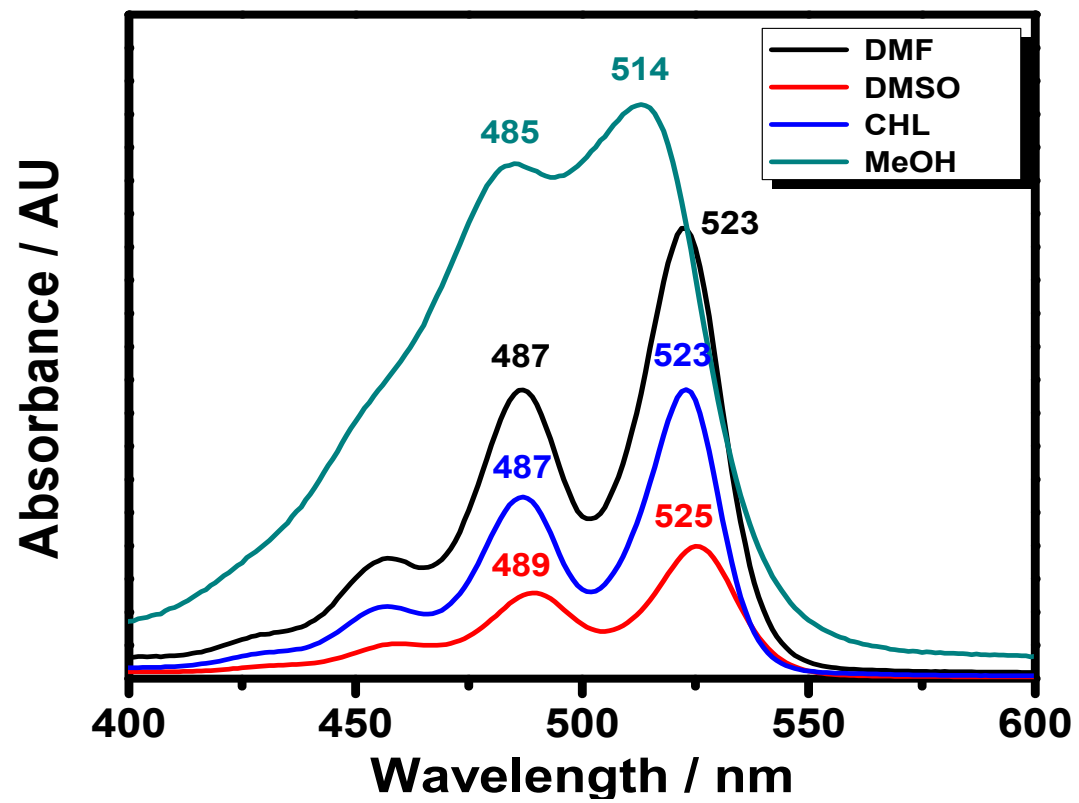


Figure 4.20 Absorption spectrum of R-CPMI in DMF, DMSO, CHL and MeOH

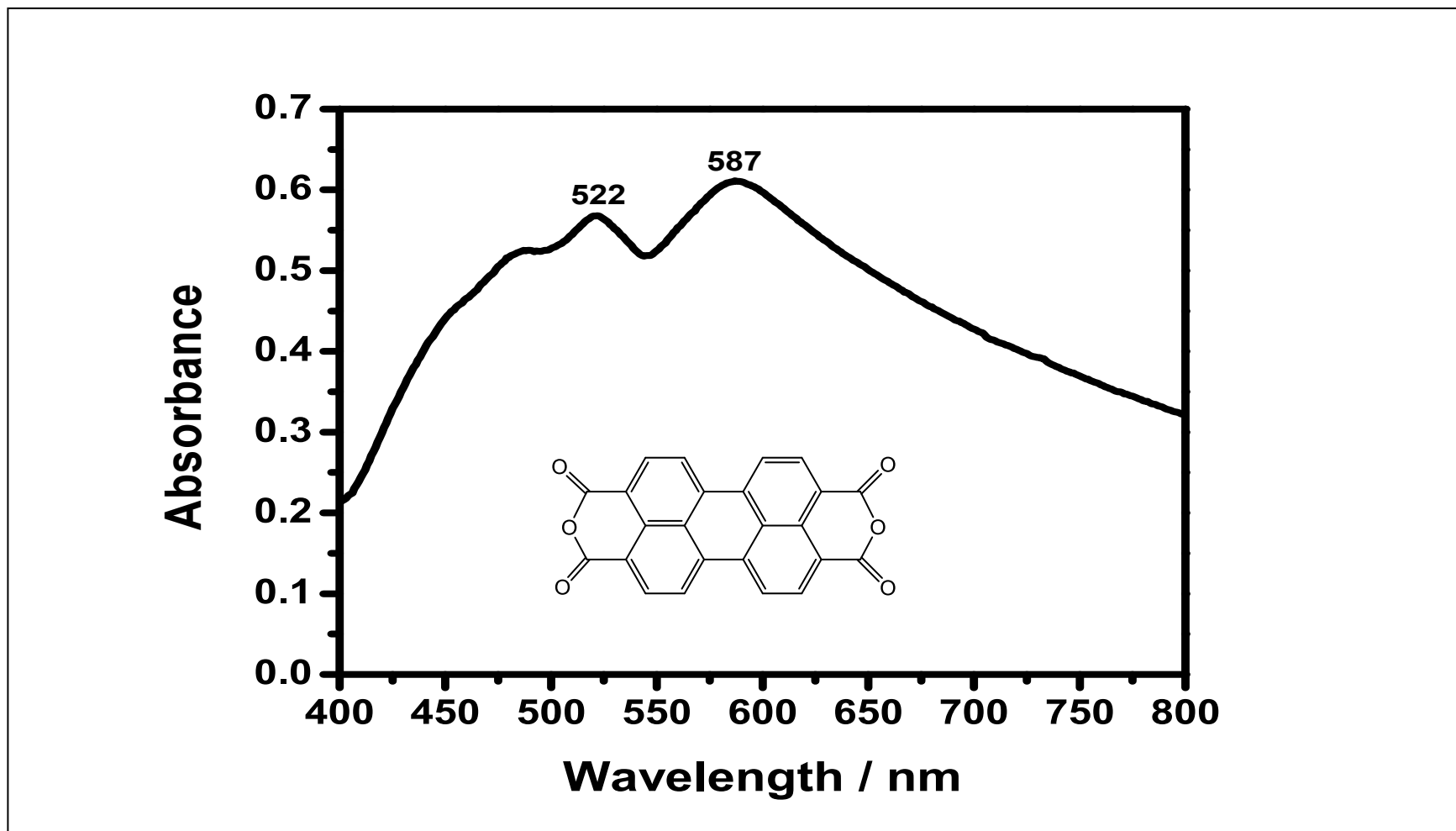


Figure 4.21 Absorption spectrum of PDA in DMSO

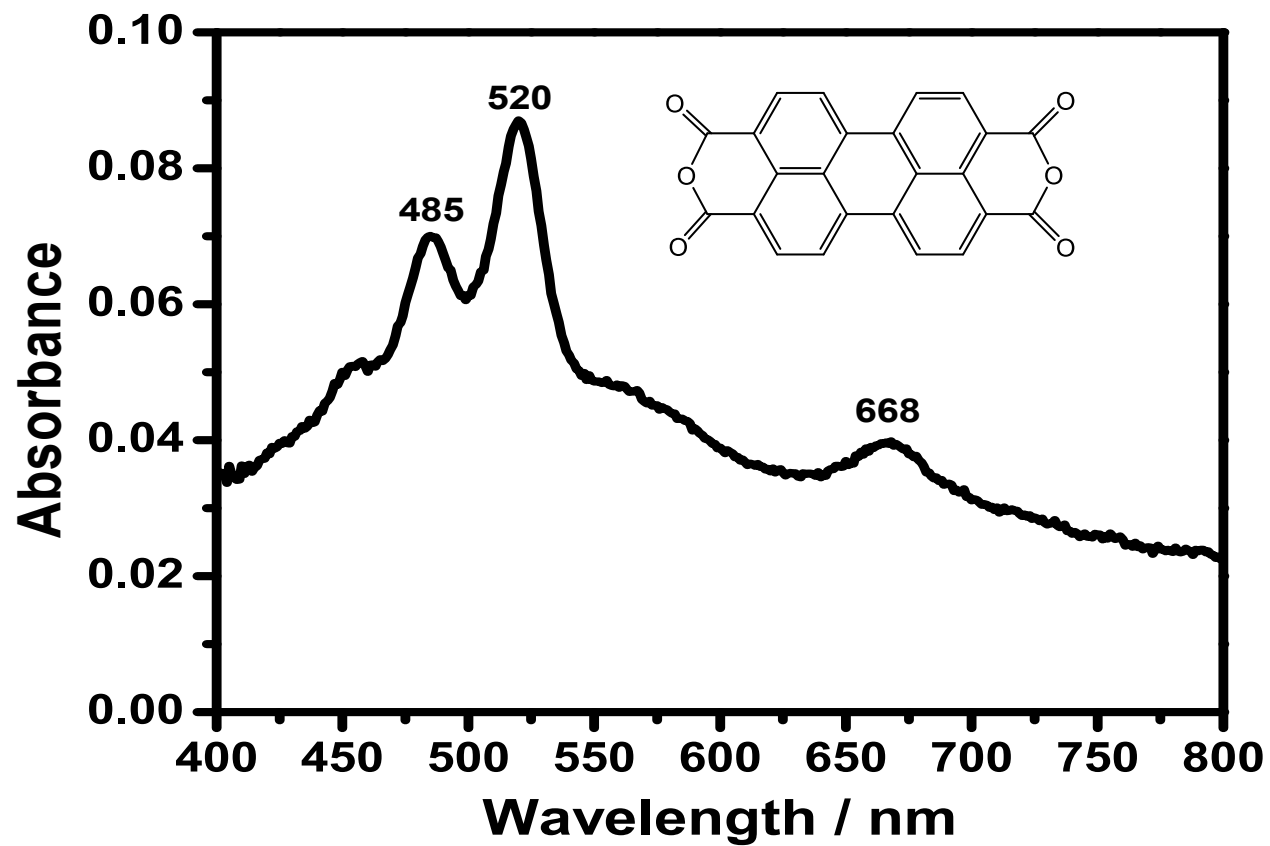


Figure 4.22 Absorption spectrum of PDA in DMSO microfiltered

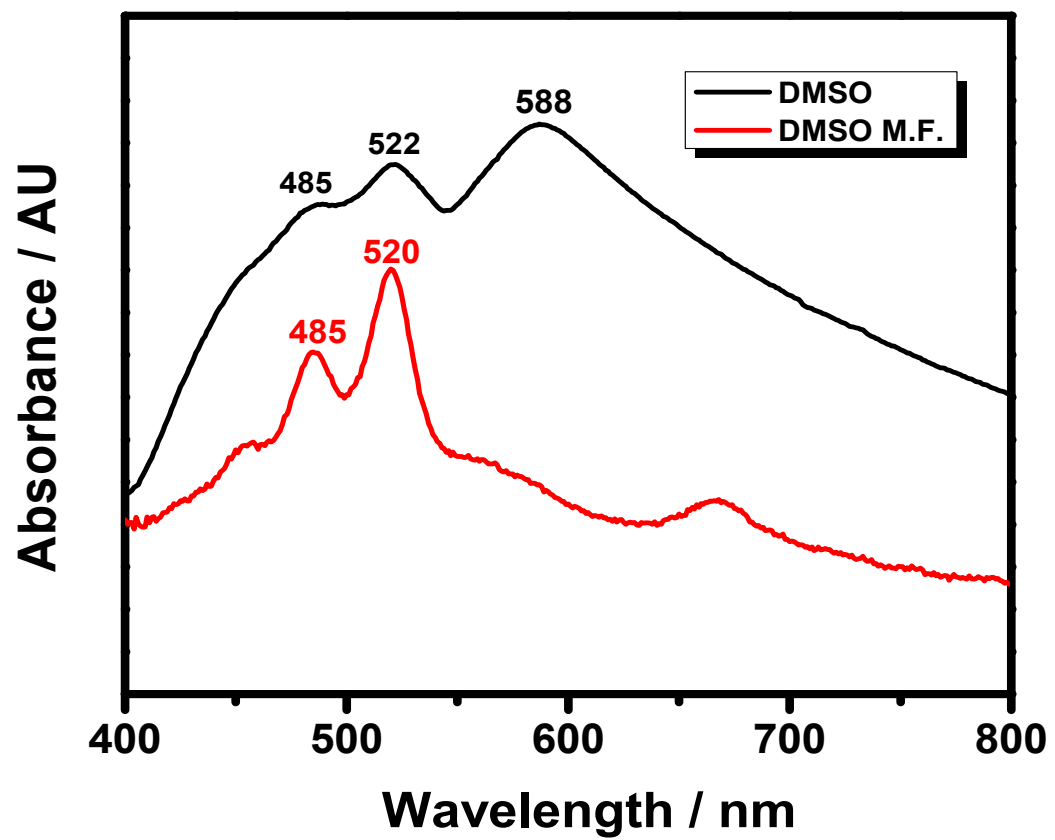


Figure 4.23 Absorption spectrum of PDA in DMSO and DMSO microfiltered

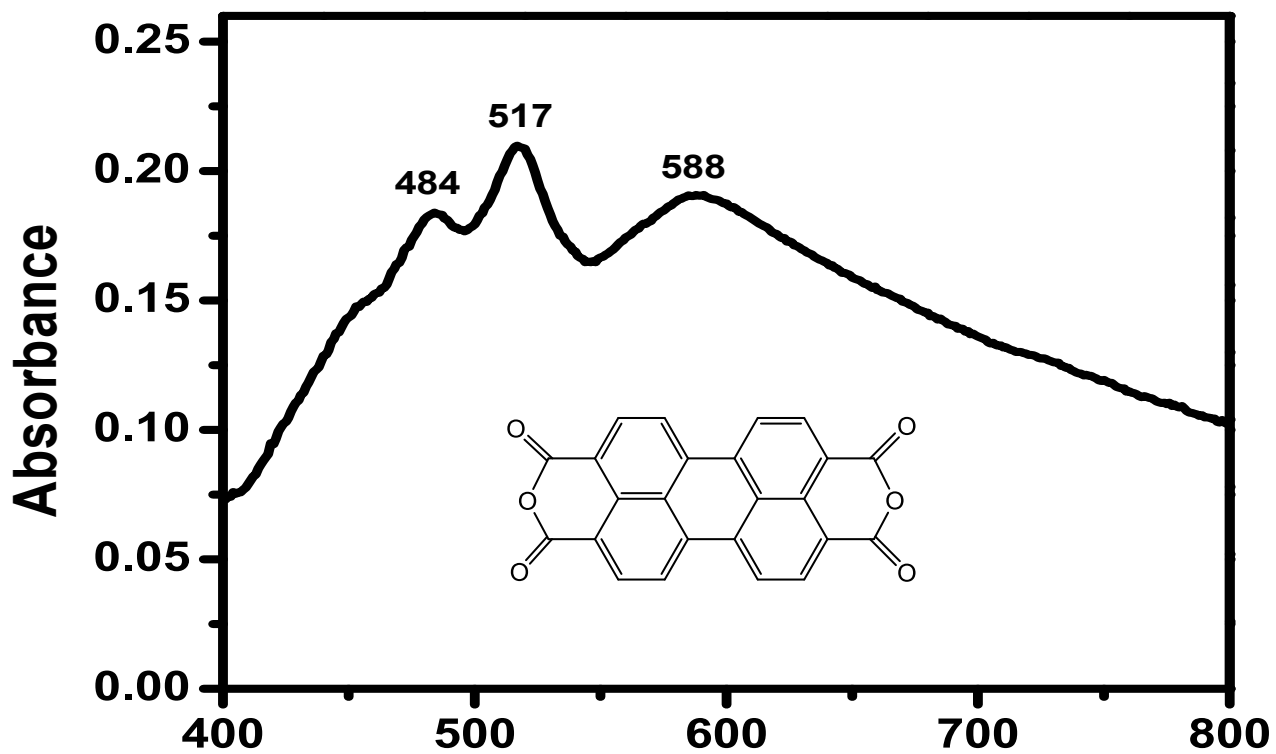


Figure 4.24 Absorption spectrum of PDA in DMF

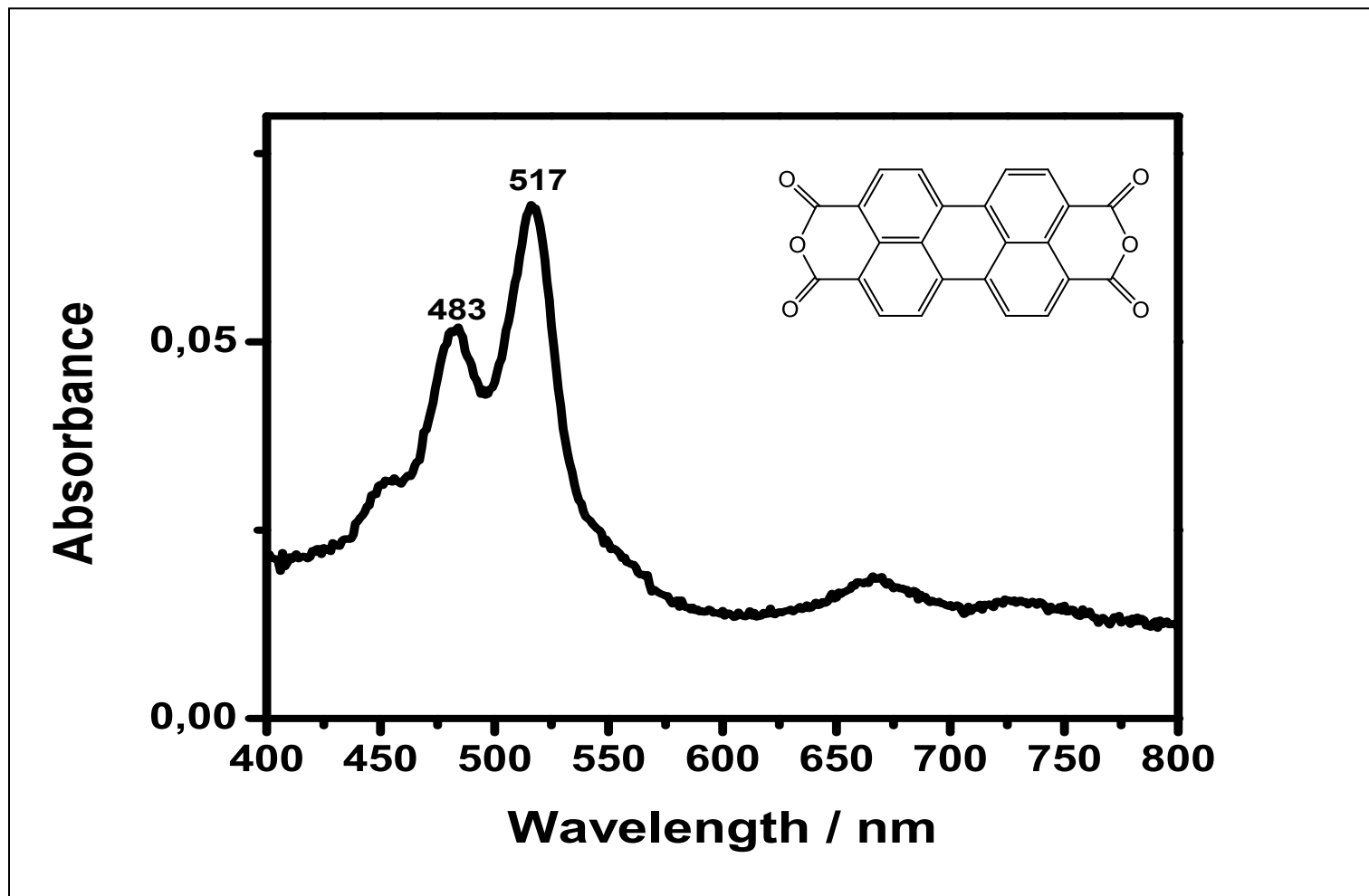


Figure 4.25 Absorption spectrum of PDA in DMF microfiltered

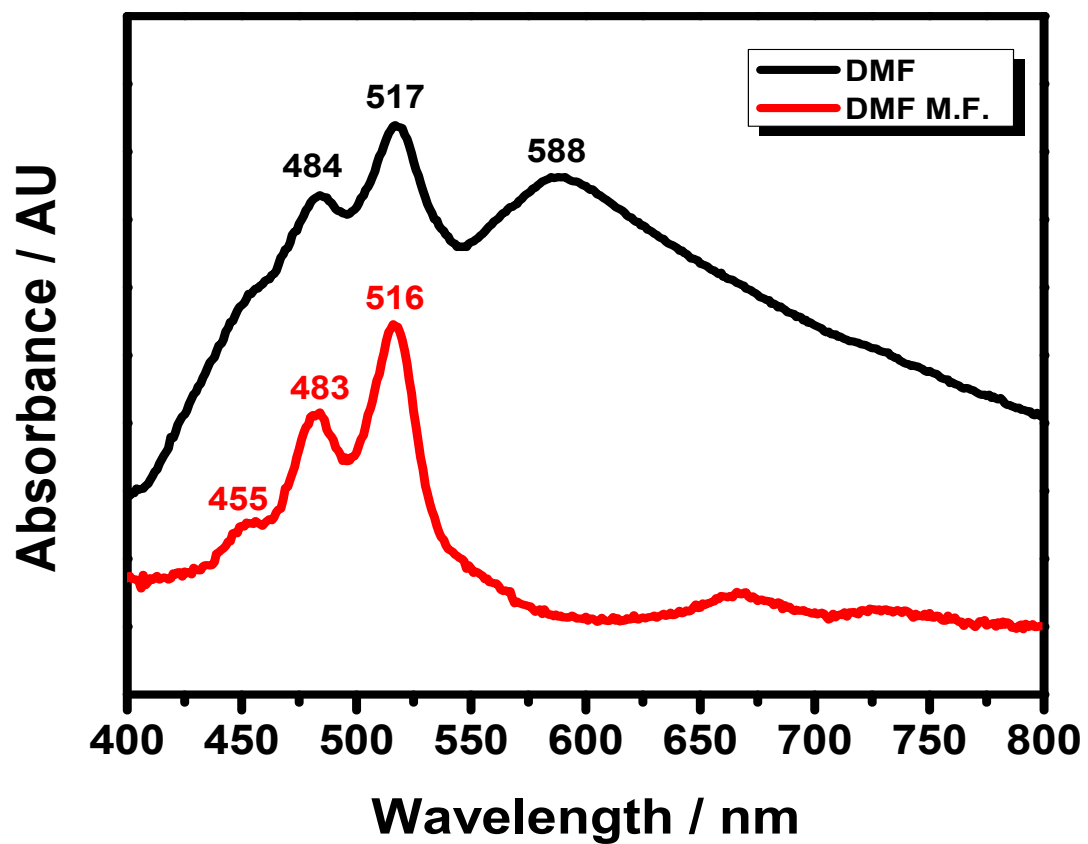


Figure 4. 26 Absorption spectrum of PDA in DMF and DMF microfiltered

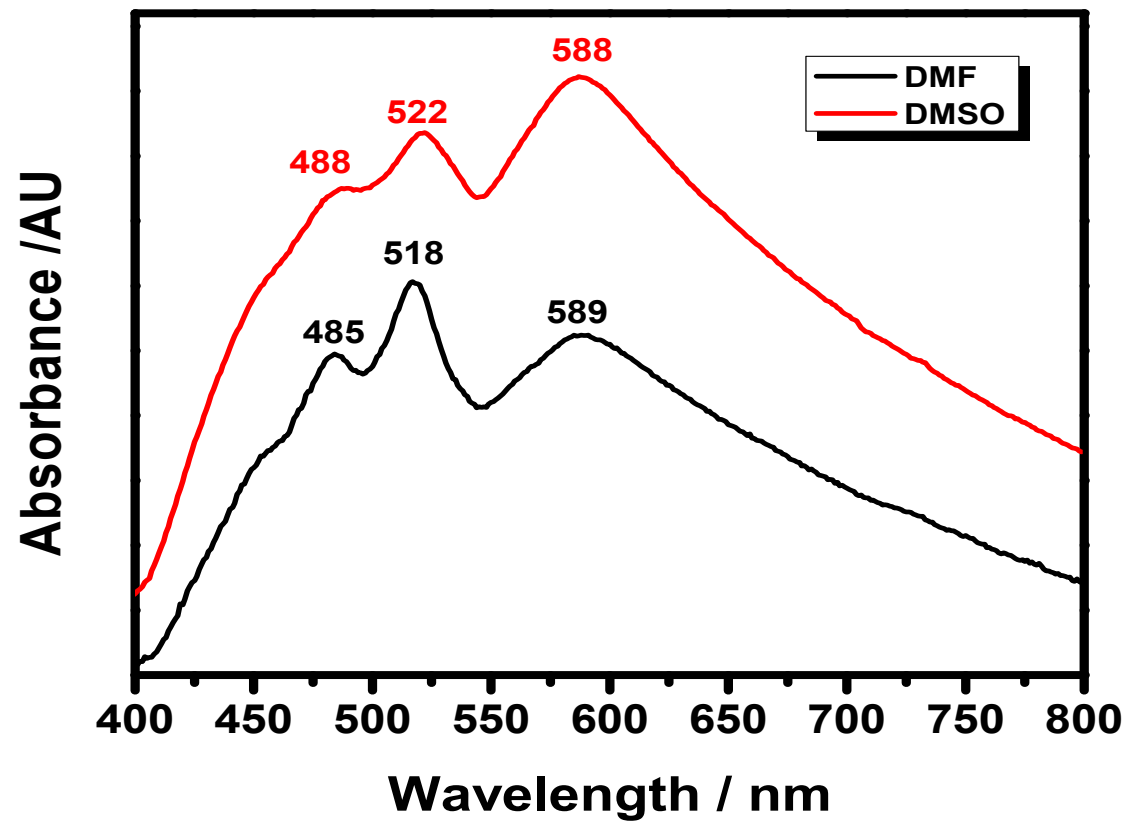


Figure 4. 27 Absorption spectrum of PDA in DMF and DMSO

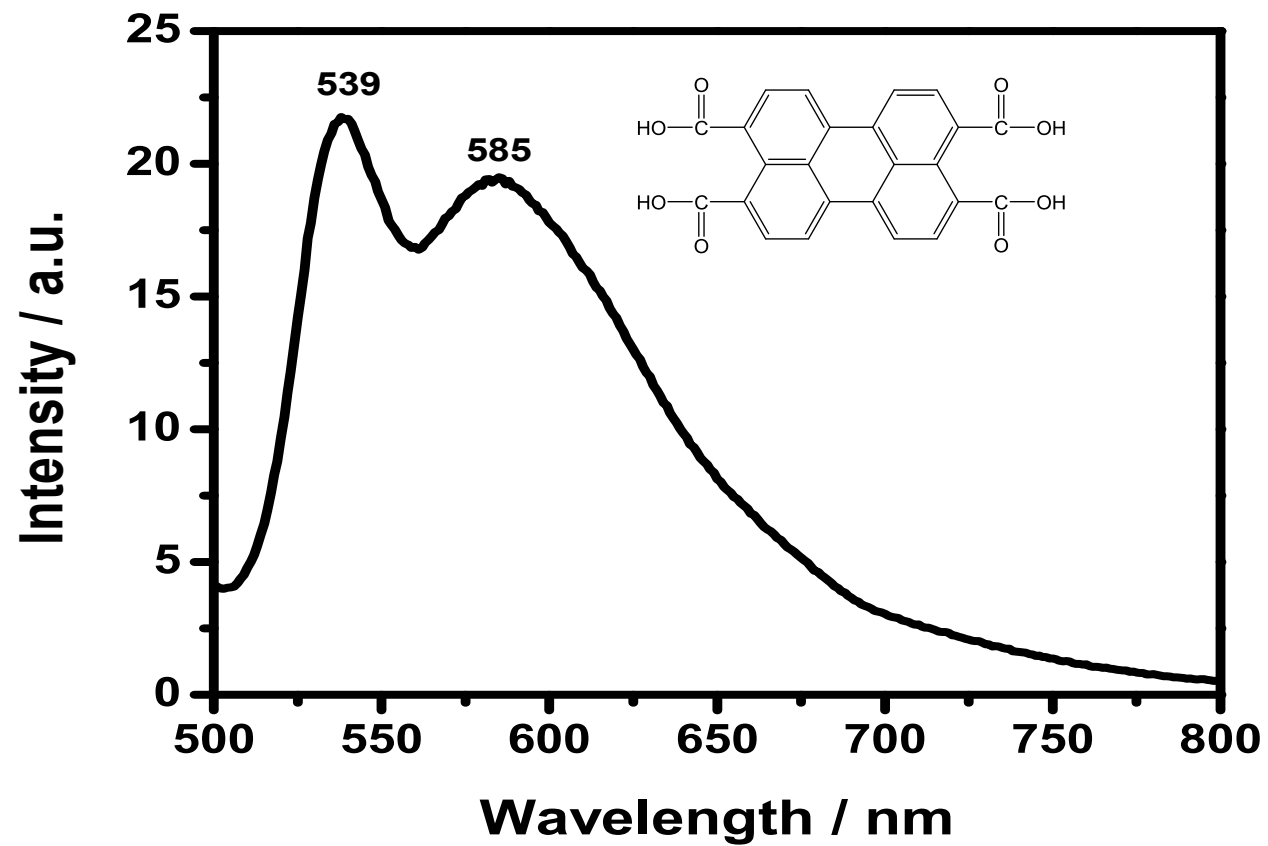


Figure 4.28 Emission spectrum of PTCA in DMSO at  $\lambda_{\text{exc}} = 485 \text{ nm}$

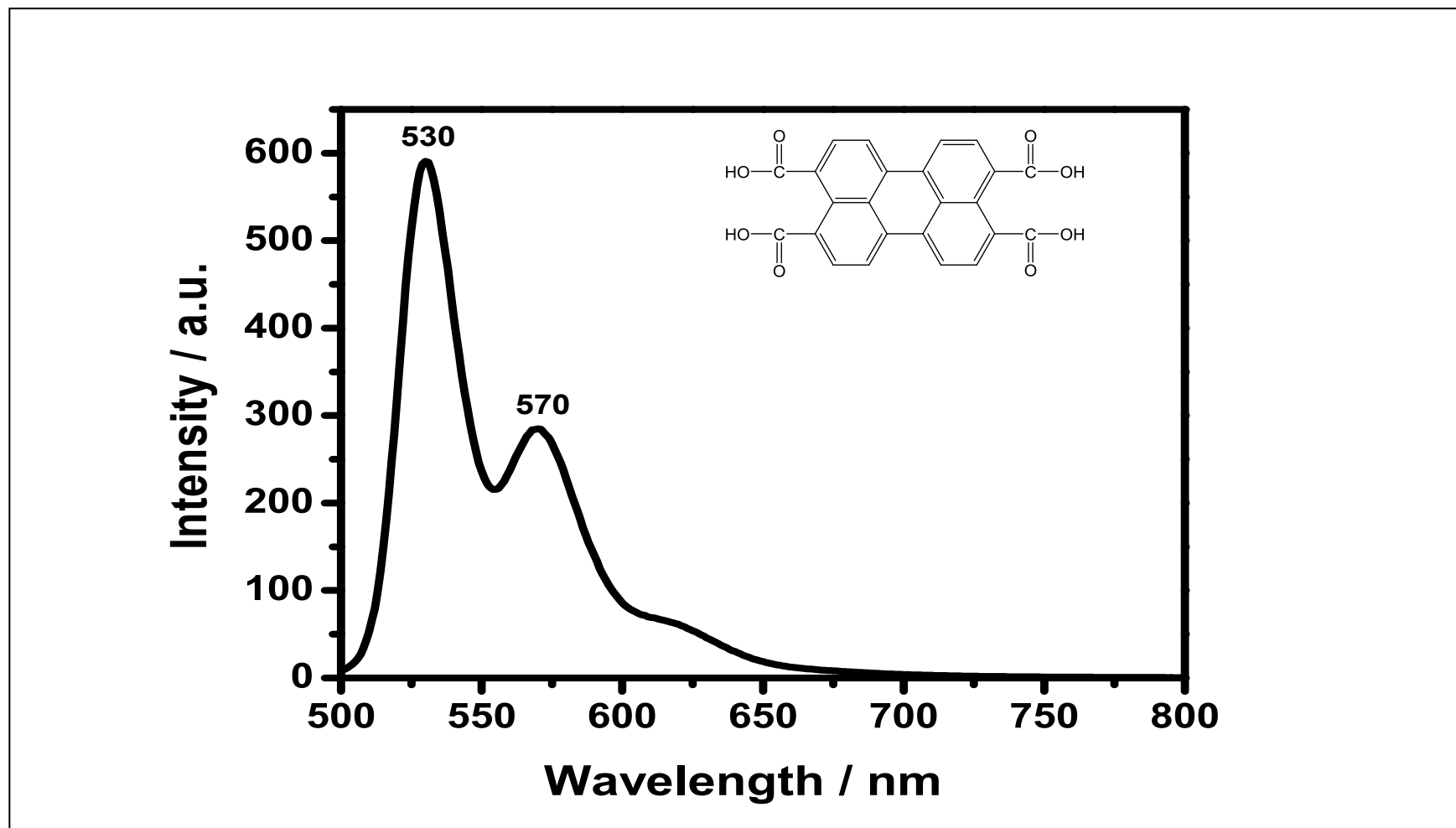


Figure 4. 29 Emission spectrum of PTCA in DMF at  $\lambda_{\text{exc}} = 485 \text{ nm}$

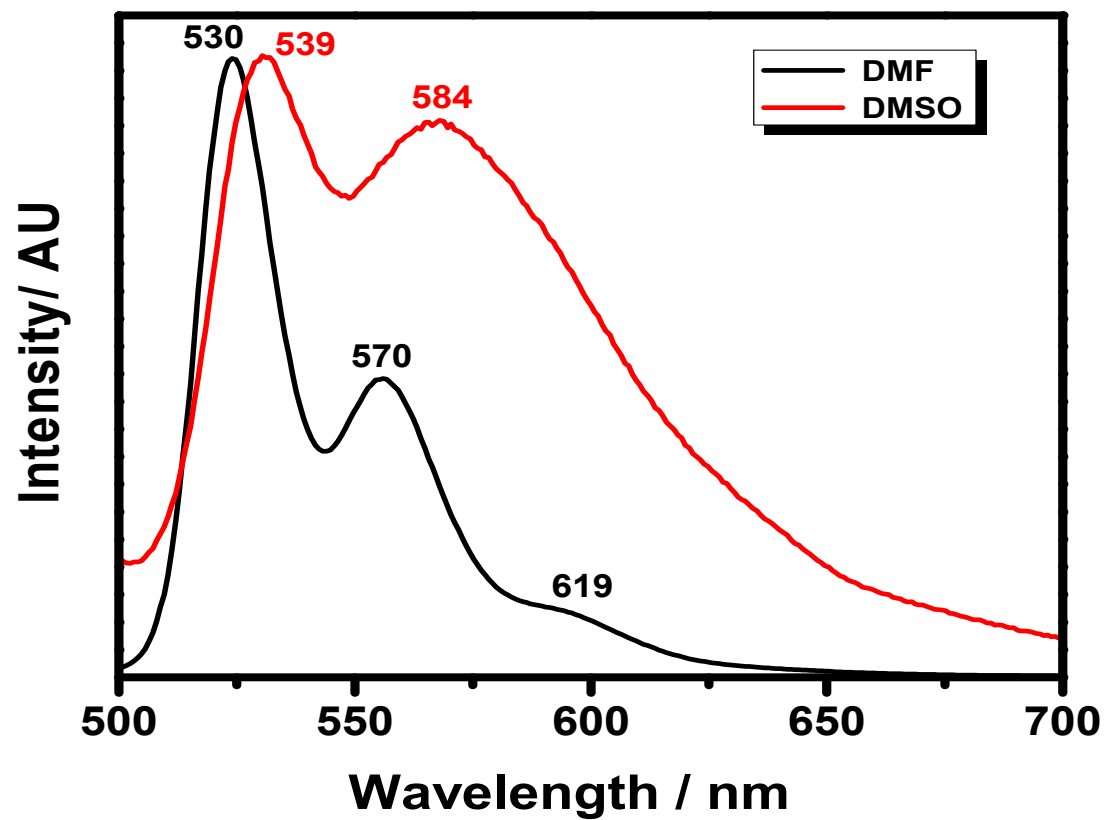


Figure 4.30 Emission spectrum of PTCA in DMF and DMSO at  $\lambda_{\text{exc}} = 485$  nm

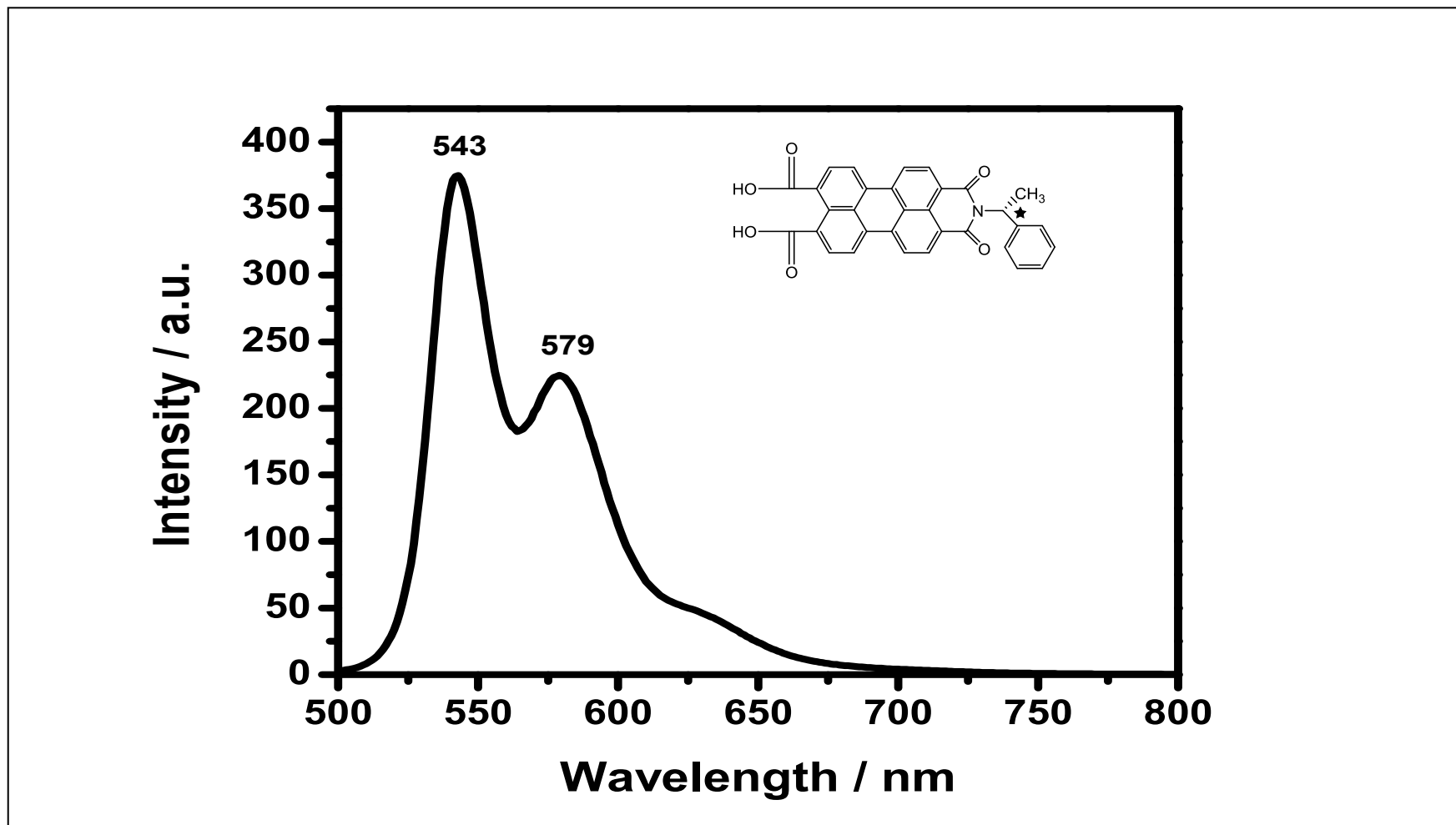


Figure 4.31 Emission spectrum of R-CPMI in DMSO at  $\lambda_{\text{exc}} = 485$  nm

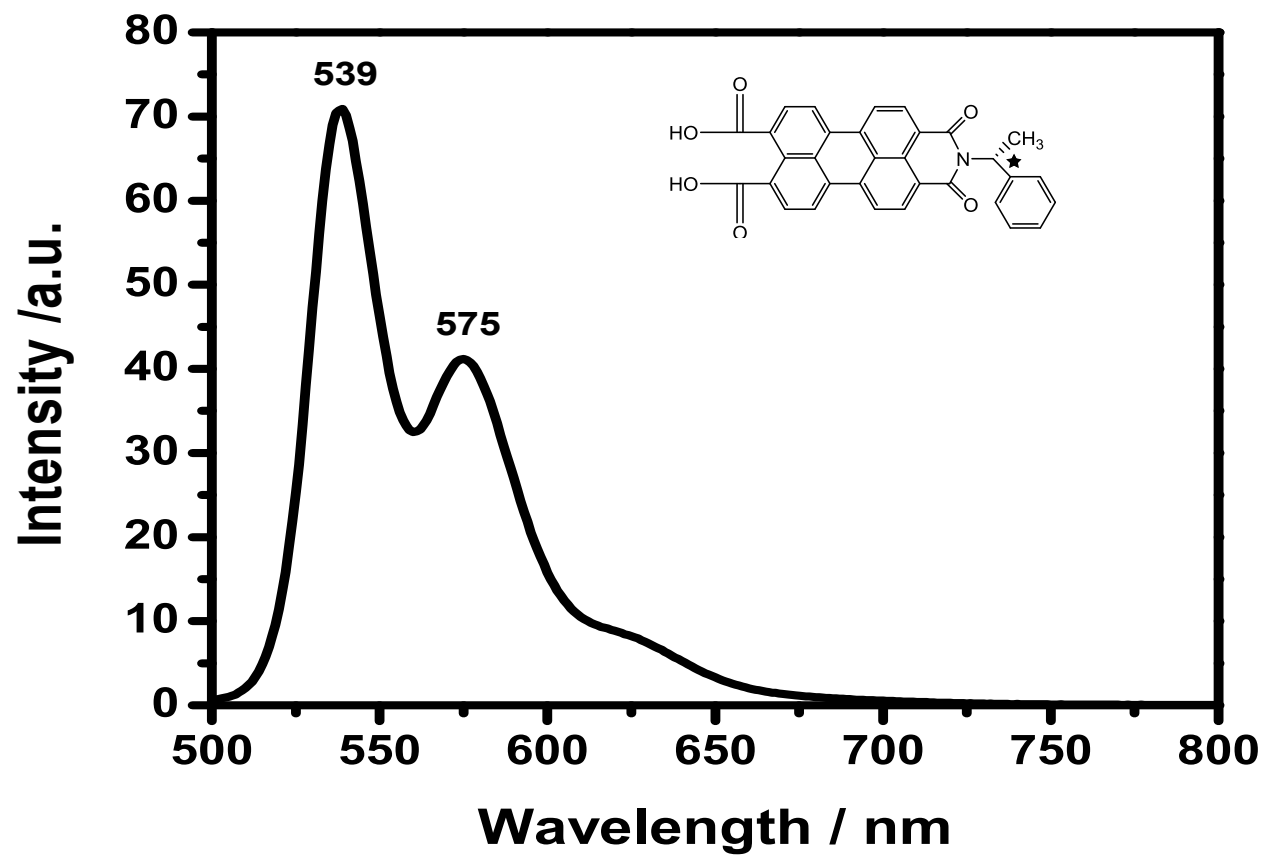


Figure 4.32 Emission spectrum of R-CPMI in DMF at  $\lambda_{\text{exc}} = 485 \text{ nm}$

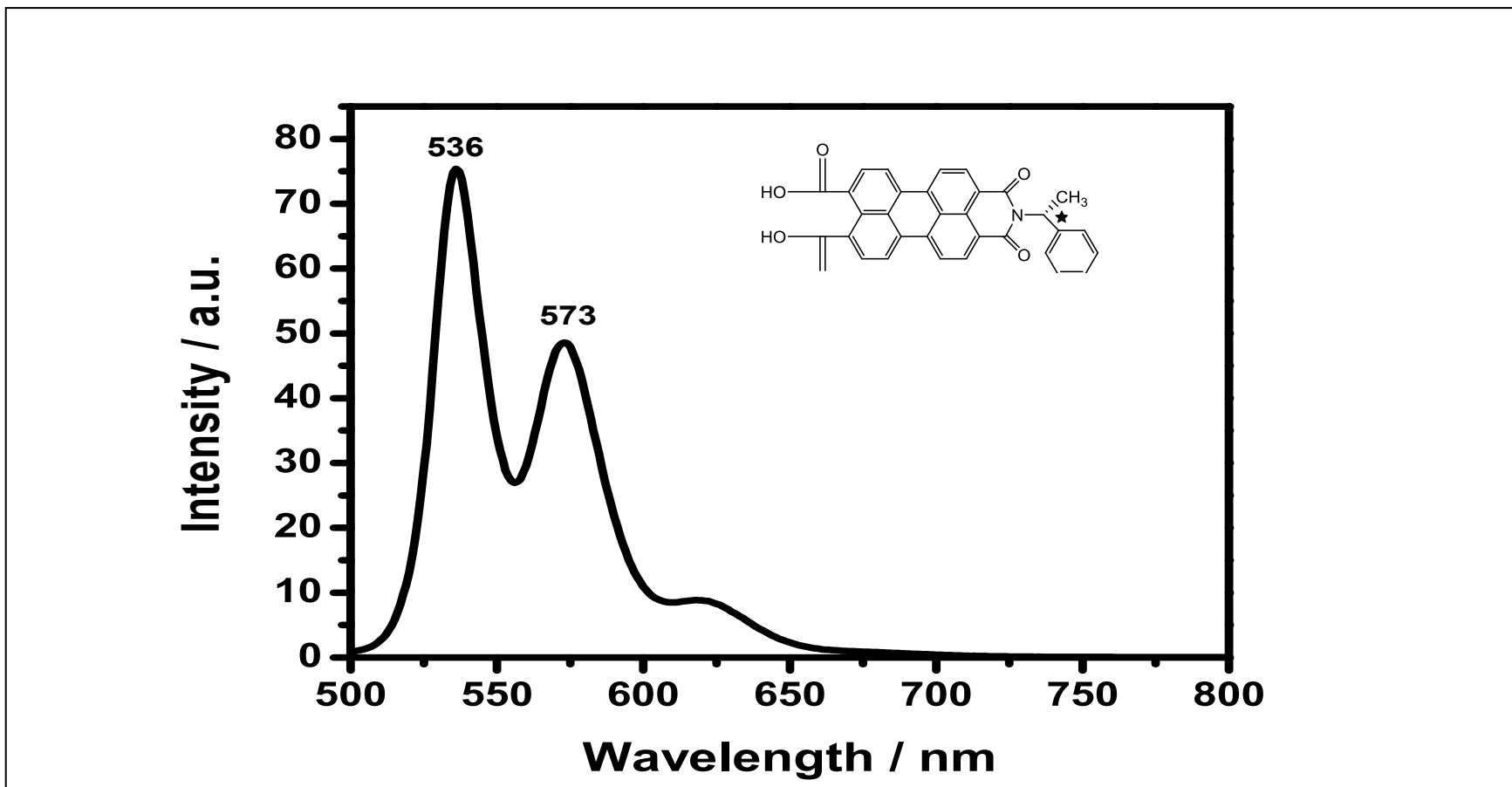


Figure 4.33 Emission spectrum of R-CPMI in Chloroform at  $\lambda_{exc} = 485$  nm

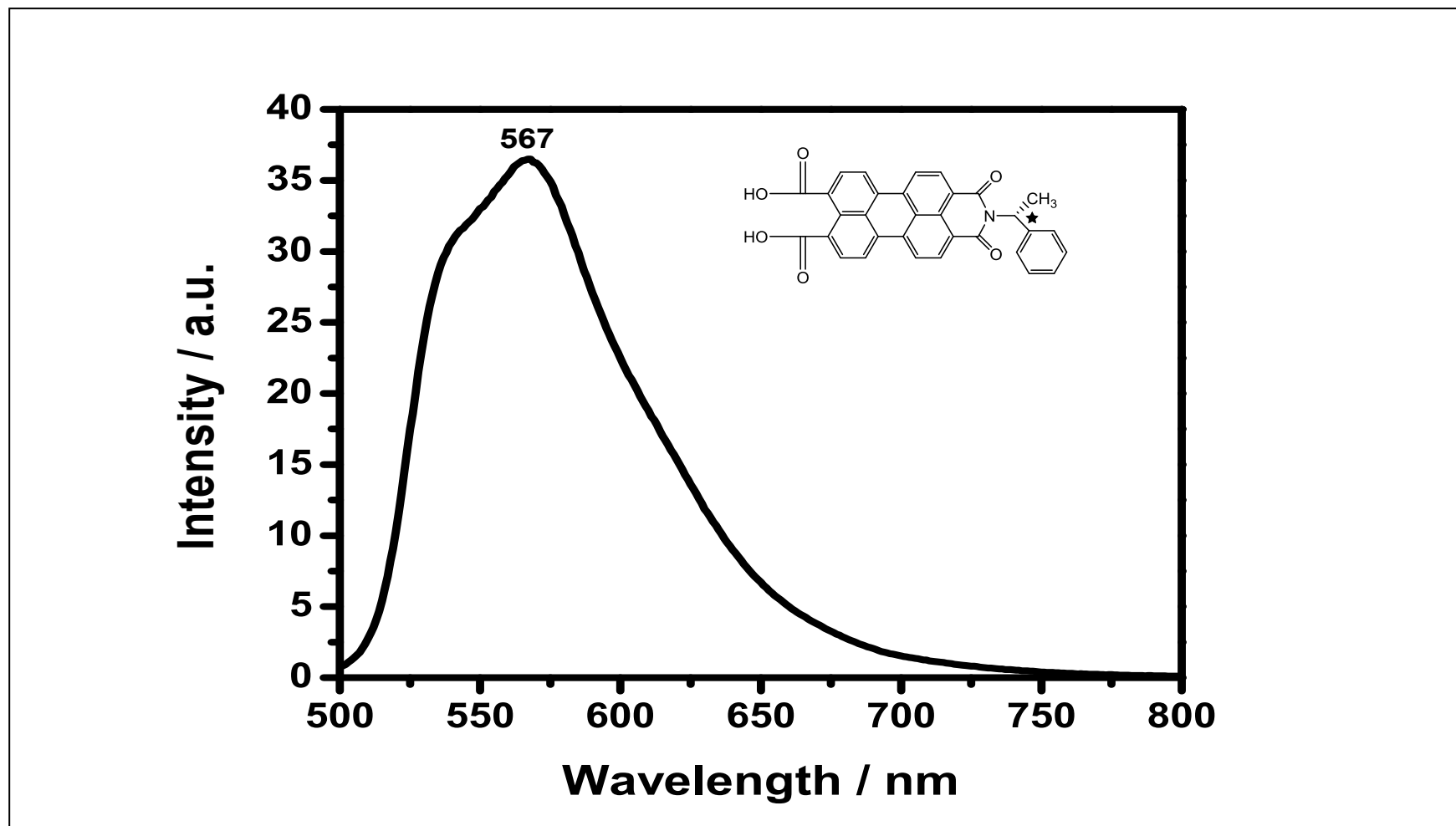


Figure 4.34 Emission spectrum of R-CPMI in MeOH at  $\lambda_{\text{exc}} = 485 \text{ nm}$

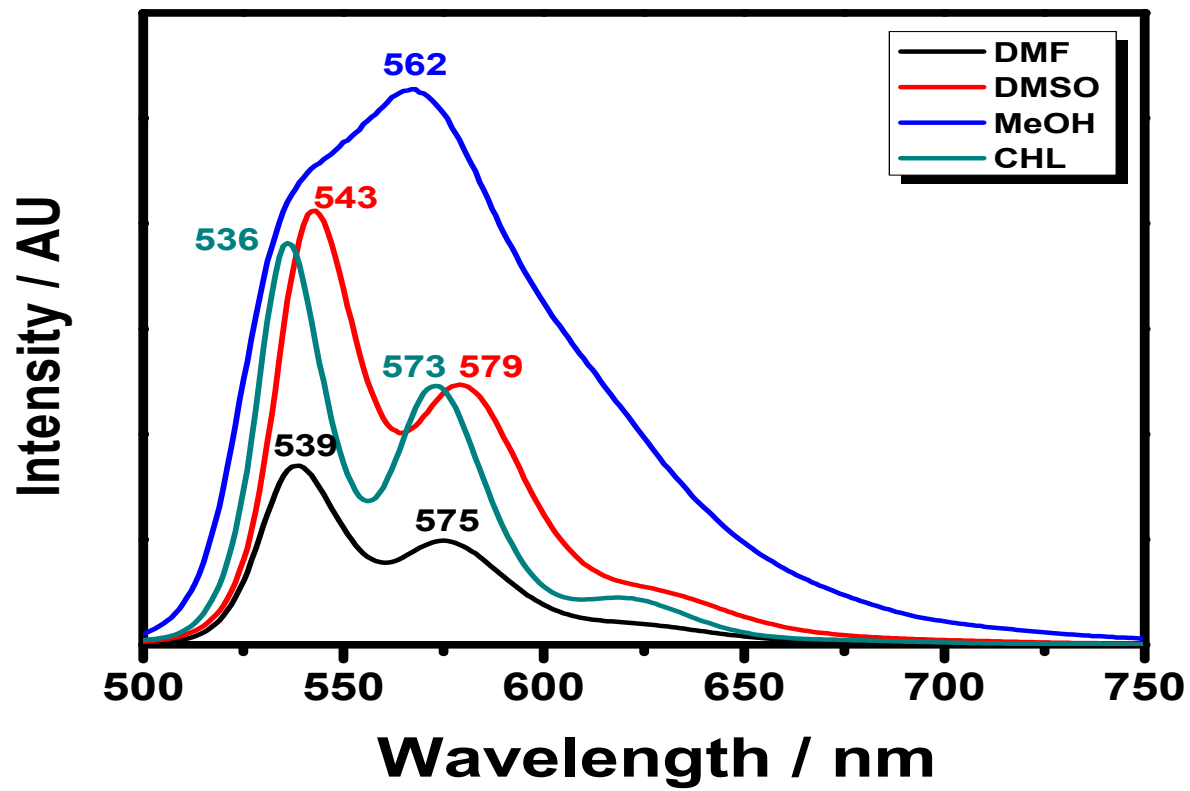


Figure 4.35 Emission spectrum of R-CPMI in DMF, DMSO, CHL and MeOH at  $\lambda_{exc} = 485$  nm

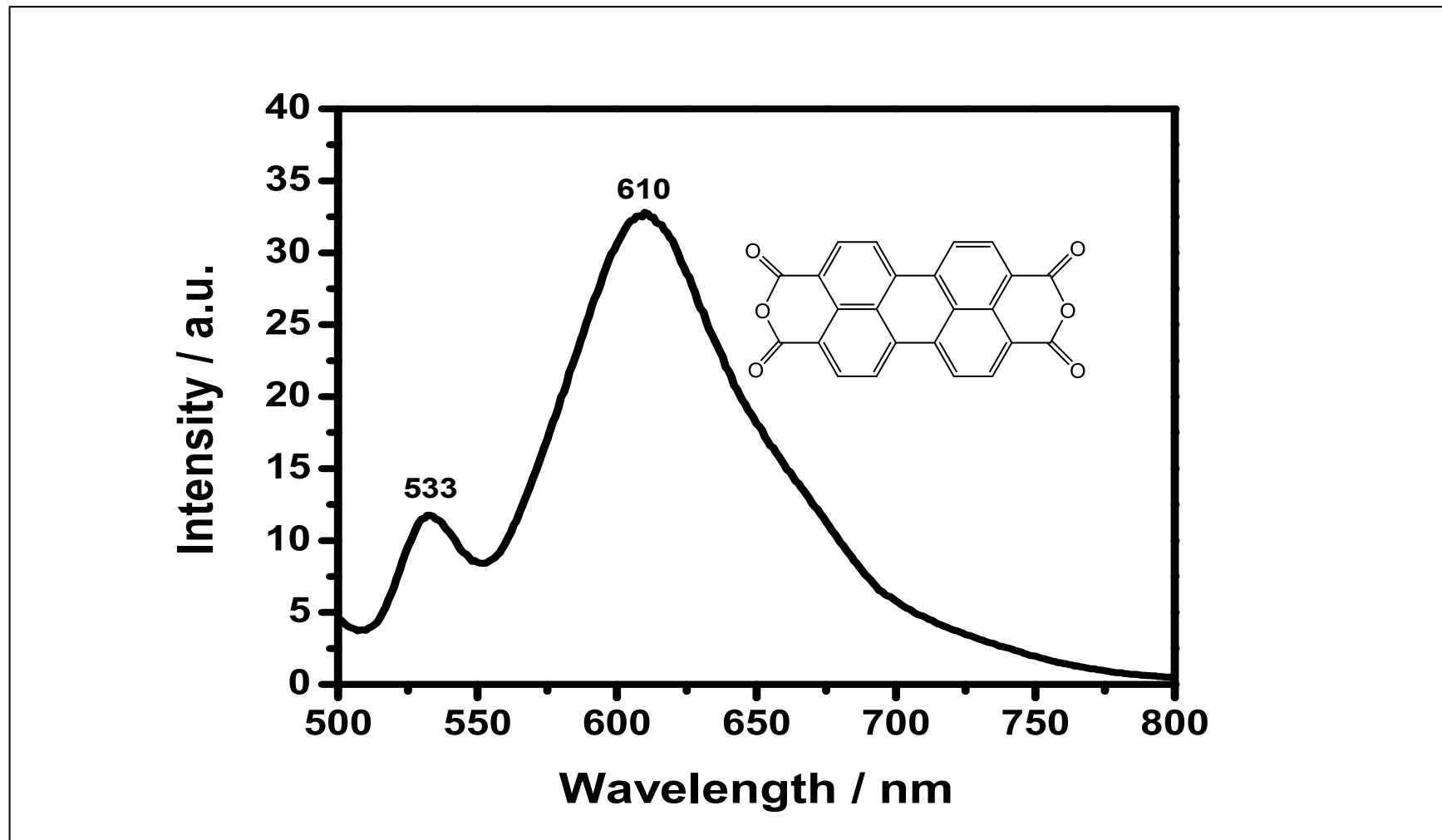


Figure 4.36 Emission spectrum of PDA in DMSO M.F. at  $\lambda_{\text{exc}} = 485$  nm

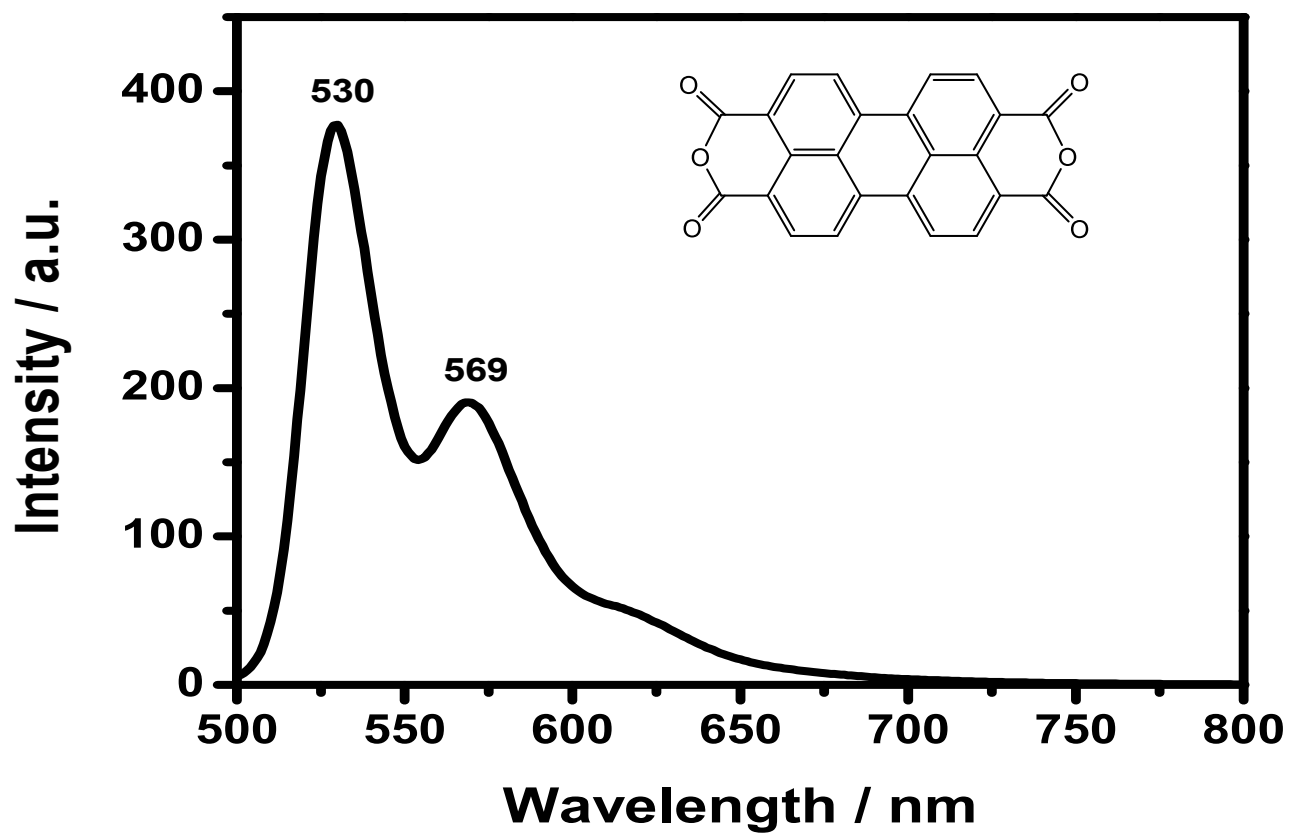


Figure 4.37 Emission spectrum of PDA in DMF M.F. at  $\lambda_{\text{exc}} = 485 \text{ nm}$

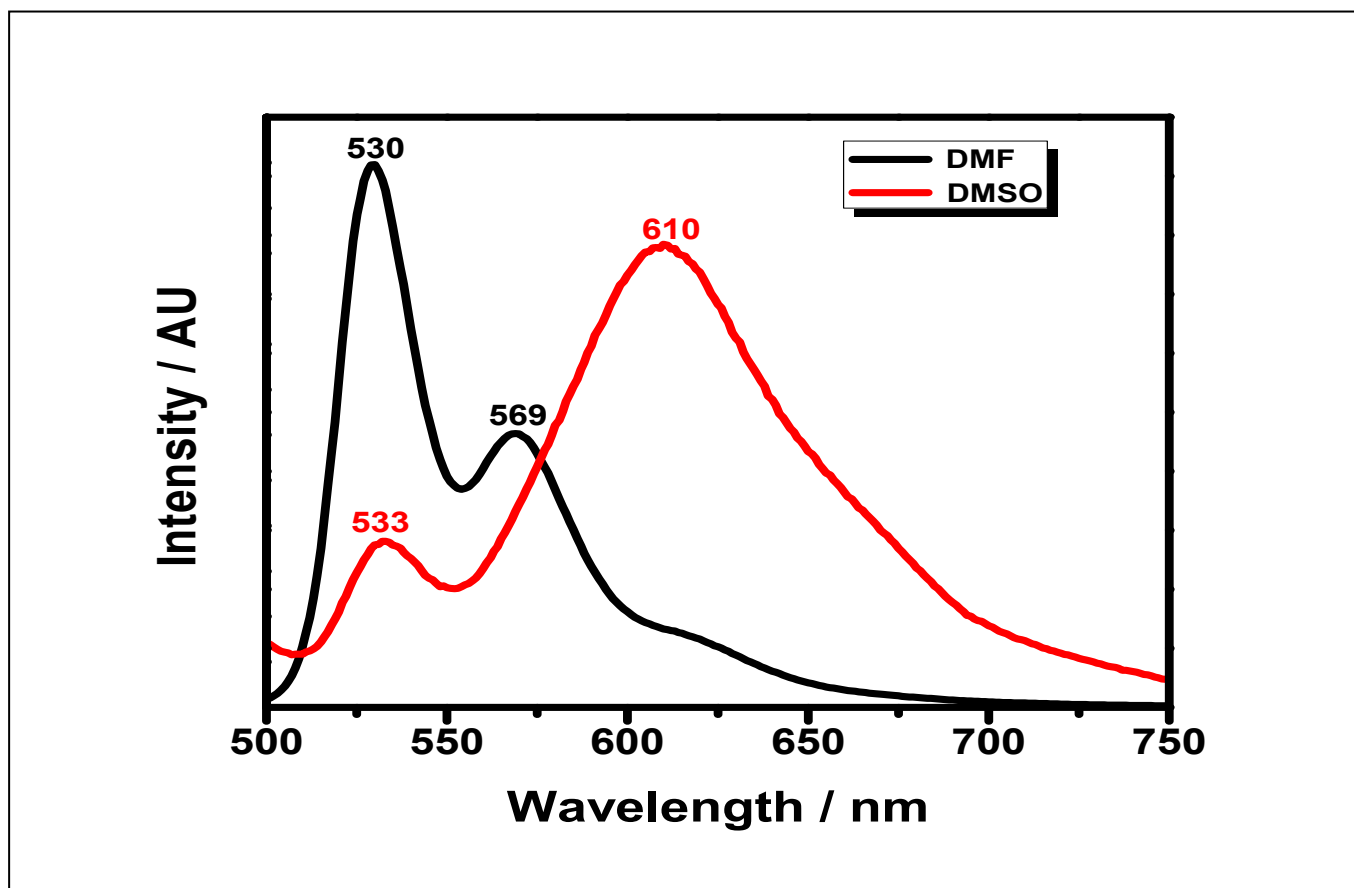


Figure 4.38 Emission spectrum of PDA in DMF and DMSO at  $\lambda_{\text{exc}} = 485$  nm

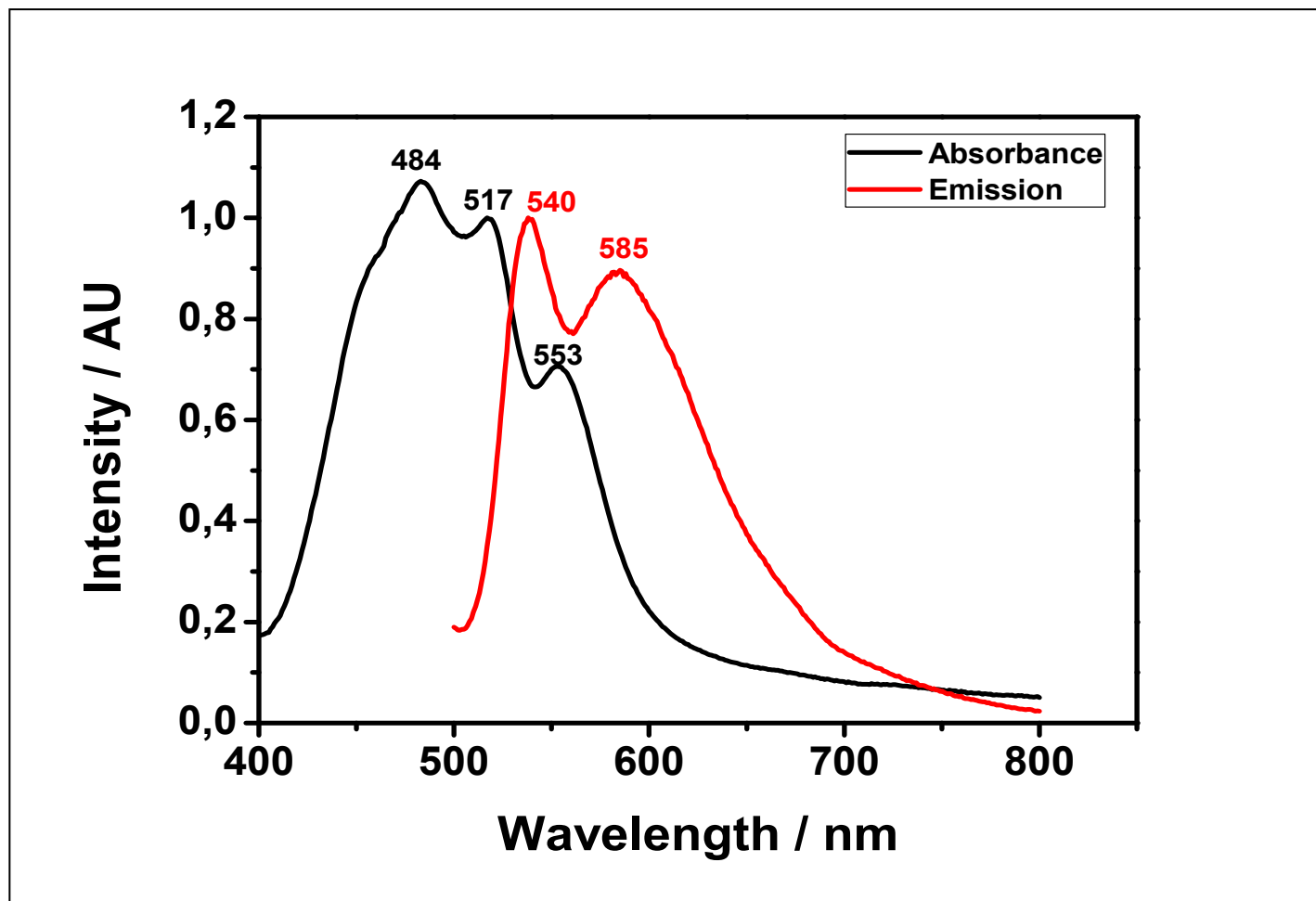


Figure 4.39 Comparison of Absorbance and Emission of PTCA in DMSO

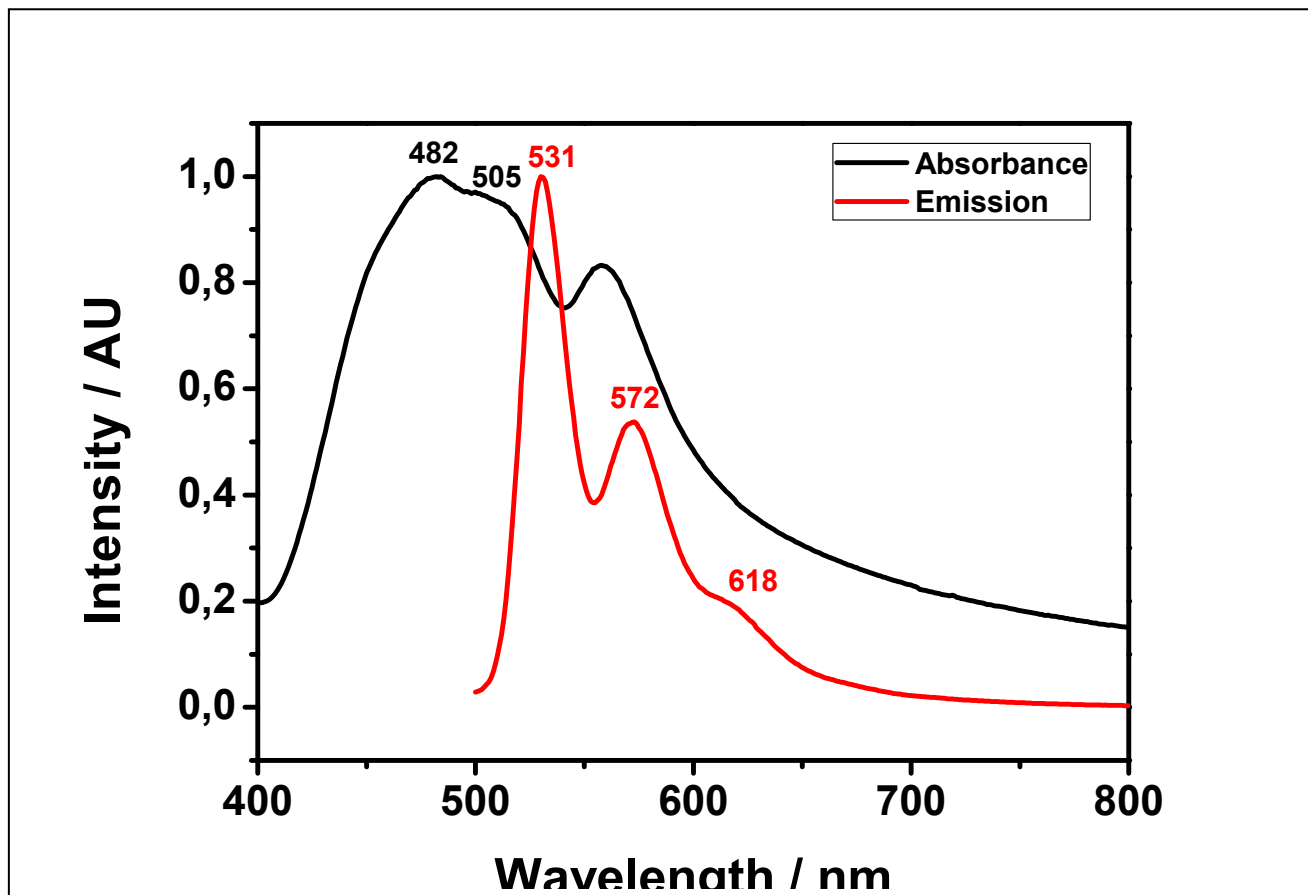


Figure 4.40 Comparison of Absorbance and Emission of PTCA in DMF

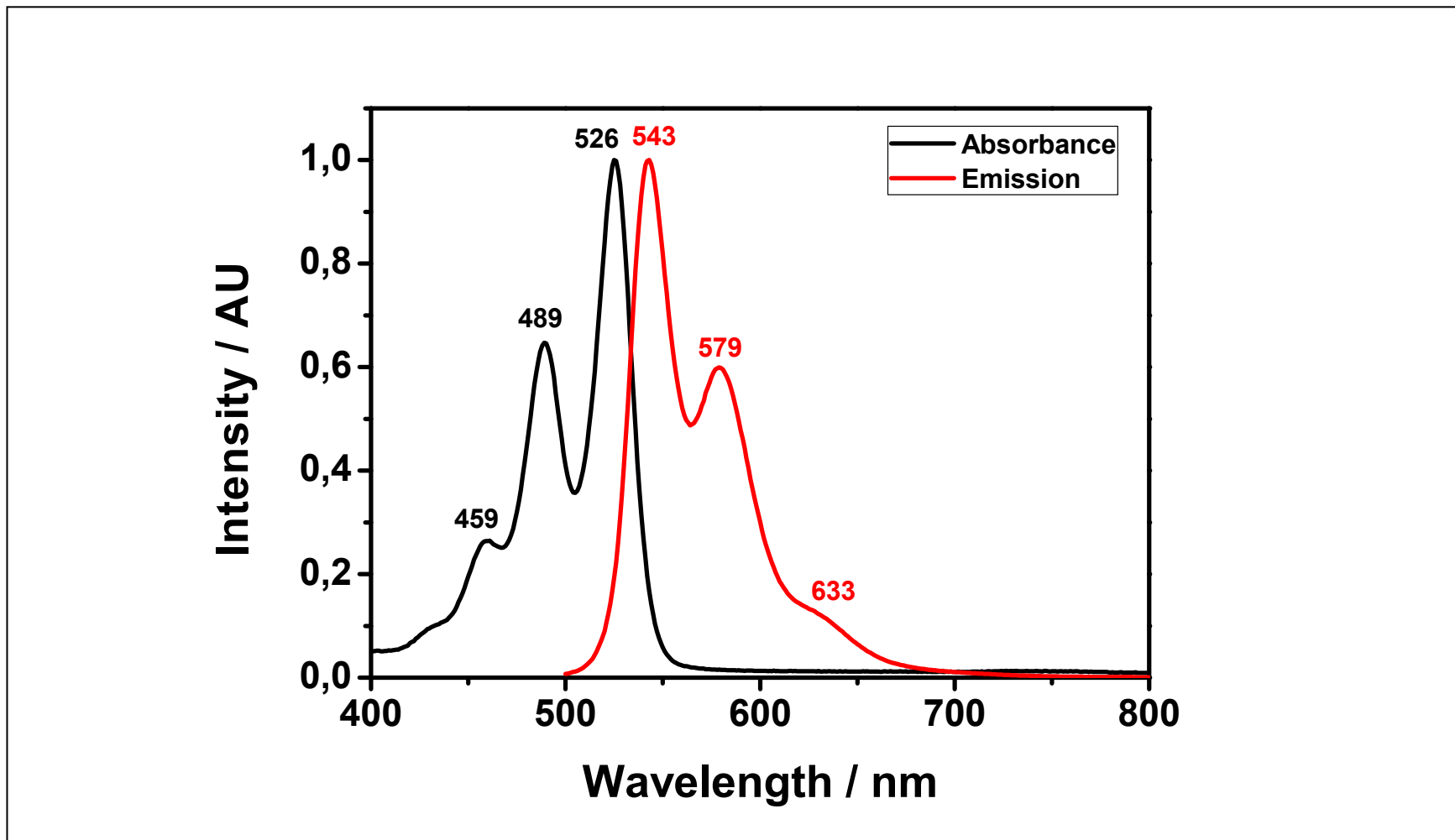


Figure 4.41 Comparison of Absorbance and Emission of R-CPMI in DMSO

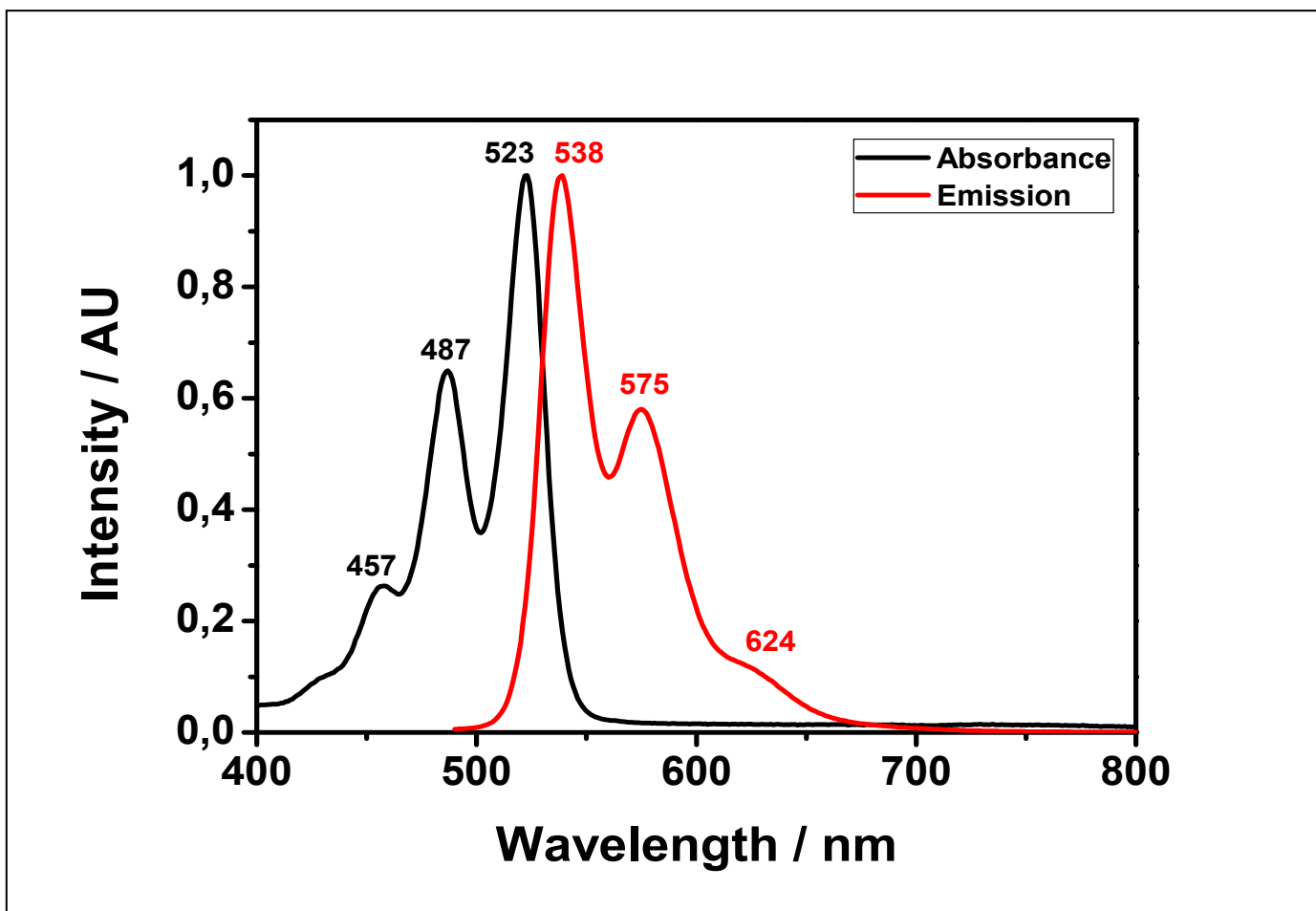


Figure 4.42 Comparison of Absorbance and Emission of R-CPMI in DMF

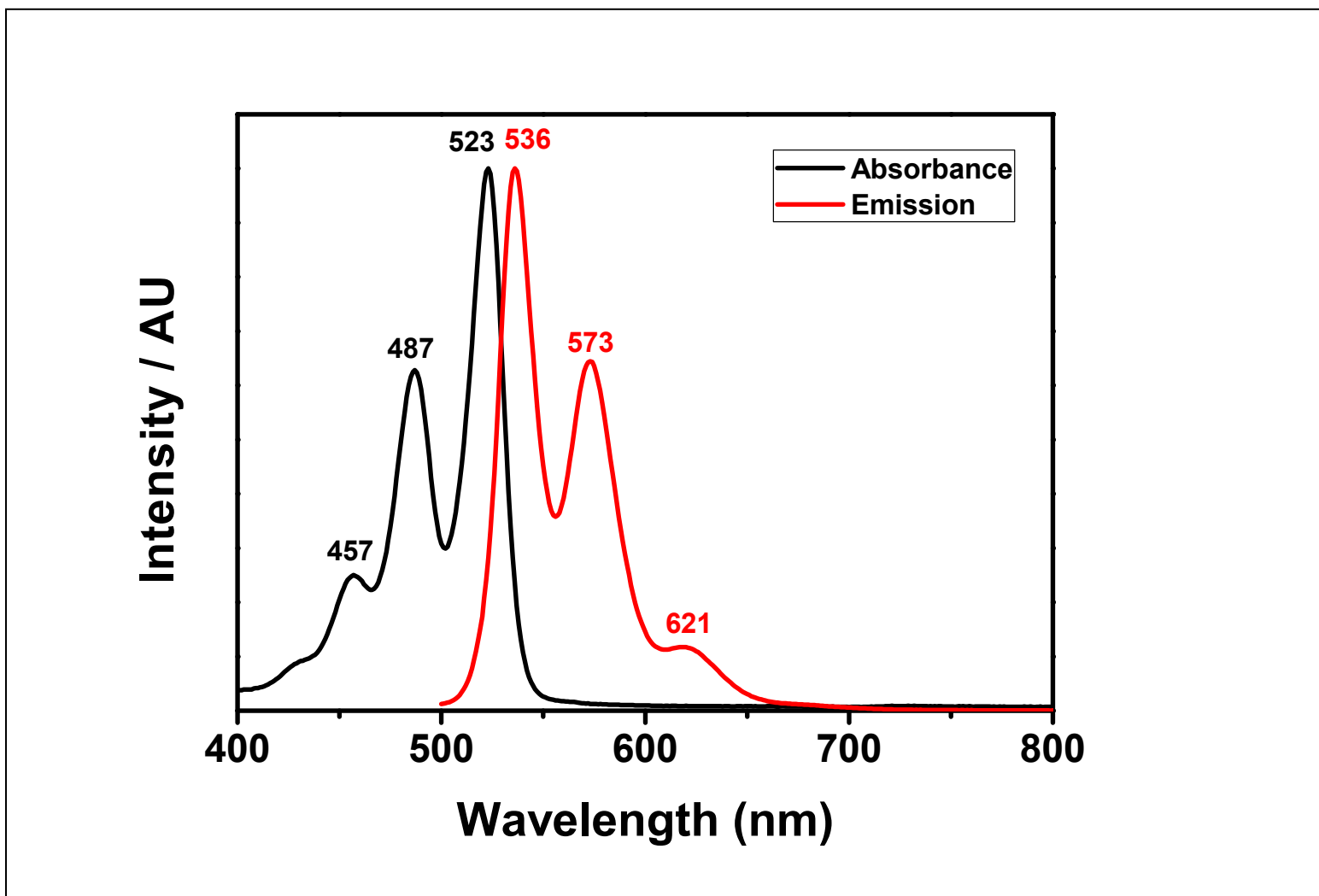


Figure 4.43 Comparison of Absorbance and Emission of R-CPMI in CHL

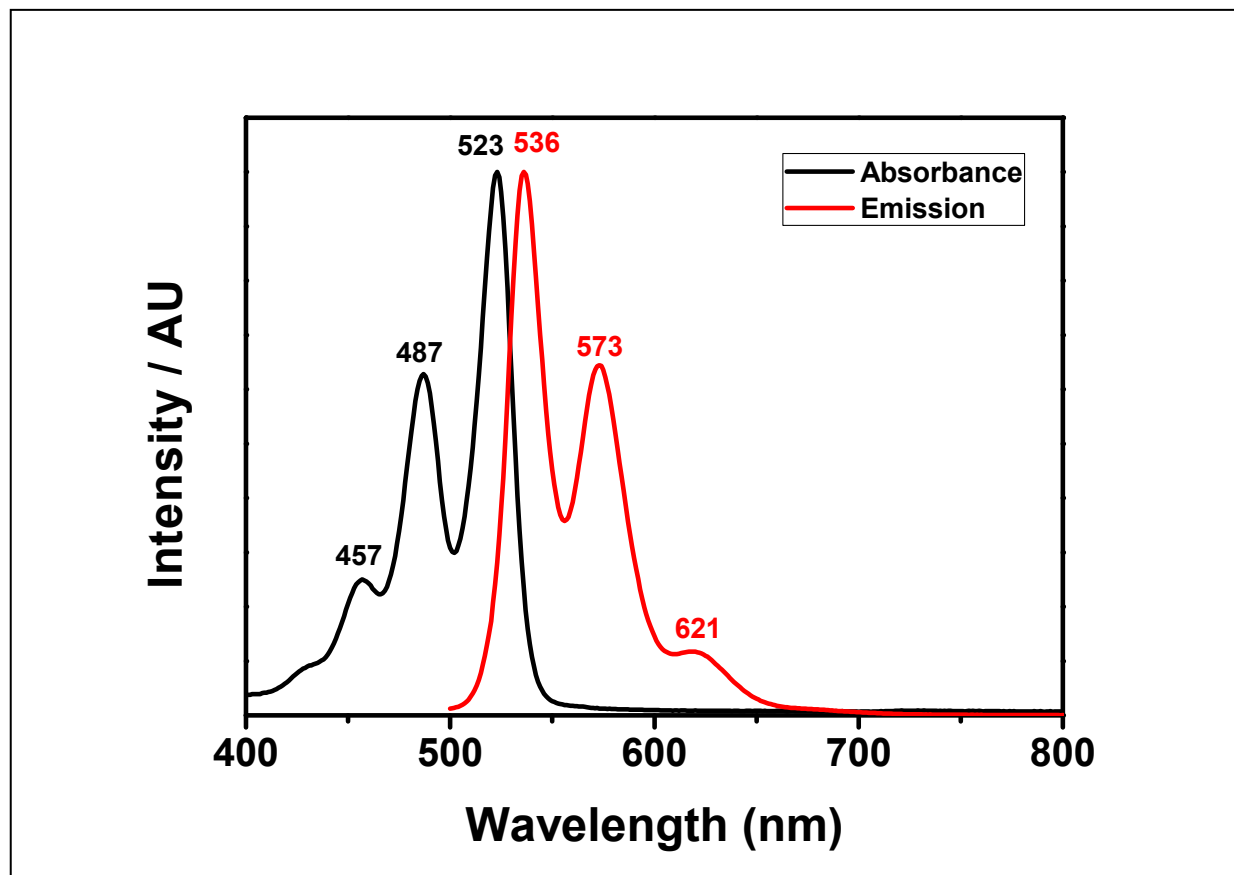


Figure 4.44 Comparison of Absorbance and Emission of R-CPMI in MeOH

## Chapter 5

### RESULTS AND DISCUSSION

#### 5.1 Synthesis of the Perylene Dyes

Perylene dyes are playing very important role in the solar cell applications. Binding properties of perylene dyes to the  $\text{TiO}_2$  is also a key step in the solar cell preparations. In this thesis, a perylene tetracarboxylic acid (PTCA), a chiral PDI, a chiral R-PMI and chiral R-CPMI were successfully synthesized.

The PTCA was synthesized from perylene dianhydride. The chiral R-CPMI was synthesized in three steps. In the first step, the chiral PDI was synthesized and then the chiral R-PMI was synthesized from chiral PDI in the second step. In the third step, the chiral R-CPMI was synthesized from chiral R-PMI.

All the perylene dyes were carefully synthesized according to the procedures where progress of reactions were followed by thin layer chromatography and FT-IR spectra. All the products were obtained with high yields. Perylene dianhydride was used in order to compare the results. Therefore, the photophysical properties of PDA, PTCA and R-CPMI were compared in this thesis.

## 5.2 Solubility of the Perylene Dyes

The solubility of PTCA, PDA and R-CPMI were poor in common organic solvents. Different solvents were used to dissolve these three compounds. It was found that PTCA and PDA were only partially soluble in DMSO and DMF. On the other hand, R-CPMI beside DMF and DMSO, it is soluble in methanol and chloroform with fluorescent color. Table 5.1 shows the solubility properties of PTCA, PDA and R-CPMI in different solvents. The higher solubility of R-CPMI with fluorescent colors indicates that it has wide application area in industry.

Table 5.1 Solubility of PTCA, PDA and R-CPMI

<b>Solubility/color</b>			
<b>Solvent</b>	<b>PTCA</b>	<b>PDA</b>	<b>CPMI</b>
<b>DMSO</b>	(- +) / Red	(- +) / Red	( + + ) / F Pink
<b>DMF</b>	( - +) / Red	(- +) / Red	( + + ) / F Orange
<b>Methanol</b>	( - - )	( - - )	( + + ) / F Orange
<b>CHCl<sub>3</sub></b>	( - - )	( - - )	( + + ) / F Orange

(+ +) is soluble at room temperature, (- +) is soluble on heating at 60 °C and (- -) is insoluble, F: fluorescent.

### 5.3 Analysis of FTIR Spectra

FT-IR spectra of all the synthesized compounds were used to characterize them from their functional groups. All the functional groups of the synthesized compounds exist in their FT-IR spectra that proves the formation and structure of the compounds. The FT-IR spectra of all the compounds are analyzed below.

Figure 4.4 shows at 3059 and 3025  $\text{cm}^{-1}$  aromatic C—H stretch, at 2970  $\text{cm}^{-1}$  and 2874  $\text{cm}^{-1}$  aliphatic C—H stretch, at 1698  $\text{cm}^{-1}$  and 1665  $\text{cm}^{-1}$  imide C=O stretch, at 1592  $\text{cm}^{-1}$  conjugated C=C stretch, at 1335  $\text{cm}^{-1}$  C—N stretch, at 809  $\text{cm}^{-1}$ , 745  $\text{cm}^{-1}$  and 697  $\text{cm}^{-1}$  aromatic C—H bend that confirms the structure of chiral PDI.

Figure 4.5 shows at 3062  $\text{cm}^{-1}$  aromatic C—H stretch, at 2974  $\text{cm}^{-1}$  aliphatic C—H stretch, at 1769 and 1732  $\text{cm}^{-1}$  anhydride C=O stretching, at 1699  $\text{cm}^{-1}$  and 1656  $\text{cm}^{-1}$  imide C=O stretching, at 1594  $\text{cm}^{-1}$  conjugated C=C stretch, at 1317  $\text{cm}^{-1}$  C—N stretch, at 810  $\text{cm}^{-1}$  and 739  $\text{cm}^{-1}$  aromatic C—H bend that confirms the structure of R-PMI.

Figure 4.6 shows at 3450  $\text{cm}^{-1}$  broad carboxylic O—H stretch, at 3096  $\text{cm}^{-1}$  aromatic C—H stretch, at 2925 and 2852  $\text{cm}^{-1}$  aliphatic C—H stretch, at 1769 and 1732  $\text{cm}^{-1}$  carboxylic acid C=O stretching, at 1699  $\text{cm}^{-1}$  and 1657  $\text{cm}^{-1}$  imide (N—C=O) stretching, at 1594  $\text{cm}^{-1}$  conjugated C=C stretch, at 1318  $\text{cm}^{-1}$  C—N stretch, at 810  $\text{cm}^{-1}$  and 739  $\text{cm}^{-1}$  aromatic C—H bend that confirms the structure of R-CPMI.

Figure 4.7 shows at 3440  $\text{cm}^{-1}$  broad carboxylic acid O—H stretch, at 3114  $\text{cm}^{-1}$  aromatic C—H stretch, at 2924  $\text{cm}^{-1}$  aliphatic C—H stretch, at 1777  $\text{cm}^{-1}$  carboxylic

acid C=O stretching, at  $1596\text{ cm}^{-1}$  conjugated C=C stretch, at  $810$  and  $734\text{ cm}^{-1}$  aromatic C–H bending that confirms the structure of PTCA.

Figure 4.8 shows at  $3118\text{ cm}^{-1}$  aromatic C–H stretch, at  $1772$ ,  $1759$  and  $1739\text{ cm}^{-1}$  anhydride C=O stretching, at  $1594\text{ cm}^{-1}$  conjugated C=C stretch, at  $1024\text{ cm}^{-1}$  anhydride C–O stretch and at  $809$  and  $735\text{ cm}^{-1}$  aromatic C–H bending that confirms the structure of PDA.

#### **5.4 Interpretation of UV-vis Spectra**

The absorption spectra of all the compounds were studied in different solvents. Each compound has different solubility and has different absorption properties. The absorption spectrum of each compound were discussed below.

Figures 4.9 – 4.15 show the absorption spectra of PTCA in DMSO and DMF. The absorption spectra of PTCA shows three absorption bands at  $483$ ,  $516$  and  $557\text{ nm}$ . The absorption bands at  $483$  and  $516\text{ nm}$  belongs to the  $\pi$ – $\pi$  interactions of the perylene structure. On the other hand, the band at  $557\text{ nm}$  is attributed to aggregate formation due to a decrease in the intensity of this band after microfiltration. Also, the other bands that belongs to the perylene structure became more resolved. Figure 4.11 and Figure 4.14 shows this difference. Table 4.2 depicted the high molar extinction co-efficient of PTCA which indicates good absorption in the visible region (at  $557\text{ nm}$   $\epsilon_{\text{max}} = 51000\text{ M}^{-1}\text{ cm}^{-1}$  and at  $516\text{ nm}$   $\epsilon_{\text{max}} = 64000\text{ M}^{-1}\text{ cm}^{-1}$ ). The calculated singlet energy values that were listed in Tables 4.8 proves this good absorption from ground state to excited state.

Figure 4.11 and Figure 4.14 shows that the aggregation in DMSO is higher than in DMF. After microfiltration there is a small change in the absorption bands in DMSO. On the other hand, after microfiltration three characteristic absorption bands of perylene core structure become more visible in DMF where aggregation band intensity decreased.

As shown in Figure 4.15, the general absorption behavior of PTCA in polar aprotic solvents DMSO and DMF are very similar to each other.

Figure 4.16 – 4.20 shows the absorption spectra of R-CPMI at different solvents. The absorption spectra of R-CMPI has been studied in polar aprotic solvents, DMSO and DMF, nonpolar solvent, chloroform and polar protic solvent, methanol. The absorption spectra of R-CMPI in DMF, DMSO and CHL have three characteristic absorption bands at 459, 489 and 525 nm.. These absorption bands belong to the  $\pi-\pi$  interactions of the perylene structure. There is no specific difference in the absorption spectra of R-CPMI in polar aprotic solvents and nonpolar solvents. Table 4.2 depicted the high molar extinction coefficient of PTCA and indicates good absorption in the visible region ( $\epsilon_{\max} = 114000 \text{ M}^{-1} \text{ cm}^{-1}$  in DMF). The calculated singlet energy values that were listed in Tables 4.8 proves this good absorption from ground state to excited state.

R-CPMI has different absorption properties in MeOH. Due to the carboxylic acid presence in the structure, in polar protic solvents, they form hydrogen bond (Figure 4.19). R-CPMI absorption spectrum in polar protic solvent display 9 nm blue shift due to hydrogen bonding (Figure 4.20).

Figure 4.21 – 4.27 display the absorption spectra of PDA in DMSO and DMF. In both solvents, PDA displays two absorption bands at 488 and 522 nm due to  $\pi$ - $\pi$  interactions of perylene structure. The third absorption band at 588 nm is attributed to the aggregate formation.

As it is shown in Table 4.2 it also has higher molar absorptivity in DMF and DMSO and has good absorption properties in the visible region. The poor solubility of PDA is a disadvantage for PDA in applications.

Figure 4.23 and 4.26 display the absorption spectra of PDA in DMSO and DMF, respectively, before and after microfiltration. These figures proved that the absorption band at 588 nm belong to the aggregate since after microfiltration that band disappeared. Figure 4.27 shows 4 nm blue shift in DMF by comparing DMSO.

### **5.5 Interpretation of Emission Spectra**

Figure 4.28 display the emission spectra of PTCA in DMSO ( $\lambda_{exc} = 485$  nm). There are two emission peaks at 539 and 585 nm due to the presence of conjugated perylene chromophoric  $\pi$ - $\pi$  interactions. The broad excimer-like peak at 585 nm is attributed to the aggregate formation in DMSO.

Figure 4.29 displays the emission spectra of PTCA in DMF. There are three characteristic emission peaks at 530 nm, 570 nm and 619 nm due to the presence of conjugated perylene chromophoric  $\pi$ - $\pi$  interactions in DMF.

Figure 4.30 displays comparison of the emission spectra of PTCA in DMSO and DMF. A 9 nm blue shift is observed in DMF by comparing DMSO.

Figure 4.31 – Figure 4.35 display the emission spectra of R-CPMI in different solvents. In polar aprotic and nonpolar solvents R-CPMI shows similar emission properties due to the presence of conjugated perylene chromophoric  $\pi$ – $\pi$  interactions by small shifts. Three characteristic emission peaks observed in these solvents at 539 nm, 575 nm and 630 nm (in DMF).

On the other hand, the emission spectrum of R-CPMI in MeOH has great difference than the emission spectra of DMF, DMSO and CHL. A broad excimer like emission spectrum in MeOH is attributed to the possible hydrogen bonding.

Figure 4.35 displays the comparison of the emission behavior of R-CPMI in polar aprotic, polar protic and nonpolar solvents.

Figure 4.36 – Figure 4.38 display the emission spectrum of PDA in DMSO and DMF. Broad excimer-like emission spectrum is observed in DMSO with the emission peaks at 533 nm and 610 nm. In DMF, characteristic emission peaks observed at 530 nm and 569 nm.

Figures 4.39 – Figure 4.44 display the comparison of absorption and emission spectra and Stokes' shifts of PTCA, R-CPMI and PDA in DMF, DMSO, CHL and MeOH. The absorption and emission spectra of PTCA are not mirror image to each other due to the aggregation band in the absorption spectrum in DMSO and DMF and display 23 nm and 26 nm Stokes' shift, respectively (Figure 4.39 and Figure 4.40).

Figure 4.41 – Figure 4.43 shows the comparison of absorption and emission spectra of R-CPMI in polar aprotic and nonpolar solvents. All the comparison spectra show mirror images. The Stokes' shifts observed 17 nm, 15 nm and 13 nm in DMSO, DMF and CHL, respectively.

Figure 4.44 display the comparison of absorption and emission spectra of R-CPMI in MeOH and due to the hydrogen bonding they are not mirror images.

The fluorescence quantum yields were also calculated. Table 4.1 shows the  $\Phi_f$  values. Due to the aggregation, PTCA in DMSO and R-PCPMI in MeOH have the lower  $\Phi_f$ .

## Chapter 6

### CONCLUSION

Perylene tetracarboxylic acid synthesized in high yield. Chiral R-CPMI synthesized according to Hamidu Ahmed thesis and Perylene-3,4,9,10-tetracarboxylic dianhydride (PDA) obtained commercially.

PTCA and PDA have poor solubility in common organic solvents. They are partially soluble in DMSO and DMF. R-CPMI has higher solubility in DMSO and DMF. R-CPMI has solubility in nonpolar solvent CHL and polar protic solvent MeOH with fluorescent color. High solubility and fluorescent color of R-CPMI indicates a potential for a wide range of applications in industry.

The structures of the synthesized perylene dyes were all confirmed by the Fourier transform of infrared spectra (FTIR).

Absorption spectra in different solvents indicate that almost all the synthesized dyes have very high molar absorptivities. The highest value is obtained for R-CPMI as  $113000 \text{ M}^{-1} \text{ cm}^{-1}$ .

PTCA and PDA absorption spectra indicates the formation of aggregates where dye-dye molecular interaction in PTCA is higher than PDA. PTCA and R-CPMI absorption spectra indicate that introducing a chiral substituent at one end of the

PTCA breaks dye-dye molecular interaction in polar aprotic solvents. R-CPMI absorption spectrum in polar protic solvent displays 9 nm blue shift due to hydrogen bonding.

The emission spectra of PTCA, PDA and R-CPMI display unique emission peaks in different solvents relating to the conjugated perylene chromophoric  $\pi$ - $\pi$  interactions.

The emission spectrum of R-CPMI in polar protic solvent MeOH displays hydrogen bonding. Introducing a chiral substituent on one end of PTCA change its photophysical properties.

The absorbance and emission spectra of PTCA are not mirror image to each other due to aggregation.

The Stokes' shifts of PTCA observed 23 nm and 26 nm in DMSO and DMF, respectively.

The absorbance and emission spectra of R-CPMI are mirror image to each other in DMF, DMSO and CHL.

The fluorescence quantum yields of PTCA and R-CPMI are low due to aggregation and hydrogen bond formation.

Introducing a chiral substituent on one end of PTCA changed its photophysical properties.

The properties of both PTCA and R-CPMI indicate that they have a high application potential especially in solar cell. On the other hand, in methanol due to hydrogen bonding they are not mirror images.

The Stokes' shifts of R-CPMI observed 17 nm, 15 nm and 13 nm in DMSO, DMF and CHL, respectively.

The properties of both PTCA and R-CPMI indicate that they have a high application potential especially in solar cell. They have high potential to bind to  $\text{TiO}_2$ .

## REFERENCES

- [1] Pasaogullari, N., Icil, H., & Demuth, M. (2005). Symmetrical and Unsymmetrical Perylene Diimides: Their Synthesis, Photophysical and Electrochemical Properties. *Dyes and Pigments*. 69, 118–127.
- [2] Wan, H. (2004). Dye Sensitized Solar Cells. Literature Seminar, University of Alabama.
- [3] Dinçalp, H., Kızılok, S., & Icil, S. (2010). Fluorescent Macromolecular Perylene Diimides Containing Pyrene or Indole Units in Bay Positions. *Dyes and Pigments* 86, 32–41.
- [4] Mikroyannidis, J. A., Stylianakis, M. M., Roy, M. S., Suresh, P., & Sharma, G. D. (2009). Synthesis, Photophysics of Two New Perylene Bisimides and Their Photovoltaic Performances in Quasi Solid State Dye Sensitized Solar Cells. *Journal of Power Sources*. 194, 1171–1179.
- [5] Langhals, H., & Pust, T., Axially Extended Perylene Dyes. *Eur. J. Org. Chem.* (2010): 3140–3145.
- [6] Cappelletti, M. A., Casas, G. A., Cédola, A. P., and Peltzer y Blanc, E. L. (2013). Theoretical study of the maximum power point of n-type and p-type crystalline silicon space solar cells. *Semiconductor Science And Technology*.

- [7] Grätzel, M. (2003). Dye-Sensitized Solar Cells. *Journal of Photochemistry and Photobiology C: Photochemistry Reviews*. 4, 145–153.
- [8] Qi, G., Li R., Wang, L., & Li, X. (2012). Linear Perylenetetracarboxylic Monoanhydride Derivatives for The Sensitization of Dye-Sensitized Solar Cells. *Journal of Photochemistry and Photobiology A: Chemistry*. 239, 28–36.
- [9] Kuo, P., Jan, T., Liao, C., Chen, C., & Lee, K. (2013). Syntheses of Size-Variied Nanorods TiO<sub>2</sub> and Blending Effects on Efficiency for Dye-Sensitized Solar Cells. *Journal of Power Sources*. 235, 297–302.
- [10] Ahmed, H., Ms Thesis. (2013). Eastern Mediterranean University.
- [11] Sharma, G. D., Kurchania, R., Ball, R. J., Roy, M. S., & Mikroyannidis, J. A. (2012). Effect of Deoxycholic Acid on the Performance of Liquid Electrolyte Dye-Sensitized Solar Cells Using a Perylene Monoimide Derivative. *International Journal of Photoenergy Volume*. Article ID 983081, 7 pages.
- [12] Mikroyannidis, J. A., Stylianakis, M. M., Suresh, P., Roy, M. S., & Sharma, G. D. (2009). Synthesis of perylene monoimide derivative and its use for quasi-solid-state dye-sensitized solar cells based on bare and modified nano-crystalline ZnO photoelectrodes. *Energy & Environmental Science*, 2(12), 1293–1301.
- [13] Xu, P. (2011). Tunable Fluorescent pH Sensor Based On Water Soluble Perylene Tetracarboxylic Acid/Fe<sup>3+</sup>. *Luminescence* 2012; 27: 307–309.

- [14] Xue, C., Sun, R., Annab, R., Abadi, D., & Jin, S. (2009). Perylene Monoanhydride Diester: a Versatile Intermediate for The Synthesis of Unsymmetrically Substituted Perylene Tetracarboxylic Derivatives. *Tetrahedron Letters*. 50, 853–856.
- [15] Yang, L., Shi, M., Wang, M., & Chen, H. (2008). Synthesis, electrochemical, and spectroscopic properties of soluble perylene monoimide diesters. *Tetrahedron*, 64(22), 5404–5409.
- [16] Li, C., & Wonneberger, H. (2012). Perylene Imides for Organic Photovoltaics: Yesterday, Today, and Tomorrow. *Adv. Mater.* 24, 613–636.
- [17] Zhang, X., Wu, Y., Li, J., Li, F., & Li, M. (2008). Synthesis and characterization of perylene tetracarboxylic bisester monoimide derivatives. *Dyes and Pigments*, 76(3), 810–816.
- [18] Li, C., Schöneboom, J., Liu, Z., Pschirer, N. G., Erk, P., Herrmann, A., & Müllen, K. (2009). Rainbow perylene monoimides: easy control of optical properties. *Chemistry-A European Journal*, 15(4), 878–884.
- [19] Schmidt, Ruediger (2009). "Synthetic Routes to Core-fluorinated Perylene Bisimide Dyes and their Properties." *ChemInform* 40.45.

- [20] Wang, M., & Wang, X. (2007). P3HT/TiO<sub>2</sub> Bulk-Heterojunction Solar Cell Sensitized By a Perylene Derivative. *Solar Energy Materials & Solar Cells*. 91, 1782–1787.
- [21] Paramaguru, G., Nagarajan, N., & Renganathan, R. (2013). Effect of Number of Anchoring Groups on Binding Ability of Perylene Diimides With SnO<sub>2</sub> and TiO<sub>2</sub> Nanoparticles: A Spectroscopic Approach. *Journal of Molecular Structure*. 1038, 235–241.
- [22] Fortage, J., Severac, M., Houarner-Rassin, C., Pellegrin, Y., Blart, E., & Odobel, F. (2008). Synthesis of New Perylene Imide Dyes and Their Photovoltaic Performances in Nanocrystalline TiO<sub>2</sub> Dye Sensitized Solar Cells. *Journal of Photochemistry and Photobiology A: Chemistry*. 197, 156–169.
- [23] Nunzi, J.M. (2002). Organic Photovoltaic Materials and Devices. *C. R. Physique*. 3, 523–542.
- [24] Vilaric, M.J., Gonza'lez-Aguilar, G. (2012). Electrochemical Behaviour of ZnO/Flavonoid Pairs. *Environmental Progress & Sustainable Energy*.(804-809).
- [25] Park, S., Cho, E., Song, D., Conibeer, G., and Green, M. A. (2009). n-Type silicon quantum dots and p-type crystalline silicon heteroface solar cells. *Solar Energy Materials & Solar Cells*. 684–690.

- [26] Karlson, M. (2012). Material Development for Solid State Dye Sensitized Solar Cells. UPPSALA University.
- [27] Wang, S., Li, Y., Du, C., Shi, Z., Xiao, S., Zhu, D., Gao, E., & Cai, S. (2001). Dye sensitization of nanocrystalline TiO<sub>2</sub> by perylene derivatives. *Synthetic Metals*. 128, 299–304.
- [28] Armarego W. L. F. and Perrin D. D. (2000) Purification of Laboratory Chemicals, 4th Edition, Oxford Press.
- [29] Wang, S. M., Dong, W., Tao, R., Deng, Z., Shao, J., Hu, L., Zhu, J., & Fang, X. (2013). Optimization of Single-Crystal Rutile TiO<sub>2</sub> Nanorod Arrays Based Dye-Sensitized Solar Cells and Their Electron Transport Properties. *Journal of Power Sources*. 235, 193–201.
- [30] Qi, Pucci, A., Donati, F., Nazzi, S., Barretta, G. U., Pescitelli, G., Bari, L. D., Ruggeri, G. (2010). Association Phenomena of a Chiral Perylene Derivative in Solution and in Poly (Ethylene) Dispersion. *React. Funct. Polym.* 70, 951-960.
- [31] Scaiano, J. C. (1989) (Ed.) Handbook of Organic Photochemistry, CRC press.
- [32] Icil, H., & Icli, S. (1997). Synthesis and Properties of a New Photostable Polymer: Perylene-3,4,9,10-tetracarboxylic Acid-Bis-(N,N\_-dodecylpolyimide). *J. Poly. Sci. A: Polym. Chem.* 35, 2137–2142.

[33] Turro, N.J. (1965) *Molecular Photochemistry*, Benjamin, London, 44.